The Prediction of Smoke Detector Activation Times in a Two-Storey House Fire through CFD Modelling

---

Fire Engineering Thesis, 2010

Submitted by

Julie Saunders

Supervised by

Michael Spearpoint, University of Canterbury

A research thesis presented to the University of Canterbury in fulfilment of the requirements for the degree of Master of Engineering in Fire Engineering.

Department of Civil Engineering

University of Canterbury

Christchurch, New Zealand

Table of Contents

List of Figures

Acknowledgments

The author wishes to express sincere appreciation to Mike Spearpoint, for his assistance, guidance and patience. To the Engineering Library staff at the University of Canterbury, thank you for your endless assistance in locating references and forwarding information to Australia, I am very grateful.

To my classmate, Lizzie, who made my time in New Zealand an experience and not just about the study. To Tony, who developed into not just my mentor but also a great friend. Also thanks to Pauline and Gordon for their hospitality and generosity during my time in Christchurch.

Finally I would like to thank my parents and partner. Without my parents I would never have been able to venture upon the path of Fire Engineering, nor any of my other achievements in life. To Gibbo, thanks for the support and patience through it all, no matter if you were near or far.

Abstract

This report describes an investigation into the prediction of the activation times of domestic ionisation and photoelectric smoke detectors within a two storey dwelling, the work undertaken being an extension to that previously presented by Brammer (2002). Three fire scenarios are considered, each having been a real test fire undertaken at the Building Research Establishment in Cardington. These three fire scenarios all involved the flaming combustion of an upholstered armchair within the lounge on the Ground floor. During the experiments various results were recorded, including temperatures, optical densities and smoke detector activation times.

The fire scenarios where modelled using FDS, Version 5. Base parameters regarding the fuel load where defined to be $0.05kg_{soot}/kg_{fuel}$ and 20MJ/kg. Consideration was also given to the effect varying the effective heat of combustion and defined soot yield would have on derived smoke detector activation times. Additional simulations where thus run considering soot yields of $0.04kg_{soot}/kg_{fuel}$ and $0.10k_{soot}/kg_{fuel}$, and an effective heat of combustion of 25MJ/kg.

Three prediction methods where applied to the results of the FDS simulations for derivation of the activation times of smoke detectors located throughout the house. These methods where the temperature correlation method, Heskestad's method, and Cleary's method. The temperature correlation method considered activation criterions of 4°C, 13°C and 20°C above ambient.

The Heskestad and Cleary methods were found to derive comparable activation times for each detector location. None of the prediction algorithms where however found to predict activation times consistently comparable to the test data. Rather, it was determined that for an appropriate prediction method to be adopted for accurate assessment of a given fire scenario, consideration must be given to the:

- type of detector being assessed;
- location of the detector relative to the fire;

- mode of combustion (i.e. flaming or smouldering); and the
- growth rate of the fire.

Nomenclature

D_u	m^{-1}	Optical density per unit length outside detector
D_{ui}	m^{-1}	Optical density per unit length inside a detector
D_{uo}	m^{-1}	Optical density per unit length required inside a detector to produce response
D_{ur}	m^{-1}	Optical density per unit length outside a detector at response
L	m	Characteristic length/path length
$\dot{m}$	kg/s	Mass burning rate
$\dot{Q}$	kW	Energy release rate
T	ºC	Temperature
T_{act}	ºC	Temperature at activation
T_{amb}	ºC	Ambient temperature
T_d	ºC	Detector temperature
t	s	Time
Y	kg/kg	Smoke mass fraction
u	m/s	Velocity
α		Empirical constant
β		Empirical constant
ΔH_{eff}	kJ/kg	Effective heat of combustion
ΔT_r	ºC	Temperature rise needed for activation
τ		Time constant (characteristic lag time)
γ		Coefficient characteristic of the detailed geometry of a detector
δt_e		Characteristic filling time of entire volume
δt_c		Characteristic filling time of sensing chamber

1. Introduction

1.1. Background to Study

In developing a fire safety strategy for a building, fire engineers are typically required to model a potential fire scenario, assessing the environmental conditions over time. From the results of this analysis, the engineer is able establish both the time at which conditions are deemed untenable for occupants (Available Safe Egress Time; ASET), and the time required for occupants to evacuate to a place of relative safety (Required Safe Egress Time; RSET). A comparative assessment would then be undertaken to determine if an acceptable level of life safety is provided for occupants, i.e. an appropriate safety margin is present.

In design, one cannot account for all fire scenarios and thus has to make many assumptions as part of an assessment process. Such assumptions may relate to factors such as fuel load, ventilation conditions, fire growth rate and detection algorithms, in addition to any assumptions included within the development of any modelling program adopted. Engineers need to have an understanding as to the degree of accuracy of their analysis and assessments given the assumptions incorporated.

The first stage of establishing the time taken by occupants to evacuate is to determine the time at which occupants become aware of the fire. This awareness will be the result of receipt and interpretation of a given cue, such as the sounding of an alarm. The alarm could be part of a building wide alarm system, or alternatively from an individual smoke alarm, comprising of a sensor and alarm within the one unit.

The establishment of an accurate smoke detector activation time is therefore an important factor in determining the overall level of safety provided to occupants for a given fire scenario. Underestimation of this time period could result in a building having insufficient fire safety measures present for occupants to be able to evacuate prior to exposure to hazardous conditions.

The research undertaken addresses this component of an ASET-RSET analysis, assessing real test fire scenarios for comparison of derived smoke detector activation

times to the test data. The aim is not to consider all the finite details of such an assessment, but rather adopt an approach which is considered to be representative of that used for typical fire engineering analysis. Assumptions made are therefore considered to be representative of those which would be adopted within a typical analysis by a fire engineering consultant for the given fire scenarios.

1.1.1. Smoke Detector Activation Prediction

Ierardi and Barnett (2000) suggest that the overall methodology for predicting smoke detector response can be divided into five categories, all of which need consideration to derive an accurate result:

- *Property Generation*: Knowledge of the production of detectable properties during the combustion process is critical to predicting detector response. Adopting the most sophisticated prediction algorithm is pointless without accurate input data. In general terms, property generation is primarily influenced by the chemical composition of the fuel, local oxygen concentration, the combustion mode and the heat release rate.

- *Bulk Property Transport*: As combustion products move away from their source of origin to a detector, their properties change with time. As a result, detectors sited in varying locations will be subjected to slightly different conditions. This change is a function of a number of processes, including coagulation, deposition, dilution and sedimentation of the particulates.

- *Local Property Transport*: This refers to the transport of combustion products from a detectors location into the sensing chamber. It is not accurate to assume that the conditions inside a detector are identical to those outside at a specific moment in time, i.e. a time lag exists. The difference between these conditions is dependent upon the geometry of the detector and the ceiling jet properties at that position.

- *Sensor Modulation*: Account must be taken for the interaction between the sensor environment and the current in the sensor circuits.

- *Alarm Condition*: Typically this is a threshold value of current in the sensor circuit which, when surpassed, triggers a detector to activate. For ionisation type detectors, an alarm condition exits when the current in the sensor circuit decreases below a threshold value. For photoelectric type smoke detectors an alarm condition exists when the current in the sensor circuit increases beyond a threshold value.

These five categories can be combined into a two stage assessment process; determination of the changing environmental conditions, and application of an activation prediction algorithm. The first stage is typically undertaken through the use of a computer modelling package, whilst the second stage applies the data derived in stage one to a detector model in order to calculate an activation time. The particular modelling package and predictor algorithm adopted is dependent on a number of factors, including the context of the scenario, the extent of information available and the reason for requiring the solution.

One such computer modelling program that has been developed for simulating a fire scenario is Fire Dynamics Simulator (FDS). This program is adopted within the research undertaken for determination of environmental conditions throughout a two storey house during the fire scenarios considered. Section 2.3 provides further information on the underlying principles of FDS.

Three prediction algorithms developed for the subsequent determination of smoke detector activation times once environmental conditions are established are the temperature correlation method, Heskestad's method and Cleary's method. These algorithms are applied to the results of the FDS simulations for the determination of smoke detector activation times. Section 2.4 provides further information on these detector prediction algorithms.

Researchers formulating the models and algorithms adopted by fire engineers in both design and analysis problems such as those noted above, must consider three issues (McGrattan et al 2009a):

- *Accuracy*: provide an accurate solution to a problem.

- *Simplicity*: be simple to use and ensure that the underlying principles and situations in which the model/method is applicable be clear.

- *Efficiency*: not be too time consuming to run or evaluate.

Unfortunately, meeting the second and third issues listed tends to offset the achievement of the first. In order to reduce the degree of complexity and the time involved, simplifications of the real world are incorporated into model packages through assumptions. Researchers are required to formulate idealised descriptions of fires and approximate solutions to the idealised equations. These assumptions will affect the accuracy of desired results, and thus need to be both understood and accounted for by an engineer within any fire engineering analysis.

1.1.2. Cardington Tests

As part of ongoing research, a number of test fires where undertaken within a full scale house rig in the Building Research Establishment (BRE) test facility located in Cardington, United Kingdom. The design of the house was such that it represented a typical 1970's two storey, three bedroom detached home. The tests considered the effects of fires in upholstered furniture within a domestic environment, with each experiment involving the combustion of either one or two armchairs located within the lounge. The door to the lounge and other rooms of the house where either closed, or fully or partially opened, across the experiments, allowing the extent of ventilation available to the room of fire origin to be modified. A total of ten tests, CDT14 – CDT23, were carried out using the full scale house rig, which assessed both flaming and non-flaming fire scenarios.

The results of these tests have been assessed and discussed in a number of published references with regards to tenability conditions within the house, including Purser et al (1995, 1998). Spearpoint (1996) discusses the activation times of the smoke detectors throughout the house, analysing the ability of smoke alarms to detect the fires, the relative performance of smoke alarms in the different locations and the resulting escape time available to occupants within the dwelling.

Thomas (2008) and Brammer (2002) have both undertaken modelling of a number of the fire scenarios, assessing the derived environmental conditions against the real test data. Thomas's work involved modelling three of the test fire scenarios; CDT16, CDT17 and CDT18, using the zone modelling program BRANZFIRE. Included within the assessment of the derived environmental conditions is consideration of smoke detector activation times. Brammer assessed two test fire scenarios; CDT17 and CDT20, on which further detail is provided in the following section.

The research presented in this report stemmed as an extension to Brammer's work. Three of the fire scenarios are considered; CDT16, CDT17 and CDT19, all involving the flaming combustion of an armchair(s). Details relating to each of these experiments are provided in Section 3.

1.1.3. Brammer's Research

Brammer (2002) assessed two of the Cardington tests, CDT17 and CDT20, using FDS Version 2[1], comparing the actual test behaviour with predicted smoke detector activation results. The objectives of the research were to create an effective analysis model for the test house, placing an emphasis on temperature and optical density as these are most relevant to the derivation of smoke detector activation times. From comparison of the predicted to actual test data, recommendations relating to the parameters and methods of prediction for use within current analysis software were provided. Further information is provided on the work undertaken by Brammer in Section 3.5.

As previously stated, the research undertaken by the author is considered to be an extension to the work undertaken by Brammer. As such, some of the initial model development work has not been repeated, but rather, based on the information presented, is considered to be accurate and therefore utilised to carry out further analysis.

[1] It is noted that use of Version 2 of FDS by Brammer is assumed given the date of the research, however this is not stated within the referenced document.

1.2. Objectives of Study

Since the initial work undertaken by Brammer, a number of developments have occurred within FDS as a result of advancements in both the physical insight and computing power requirement necessary for assessment of a fire scenario. It was thus considered desirable to update and extend the research previously undertaken. The objectives of this research are as follows:

- Update and extend the work undertaken by Brammer given the developments in the FDS program since his work
    - Establish base parameter input data as would typically be used by Fire Engineers for the modelling of the subject fire scenarios using FDS.
    - Compare the results of the modelled scenarios to the actual test data, considering high level temperatures and smoke detector activation times.
    - Undertake sensitivity analysis to assess the impact that changes to the input data, specifically effective heat of combustion and soot yield, have on the derived smoke detector activation times, and comparison of these times to that recorded during the experiments.
- Provide recommendations on the derivation of smoke detector activation times as applicable to fire engineers.

1.3. Scope of Study

In this study, three fire tests from the Cardington house fire experiments are considered; CDT16, CDT17 and CDT19. These tests are analysed as they involve flaming fire scenarios and utilise a similar make-up arm-chair(s) as the primary fuel load. The experiments are modelled within FDS for various soot yield (0.04, 0.05 and 0.10kg_{soot}/kg_{fuel}) and effective heat of combustion values (20 and 25MJ/kg). Prediction of the activation time of domestic detectors located throughout the house is undertaken using the temperature approximation method, Heskestad's method and Cleary's

method. The results are then compared to the detector activation times recorded during the experiments. Comparison is also made within Section 6 to the derived activation times by Thomas (2008) for CDT16, and both Thomas (2008) and Brammer (2002) for CDT17.

2. Modelling and Smoke Detection Prediction

2.1. Introduction

There are various ways in which fire conditions and the behaviour of smoke detectors can be modelled and assessed. This chapter provides an overview of the modelling parameters and methods of analysis used within the research undertaken and justification of their applicability to the fire scenarios under consideration. Chapter 3 provides a summary of the subject Cardington tests and Brammer's subsequent research.

2.2. Field Models

Field models are based on computational fluid dynamics (CFD); the process of solving, using numerical methods, governing equations of fluid flows. Although first demonstrated in the 1920's by Lewis Richardson (Richardson 1993), it was not for another fifty years that CFD techniques began to emerge as a general analysis tool for fluid flow problems, including that of combustion (Cox and Kumar 2002). It was then not until as recently as the last two decades that these principles have been applied to the general practices of everyday design and analysis problems tackled by fire engineers. Prior to this, and still adopted today, zone models were utilised for such analysis.

Zone models typically consider a volume to be comprised of two layers; a hot upper layer and a cooler lower layer. Conditions within a layer are isotropic, changing only with time, with the conservation of mass and energy equations applied between the upper and lower layer control volumes. Examples of two zone computer modelling programs include CFAST and BRANZFIRE. In contrast, within a field model, a full partial differential equation set, expressing the principles of local conservation of mass, momentum, energy and species, are solved using numerical methods subject only to the boundary conditions of the problem (McGrattan el at 2009a). This equation set is typically referred to as the field equations. By adopting field models rather than zone models, a number of the underlying assumptions incorporated within zone models that limit the accuracy of an analysis are removed.

The starting point for CFD models is the system of coupled partial differential equations that describe the balance between the competing influences on the transport of mass, momentum, chemical species, and energy within the fire and throughout the enclosure containing it. Large scale turbulence is generated typically on the order of a few metres. Without any further stimulus, the turbulent energy decays resulting in the size of turbulent eddies becoming smaller and smaller. At some point, the size of these eddies will become small enough such that the remaining energy is dissipated by viscous forces. These fine length scales are those at which the fuel/air mixing takes place and chemical reaction occurs. Solving the equations at the length and time scales that occur in the flows associated with the turbulent combustion characteristics of fire is beyond the capabilities of computing powers to date and simplifications of the equations are thus required.

The original work on CFD is virtually all based on the conceptual framework provided by the Reynolds-averaged form of the Navier Stokes equations (RANS) (McGrattan and Forney 2005). These equations are obtained from the Navier Stokes equations through time-averaging and then solving in discretized form over the domain of interest. The terms describing the contributions of turbulent mixing and its influences on chemical kinetics and radiant heat transfer are modelled by various techniques. Typically this has been achieved by use of the k–ε turbulence model, where k is the kinetic energy of the turbulence and ε its rate of dissipation (Cox and Kumar 2002).

An alternative approach to RANS is the application of Large Eddy Simulation (LES) techniques. The basic theory behind this being that the eddies accounting for most of the mixing are large enough to be calculated with reasonable accuracy from the equations of fluid dynamics. Small scale eddy motion is then either crudely accounted for or ignored. The application of LES techniques to fire is aimed at extracting greater temporal and spatial fidelity from simulations of fire performed on a more finely meshed grid as is allowed by faster computers (McGrattan el at 2009a).

An extension of LES is Direct Numerical Simulation (DNS), where the computational grid is fine enough such that all the motion that occurs on a scale influencing the flow field is resolved from the governing equations. No subsequent turbulence modelling is

therefore required. The restriction of DNS in terms of its application to fire engineering is the required grid size for the analysis. Current computational powers make it impossible to solve even a single room scenario on this scale on a standard PC, restricting its application to very small physical domains (Clement 2000).

The simplified combustion equations describing the transport of mass, momentum and energy by fire-induced flows are referred to as the 'low Mach number' equations, developed by Rehm and Baum (McGrattan el at 2009a). Within a CFD model, these equations are solved numerically at each time step for each cell. The accuracy of a simulation is therefore dependent on the grid size within a model space, however as alluded to previously, this also influences the computational power and time required for a simulation. Fire Engineers must therefore determine an acceptable balance between grid size, i.e. accuracy, and computational requirements, dependent on the problem at hand.

2.3. FDS Overview

2.3.1. Overview

FDS is a CFD computer modelling program produced by the National Institute of Standards and Technology (NIST), which is free to download from their website, http://fire.nist.gov/fds/. The companion program Smokeview is a visualisation tool, used to produce images and animations of the results of a simulation. FDS Version One was publicly released in February 2000, with continual upgrades and releases being made as both computational resources and knowledge and understanding of the physical and chemical process of combustion improve over time. Initial simulations undertaken as a component of the research work were modelled using Version 4, however all the results presented within this report are from simulations run using Version 5.3.1, released April 8th 2009.

The major components of the FDS program are summarised as follows:

- *Hydrodynamic Model*: FDS solves numerically a form of the Navier-Stokes equations, appropriate for low-speed, thermally driven flow with an emphasis

on smoke and heat transport from fires. Turbulence is typically treated by means of the Smagorinsky form of LES.

- *Combustion Model*: A mixture fraction combustion model is adopted.

- *Radiation Transport*: Radiation transport is included via the solution of the radiation transport equation for a non-scattering grey gas. The equation is solved using a technique similar to a finite volume method for convective transport.

- *Boundary Conditions*: All solid surfaces are assigned thermal boundary conditions, plus information about their burning behaviour. Heat and mass transfer to and from solid surfaces is handled with empirical correlations.

- *Geometry:* Governing equations are approximated on one or more rectilinear grids. Objects and boundaries for inclusion must conform to the grid, disallowing the use of curves or slopes. Objects that are defined as smaller than a single cell are either approximated as being equal in size to that of one grid cell, or are simply ignored.

2.3.2. Program Limitations

FDS can be used to assess most fire scenarios however, as occurs whenever simplifications of reality are required and assumptions adopted, limitations to the model do exist. Two of the more prominent limitations that are relevant to the research undertaken are:

- *Rectilinear Geometry*: As noted previously, the program adopts a rectilinear grid, which requires curved geometry to be modelled in a step-wise manner and the alignment of objects to the grid. To reduce the errors that result from fluid flow over a jagged surface rather than a smooth surface, FDS does incorporate an inbuilt ‘sawtooth’ algorithm, which prevents vorticity being generated at sharp corners.

- *Simulation Time*: Zone models have the benefit over CFD models in that they do not entail extensive computational power. As the technology of computers rapidly advances this is becoming less of an issue, however, dependent on the number of cells defined within a model space, a simulation may still take a few days to complete on a standard PC. Engineers are therefore typically required to compromise between the required accuracy of a simulation and the length of time available to run it.

One of the more prominent limitations applicable to all modelling programs, not just FDS, is that the output is only as accurate as the input parameters assigned by the user. As stated by Versteeg and Malalasekera (1995),

> '... the results generated are at best as good as the underlying theory of the program and at worst as good as its operator's input.'

2.3.3. Validation

Various versions of FDS have been assessed for its validation for the accurate prediction of smoke detector activation. A number of these are detailed within the Fire Dynamics Simulator (Version 5) Technical Reference Guide Volume 3: Validation (NIST 2009b), including work undertaken by D'Souza, Roby et al, Zhang et al and Cleary. Cleary's work provided comparison between FDS computed gas velocity, temperature and concentrations at various detector locations in a multi-room fire scenario. The research concluded that the model can accurately predict the conditions that a sensor might experience during a real fire event, predicting smoke and gas concentrations, heat, and flow velocities at the detector locations, to within 15% of measurements (NIST 2009a).

2.4. Smoke Detector Activation Prediction

2.4.1. Ionisation and Photoelectric Smoke Detectors

Smoke detectors are fundamentally based on the mechanism of detecting changes to surrounding environmental properties caused by the fluid-mechanical transport of combustion products from a fire (Heskestad 1975). Ionisation and photoelectric smoke

detectors are the two most common detector types installed in residential buildings. Both are considered to be products of combustion detectors, yet operate on two fundamentally different physical principles.

- *Ionisation Detectors*: An ionisation detector typically consists of two chambers. The first, a sensing chamber that is open to the atmosphere in order to be able to sense aerosols and vapours. Secondly, a sealed chamber, not permitting the entry of smoke, that is connected electronically in series with the first. When a small current is allowed to flow through the two chambers, a voltage divider forms across the supply. This current is defined by a small radioactive source (an alpha emitter) that ionises the oxygen and nitrogen molecules present in the air within the sensing chamber. The ionisation of the molecules in the air permits the current flow between the two charged electrodes giving the sensing chamber an effective electrical conductance. Combustion products, upon entering the sensing chamber, are able to attach themselves to the ionised molecules, slowing their movement due to their increase in mass. The drop in current flow corresponds to a proportional drop in the voltage, which is sensed by the detector (Buchanan ed 2001). Activation of the detector occurs once the voltage drops below the inbuilt threshold.

  The signal produced by an ionisation chamber is known to be proportional to the number of smoke particles and their size, present in a detectors sensing chamber. As a result, ionisation detectors tend to provide a somewhat faster response to high energy (open flaming) fires, which are known to produce a larger number of smaller smoke particles (Farouk et al 2001).

- *Photoelectric Detectors:* Two types of photoelectric smoke detectors exist; scattering and extinction. This report focuses on the scattering model. Activation of scattering photoelectric type smoke detectors[2], is based on the principal of light scatter by smoke particles migrating into the sensing

[2] Scattering photoelectric type smoke detectors are noted as simply being referred to as photoelectric detectors for the remainder of this report.

chamber. Photoelectric detectors consist of a light source and a photoelectric device arranged in such a manner that the light rays do not normally fall onto the device. The amount of light reaching the receiver is increased by being either reflected or refracted by smoke particles. The total of these two effects is referred to as scattering. The detector is designed to activate when sufficient light is scattered onto the photosensitive device, i.e. when the responsive optical density threshold is met.

In contrast to ionisation detectors, a photoelectric detector's signal is proportional to the mass concentration of particles present. Photoelectric detectors respond to the volume (mass) density of smoke particles, unlike ionisation detectors, which are more affected by the number density (Farouk et al 2001). This method of detection favours lighter coloured and larger diameter particles, characteristics tending to be associated with smouldering fires. The darker carbon particles associated with flaming fires tend to absorb a greater proportion of the incident light, reducing the amount that reaches the receiver, and thus photoelectric detectors are not as effective in this instance.

2.4.2. Prediction Algorithm Overview

To date there are no direct methods for modelling the response of spot type ionisation or photoelectric smoke detectors. As has been noted, their activation is influenced by a large number of factors which themselves consist of a number of variables that are influenced by the composition of the combustion fuel, the combustion state and the degree of vitiation within the fire environment.

In the event that information on the environmental conditions is obtainable, a direct prediction method is still not available for use by engineers. The design of smoke detectors often incorporates complex response algorithms rather than simple threshold rate of change response levels. The purpose of this is to attempt to reduce the occurrence of false alarms and to enhance fire signature matching. The response algorithms vary between detectors and are generally not published. These different principles of operation of the various types of smoke detectors and their different

responses to various forms of smoke, makes it difficult to provide one universal approach for accurate detector modelling.

The other difficulty that exists in modelling the response of smoke detectors is that fire models and undertaken experiments tend to not provide data on the factors that are required. Optical density, or obscuration per unit length, tends to be the only data reported that relates to smoke, however only one commercial smoke detector currently operates on this basis, the projected beam type detector (Schifiliti 2001). Without a correlation between optical density and a particular detector's response characteristics, accurate modelling is not possible.

Within the research presented three smoke detector prediction methods are considered:

- Temperature correlation method
- Heskestad method
- Cleary method

Historically, the temperature correlation is the most common method adopted, as well as being the most frequently cited method for prediction of smoke detector activation times in fire safety engineering literature (Shifiliti et al 2002). This is primarily due to the inherent simplicity of the model and its ease of use. With recent improvements in the technology enabling the production of modern zone and field models, the use of Heskestad's method, requiring the derivation of optical density, is however gradually increasing. The International Fire Engineering Guidelines (ABCB 2005), when discussing the merits of a temperature based approach in comparison to an optical density based approach states that

> '... the temperature equivalent approach is rather empirical. Since temperature rise and smoke concentration do not always correlate well, this approach is not preferred.'

The underlying theory of each of these prediction methods are summarised in the following sections of this report.

2.4.3. Temperature Correlation Method

The temperature correlation method is seen as the simplest of the three prediction methods being discussed. The approach, originally proposed by Heskestad and Delichatsois in the late 1970's, is based on the temperature approximation theory for estimation of optical density. In short, the model assumes that a smoke detector will activate when the surrounding gas temperature rises a certain amount above ambient, ΔT_r; Equation 1.

$$T_{act} = T_{amb} + \Delta T_r \qquad \text{[Equation 1]}$$

The temperature approximation theory hypothesizes that the mass concentration of smoke particles at a point is proportional to the change in temperature at that point, due to a fire. This theory is based on four main assumptions:

- Particle size distribution is constant in both time and space.
- Mass generation rate is proportional to the mass burning rate.
- No heat transfer occurs between particles or between particles and confining surfaces, and
- Smoke does not continue to react as it travels.

Heskestad and Delichatsois carried out a number of experiments, examining the obscuration and temperature rise at various locations on a ceiling for different fuel types. For polyurethane, the experiments resulted in a range in values of 0.002 to 0.005 for the ratio of optical density to change in temperature; $D_u/\Delta T$.

From the results of the experiments, Heskestad and Delichatsois concluded that, whilst some variation existed in time at different radial positions, the optical density to temperature rise ratio could be approximated as a constant for a particular fuel and burning mode. It was further concluded that as every detector model will respond differently to optical density for each fuel type, the ratio could be used to estimate the temperature rise required for a particular fuel to alarm a given detector; Equation 2.

$$\Delta T_r = D_{ur} \frac{\Delta T}{D_u} \qquad \text{[Equation 2]}$$

Researchers have since concluded that the variations Heskestad and Delichatsois found in their experimental data was the result of slowly changing characteristics of smoke particles as they left the fire source and traveled in the plume and ceiling jet away from the point of origin, i.e. ageing effects. With this knowledge, there is a consensus amongst researchers that the concluded constant value for the ratio of $D_u/\Delta T$ is an acceptable rough approximation. Bjorkman however, is noted to have reported values for polyurethane approximately half that derived by Heskestad and Delichatsois (Shifiliti 2001).

In order to accurately apply the temperature correlation method, one would be required to know the optical density to temperature rise ratio for the burning fuel in question, in addition to the optical density at response for that particular detector. This data can be found within various reference sources for a number of fuel and burning mode combinations, however given no two fire signatures are identical, a significant amount of experimental research is still required in order for a comprehensive list to be formulated. Table 1 states some values of rise in temperature required for smoke detector activation, as derived by Heskestad and Delichatsois during their experiments, for various fuel types (Mowrer and Friedman 1999). The results listed are noted as being applicable to a flaming fire scenario.

Material	**ΔT_r**	
	Ionization	**Photoelectric**
Wood	25	75
Polyurethane	13	13
Cotton	3	50
PVC	13	13
Average	14	38

Table 1 Temperature Rise Required for Smoke Detector Activation (Mowrer and Friedman 1999)

In practice, a generic value is typically adopted for the rise in temperature above ambient necessary for detector activation. Initially, this was generally accepted as being approximately 13ºC; ΔT_r = 13ºC. Table 2 provides a list of various temperature rise values that have been published since the work undertaken by Heskestad and Delichatsois. These values were generally derived from experimental procedures

undertaken in test facilities with a ceiling height of 2.4m, typical of a residential dwelling.

Reference	ΔT_r (ºC)
SFPE (chapt 4-1) [3]	13
United Kingdom Fire Safety Engineering Guide[3]	13
Australian Fire Safety Engineering Guide[3]	13
New Zealand Fire Safety Engineering Guide[3]	4 – 5
Nordic Guide[3]	20
Heskestad and Delichatsios[3]	13
CFAST Default value[4]	13
International Fire Engineering Guidelines[5]	13
Collier[6]	2 – 4
Davis and Notarianni[7]	5

Table 2 Recommended Temperature Rise for Determination of Smoke Detector Activation

As highlighted in Table 2, recent research has indicated that a more appropriate value to adopt for the temperature rise is 4ºC or 5ºC. This has been hypothesized to be a result of the significant improvements that have occurred in sensor technology over the years. It is however generally considered that further research is required in this field prior to a change from 13ºC to 4ºC is accepted across the board (Bukowski and Averill 1998)

2.4.4. Heskestad Method

In 1975, Heskestad (1975) proposed 'a simple model for detector response' based on optical density. The fundamental theory of the model adopts the following assumptions:

- Velocity of the convective gas flow near a detector is constant.
- Rate of rise of particle mass concentration, or rate of rise of optical density is constant with time.

[3] Bukowski and Averill 1998

[4] NIST 2009

[5] ABCB 2005

[6] 1996

[7] 1996

- Optical density is proportional to the particle mass concentration for given particle properties, size distribution, and emission spectrum of light source.

- The Reynolds number associated with entry flow into a detector is high enough so that viscosity can be neglected in a first approximation.

- Within the time associated with a detectors response, the temperature of the gas near that detector has not changed appreciably from ambient (otherwise one must consider buoyancy effects).

A point type smoke detector has partially permeable walls separating the gas volume inside the detector from the volume surrounding it. These walls consist mostly of mesh or perforated plates. The sensing region of a detector is encased for various reasons, including eliminating stray light in photoelectric heads, to keep out insects etc and to protect the sensing element from damage. This provision delays fire detection in comparison to a fully open detector as there will always be a time lag between the conditions within the sensing chamber equalling that of the outside environment, as the smoke must first flow through the baffles, into the chamber.

Unlike the temperature correlation, Heskestad accounted for this delay time within his proposed detector prediction algorithm through the inclusion of a time constant, often referred to as the characteristic lag time. The optical density within a detector is thus derived in accordance with Equation 3.

$$\frac{dD_{ui}}{dt} = \frac{1}{\tau}\left(D_u - D_{ui}\right) \qquad \text{[Equation 3]}$$

As stated previously, an assumption of Heskestad's model is that the time constant and rate of change of optical density with respect to time, is constant, thus enabling Equation 3 to be solved. Substituting D_{ur} for the optical density outside the detector at response and D_{uo} for the optical density required inside the detector to produce response, the solved equation can be written as:

$$D_{ur} = D_{uo} + \tau\left(\frac{dD_u}{dt}\right)\left\{1 - \exp\left[-D_{ur}\frac{1}{\tau}\left(\frac{dD_u}{dt}\right)\right]\right\} \qquad \text{[Equation 4]}$$

Heskestad proposed that the time constant could be represented as shown in Equation 5 or more commonly as in Equation 6.

$$\tau = \frac{\gamma l}{u} \qquad \text{[Equation 5]}$$

$$\tau = \frac{L}{u} \qquad \text{[Equation 6]}$$

Substituting Equation 6 into Equation 4, Equation 7 is derived.

$$D_{ur} = D_{uo} + \frac{L}{u}\left(\frac{dD_u}{dt}\right)\left\{1 - \exp\left[-D_{ur}\frac{u}{L}\left(\frac{dD_u}{dt}\right)\right]\right\} \qquad \text{[Equation 7]}$$

Due to different detector geometries, all detector models have a specific characteristic length. One of the problems associated with Heskestad's method is that characteristic length is not a value manufacturers are required to supply and no single generic value can be adopted with great accuracy for all detector types. Various research has been undertaken in this field and a wide variety of values published, as reproduced in Table 3. It is noted that the default value within FDS (2009) for characteristic length is 1.8m.

Source/Researcher	L (m)	
	Ionization	Photoelectric
VTT, Finland[8]	1 -2 (all)	
Heskestad[8]	1 – 8	15
Bjorkman et al[8]	3.2 +/- 0.2	5.3 +/- 2.7
Bjorkman et al[9]	10 (all)	
Marrion[9]	-	7.2, 11-13, 18.4
Oldweiler[9]	4 – 9.5, 4.3 – 14.2	-
Schifihiti[10]	1.8 – 9.5	5.3 – 13.0
Bukwoski et al[10]	1 – 2 (all)	

Table 3 Characteristic Length

2.4.5. Cleary Method

Research, such as that undertaken by Brozovsky (Beyler 1984), suggests that the characteristic length at low smoke velocities may be a function of smoke momentum.

[8] Bjorkman et al 2001

[9] Bjorkman et al 1992

[10] Cleary et al 2000

It is hypothesized that there exists a critical ceiling jet velocity, below which smoke cannot reach the sensing chamber in sufficient quantities to trigger an alarm, even when the optical density outside the detector exceeds the alarm threshold. Bjorkman et al (1992) found that by decreasing the flow velocity below 0.2m/s, smoke density at response rises much faster than inversely proportional to the flow velocity. Brozovsky's experimental data was found to fit an exponential curve at values of velocity less than 0.13m/s.

It is postulated that this sway from the linear trend at lower flow velocities occurs as the influence of viscous effects on the flow resistance increases and becomes more significant. Often the early stage of a fire produces only a weak plume where transport of smoke is slow and the air velocity adjacent to a detector can be very low. This smouldering period has the possibility of continuing for a considerable length of time before conditions build up enough for flaming combustion to begin. It is important that engineers are aware of these conditions and are able to account for them in their analysis.

Clearly et al (Beyler 1984) undertook research to develop a prediction algorithm that incorporated this low-velocity anomaly. Heskestad's prediction algorithm models the time lag between conditions outside a detector and inside a detector as a first order response, with characteristic time proportional to the inverse of velocity; Equation 5 and Equation 6. Cleary et al proposed that a two-parameter model is more appropriate; the two parameters being a dwell time and a characteristic mixing time, or otherwise referred to as a characteristic filling time of the overall detector and a characteristic filling time of the sensing chamber (Cleary et al 2000).

Given that δt_e is the characteristic filling time of the entire volume enclosed by the external housing and δt_c the characteristic filling time of the sensing chamber, Clearly et al (2000) suggested that each characteristic filling time is a function of the free stream velocity outside the detector. The α and β variables within Equation 8 and Equation 9 are empirical constants related to the specific detector geometry.

$$\delta t_e = \alpha_e u^{\beta_e} \qquad \text{[Equation 8]}$$

$$\delta t_c = \alpha_c u^{\beta_c} \qquad \text{[Equation 9]}$$

The change in the mass fraction of smoke in a sensing chamber, $Y_{c,}$ is found by solving Equation 10, where Y_e is the mass fraction of smoke outside of the detector in the free stream.

$$\frac{dY_c}{dt} = \frac{Y_e\left(t - \delta t_e\right) - Y_c\left(t\right)}{\delta t_c} \qquad \text{[Equation 10]}$$

Assuming that the gas velocity external to the detector is constant and that there is no smoke within the detector's sensing chamber at time zero, the mass fraction of smoke at any time can be derived by integrating Equation 10.

Cleary et al (2000) found that at an air velocity greater than 0.5m/s, the dwell time drops below 10s and the mixing time is essentially zero, corresponding with Heskestad's single parameter model. Thus by defining α_e as zero, β_e and β_c as one, the prediction algorithm is equivalent to Heskestad's algorithm, with α_c equivalent to characteristic length.

It is noted that these above findings are accounted for in Heskestad's model through one of the assumptions adopted. Heskestad assumed that the Reynolds number associated with entry flow into a detector is high enough so that viscosity can be neglected in a first approximation; Reynolds number being a function of gas flow velocity.

2.5. Soot Yield

Smoke aerosols vary widely in both appearance and structure, with no two fires having the exact same smoke particle characteristics. Fuel composition, combustion state, i.e. flaming, pyrolysis and smouldering, and the degree of vitiation, all affect the amount and characteristics of the smoke particles produced during a fire. The soot yield during a fire is thus going to vary as different fuels ignite and ventilation conditions change. The soot yield within an enclosed fire scenario is also therefore likely to vary from that in a bench-scale experiment, where an identical fuel source is being compared. Mulholland (2002) provides a number of soot yield values, referred to as 'smoke

conversion factors' for various fuel type under both flaming and pyrolysis conditions. Some of this information is reproduced in Table 4.

Source	Soot Yield	Combustion Conditions
	(kg_{soot}/kg_{fuel})	
Polyurethane (flexible)	0.07 – 0.15	Pyrolysis
Polyurethane (flexible)	<0.01 – 0.035	Flaming
Polyurethane (flexible)	0.06 – 0.19	Pyrolysis
Polyurethane (flexible)	0.09	Flaming

Table 4 Soot Yield Vales [Mulholland 2002]

Robbins and Wade (2007) undertook research with the objective of making a recommendation on an appropriate smoke yield to be included in design fire specifications, to be published by the New Zealand Department of Building and Housing. As a component of their published report, they provide a summary of published and proposed average smoke yield values for flaming combustion of combinations of materials, natural materials and solid and foamed synthetics. Those values of relevance to the subject research are reproduced in Table 5 and Table 6.

Description	Pre-Flashover Soot Yield Value	Reference
	[kg_{soot}/kg_{fuel}]	
Using whole data set for mattress and upholstered furniture 95th percentile 99th percentile	 0.097 0.030	From analysis of data from CBUF (1995)
Using data set without outlier for mattress and upholstered furniture 95th percentile 99th percentile	 0.073 0.96	From analysis of data from CBUF (1995)

Table 5 Summary of published and proposed average smoke yield values associated with flaming combustion of combinations of materials [Robbins and Wade 2007]

The work undertaken involved the modelling of a real test fire scenario within FDS and BRANZFIRE to enable a comparison of the optical density results derived to that recorded during experiments. The scope of the study was a small single-storey residential occupancy, in which a flaming upholstered armchair fire was initiated within the living room. Models of the fire scenario considered soot yields ranging from $0.05kg_{soot}/kg_{fuel}$ to $0.20kg_{soot}/kg_{fuel}$.

Description	Pre-Flashover Soot Yield Value	Reference
	[kg_{soot}/kg_{fuel}]	
Polyurethane	0.230	Karlsson and Quintiere 2000
Polyurethane flexible foam	0.131 – 0.227	Tewarson 1988
Polyurethane rigid foam	0.104 – 0.130	Tewarson 1988
100% polyamide	0.052	Wade 2001
Nylon	0.04	Wade 2001
Nylon	0.075	Karlsson and Quintiere 2000
PMMA	0.022	Karlsson and Quintiere 2000; Guillaume 2006
Polyethylene foam	0.056 – 0.102	Guillaume 2006

Table 6 Summary of published and proposed average smoke yield values associated with flaming combustion of synthetic solids and foams [Robbins and Wade 2007]

The results of the modelling found that near to the fire, at 20mm below the ceiling, a soot yield of $0.10kg_{soot}/kg_{fuel}$ predicts conservative optical density in good agreement with that reported for the thermocouple locations closest to the fire. A soot yield of $0.05kg_{soot}/kg_{fuel}$ predicts conservative optical density in good agreement with that reported within the room of fire origin, but at a greater distance from the fire. At 900mm below the ceiling, optical density was found to be consistently over predicted within the room of fire origin for all soot yields, however as the distance from the fire increased the predicted soot yield values provided a closer approximation.

For rooms adjacent to and remote from the fire, a soot yield of $0.05kg_{soot}/kg_{fuel}$ predicted optical density to be in reasonable agreement with experimental values 20mm below the ceiling. At 900mm below, optical density is again found to be generally over-predicted.

It was recommended from the results of the study that for scenarios similar to that considered, a 'design fire value for soot/smoke yield derived from optical measurements taken during flaming combustion of full sized items of upholstered furniture' should be selected, with the upper 95^{th} percentile value of 24 items (with outlier removed) of upholstered furniture considered within the research $0.07kg_{soot}/kg_{fuel}$. It is noted that both Thomas (2008) and Brammer (2002) defined soot

yield to be 0.10kg_{soot}/kg_{fuel}, however Brammer's analysis was seen to significantly over predict the optical density throughout the house.

2.6. Effective Heat of Combustion

As referenced in Brammer (2002), Girgis undertook experimental research deriving the effective heat of combustion for a number of lounge chairs to be typically 30-38MJ/kg. The primary fuel source within the fire scenarios, as detailed in Section 3, are upholstered armchairs, consisting of combustion modified polyether foam and cotton covering. Tewarson (2002) presents effective heat of combustion values for polyurethane, as provided in Table 7.

Material	Effective Heat of Combustion
	(MJ/kg)
Polyurethane (GM21)	26.2
Polyurethane (GM21)	27.2
Polyurethane (GM21)	24.6
Polyurethane (GM21)	23.2

Table 7 Polyurethane Effective Heat of Combustion Values as Published by Tewarson (2002)

Table C.3 within The SFPE Handbook of Fire Protection Engineering (NFPA 2002) states both gross and net effective heat of combustion values for polyurethane, as provided in Table 8.

Material	Gross Effective Heat of Combustion	Net Effective Heat of Combustion
	(MJ/kg)	(MJ/kg)
Polyurethane	23.90	22.70
Polyurethane – foam	26.1 – 31.6	23.2 – 28.0
Polyurethane – foam, FR	24.0 – 25.0	-

Table 8 Polyurethane Effective Heat of Combustion Values as Published by NFPA (2002)

It is noted that Thomas (2008) defined the effective heat of combustion to be 20MJ/kg within his research and Brammer 30MJ/kg.

3. Cardington Full Scale Fire Tests and Brammer Research

3.1. Introduction

The Fire Research Station (FRS) conducted a series of ten full-scale fire tests in a typical 1970's UK three bedroom dwelling to examine the relationship between fuel load, ventilation, detection and hazard development in realistic domestic fire scenarios. These tests, CDT14 – CDT23, were part of a series of tests undertaken, often referred to as the Cardington House tests, and have been the topic of a number of papers, including Purser et al (1995), Spearpoint (1996), Purser et al (1998), Brammer (2002) and Thomas (2008).

The tests involved the burning of upholstered furniture of similar design but varying combinations of fabrics and foam. In all experiments the upholstered furniture acting as the fuel source was located within the lounge. Spearpoint (1996) noted that all furniture complied with the UK regulations at the time with regards to ignition and combustion characteristics of the foam filling and covering materials.

The work undertaken by Brammer, as detailed in Section 3.5, analysed experiments CDT17 and CDT20. The research detailed within this report considers CDT16, CDT17 and CDT19; the armchairs used as fuel load in these simulations all being of similar composition, a combustion modified high-resilience (CMHR) foam with fire retardant (FR) cotton cover.

It is noted that CDT14 and CDT15 were both smouldering fires rather than flaming fires and CDT18 used a fire retardant dralon cover in lieu of a cotton cover. CDT21, CDT 22 and CDT23 were also flaming fire scenarios, however included additional fuel loads within the lounge and also additional ventilation provisions via the lounge chimney flue. In all other experiments undertaken the chimney flue is noted as being blocked up.

3.2. Experimental Test Set Up

The experiments were undertaken at the Building Research Establishment (BRE) laboratory in Cardington. The construction and layout of the house was designed to be representative of typical domestic two storey, three bedroom dwellings in the United Kingdom in the 1970's. The ground floor comprised of an entry hall, kitchen, lounge and dining room, whilst the first floor housed the stairway landing, three bedrooms and a bathroom. Some variances do exist between reference papers (Purser et al 1998, Spearpoint 2006) as to the exact layout of the house with regards to internal wall locations and instrumentation positions, however the information provided is comparable. The layout of the building as defined within this research, following that presented by Spearpoint (1996) and Brammer (2002), is shown in Figure 1 and Figure 2.

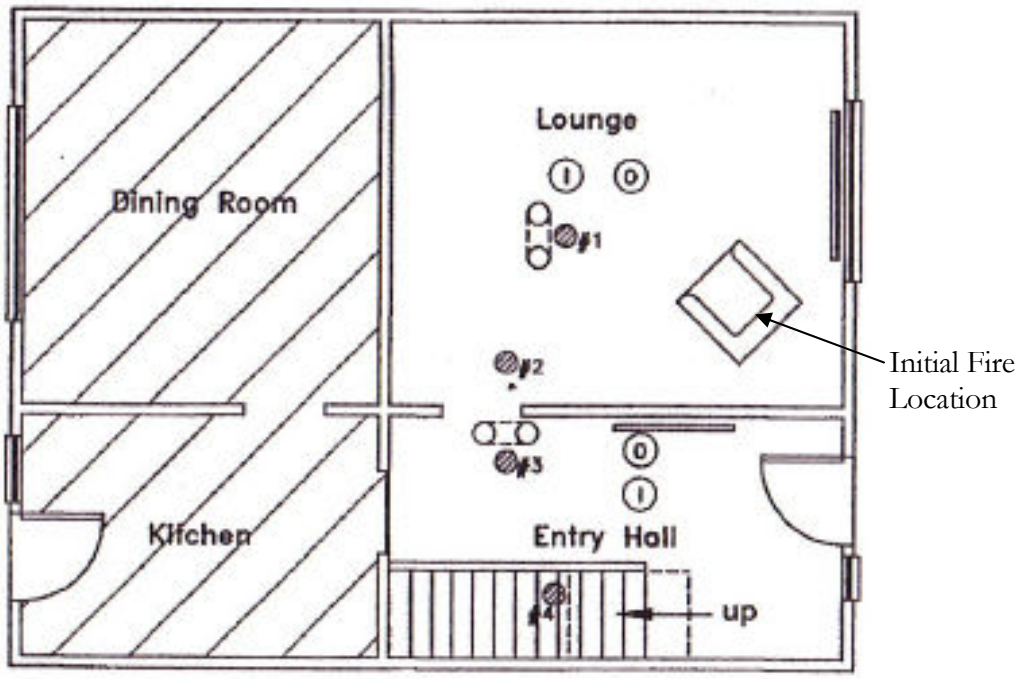

Figure 1 Ground Floor Layout

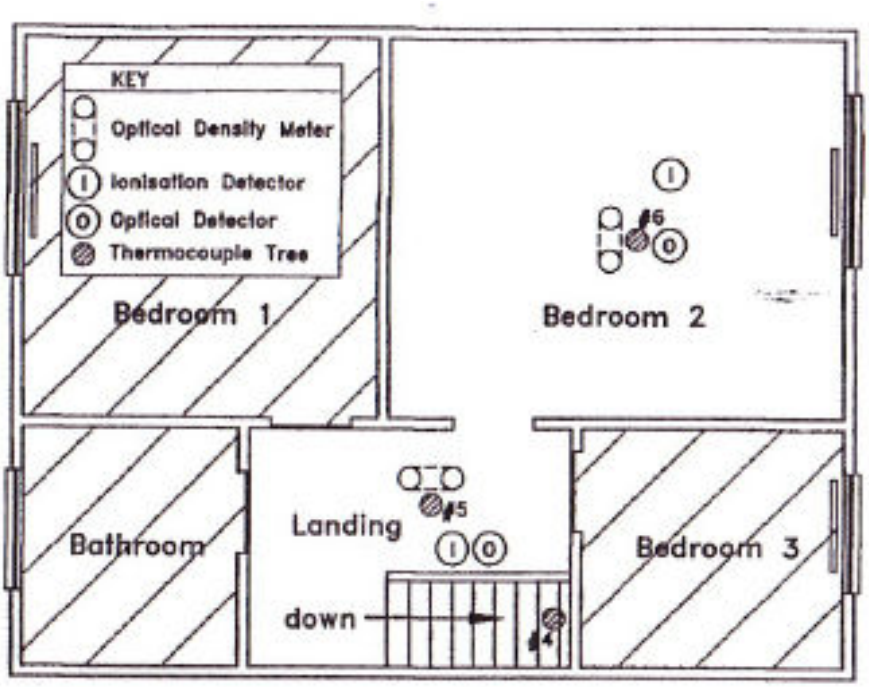

Figure 2 First Floor Layout

During the subject experiments, the dining room, kitchen, two bedrooms (bedroom 1 and bedroom3) and bathroom were sealed off from the remainder of the house. Supported by the research undertaken by Brammer (2002), and shown shaded in Figure 1 and Figure 2, these areas are thus not considered within the work undertaken. The internal door to bedroom 2[11] was fully open in all three experiments and the door to the lounge fully open in CDT 17 and CDT19, but closed in CDT16.

To simulate typical winter conditions, all external doors and windows were closed with the windows in the fire room being of wired glass to prevent failure. Several radiators were in operation prior to the commencement of the tests, these being electrically powered oil-filled domestic models. The radiators were located within the lounge, entry hall and in each of the three bedrooms. Within the lounge the radiator had an output of 2kW, 1.5kW in the hall and 1kW in bedroom 2. The radiators where turned on and left to run for some time prior to the commencement of the tests in order to allow the resulting convectional air currents to establish throughout the house. Prior to ignition of the fire in each experiment the lounge radiator was turned off and removed.

[11] As bedroom1 and 3 are not considered within the analysis, where comment is provided to 'the bedroom' within this report, this infers reference to bedroom 2.

3.3. Instrumentation & Data Collection

Various instruments were installed throughout the house for monitoring environmental conditions. Typically this instrumentation was provided such that the time at which conditions become untenable could be determined. Such instrumentation includes gas analysers (carbon monoxide, carbon dioxide and oxygen), grab vessels for comprehensive gas sampling and thermal radiometers. Also present where domestic and commercial smoke detectors, optical density meters, thermocouple trees and a load cell. It is noted that the research undertaken is concerned with the domestic rather than commercial detectors. The upholstered furniture provided as the primary fuel source was located on the load cell within the lounge for recording of its change in mass during the combustion process.

Two types of smoke alarms were used within the experiments; photoelectric type (model EI 105C) and an ionisation type (model EI 100C). In the tests described within this report the models installed were manufactured by E.I. Company Ltd and were purchased off the shelf from a local DIY store. These detectors are stated as being compliant with BS 5446 (BSI 1990), the British Standard relating to components of automatic fire alarm systems for residential premises (Spearpoint 1996). The detectors were installed in pairs within the lounge, hall, landing and bedroom, so that a photoelectric type and ionisation type detector was present in each location.

Temperature thermocouple trees were located in the hall, stairway, landing, bedrooms and two trees within the lounge. Each tree comprised of eight thermocouples, positioned at varying heights above floor level. Table 9 states the locations of these thermocouples and other recording instruments present. Their locations are also noted as being indicated on Figure 1 and Figure 2.

Instrument	Room Location	Position (x,y)	Position Above Floor Level (z)
		[m]	[m]
Ionisation Smoke Detectors	Lounge	(5.8, 4.7)	2.3
	Entry Hall	(5.9,1.6)	2.3
	Landing	(3.8, 1.2)	4.9
	Bedroom 2	(6.1, 4.6)	4.9
Photoelectric smoke detectors	Lounge	(5.3, 4.7)	2.3
	Entry Hall	(5.0, 2.0)	2.3
	Landing	(4.1, 1.2)	4.9
	Bedroom 2	(6.1, 4.0)	4.9
Optical density meters	Lounge	(5.2, 3.9)	0.5, 1.5
	Entry Hall	(4.7, 2.2)	0.5, 1.0, 1.5
	Landing	(3.6, 1.7)	3.1, 4.1
	Bedroom 2	(6.0, 4.1)	3.1, 4.1
Temperature thermocouple trees	Lounge*2	(5.2, 3.9) (4.3, 3.2)	0.1, 0.4, 0.7, 1.0, 1.4, 1.7, 2.0, 2.3
	Entry Hall	(4.7, 2.2)	0.1, 0.4, 0.7, 1.0, 1.4, 1.7, 2.0, 2.3
	Stairway	(5.3, 0.7)	0.9, 1.3, 1.6, 1.9, 2.2, 2.6, 2.9, 3.2
	Landing	(3.6, 1.7)	2.7, 3.0, 3.3, 3.7, 4.0, 4.3, 4.6, 4.9
	Bedroom 2	(6.0, 4.1)	2.7, 3.0, 3.3, 3.7, 4.0, 4.3, 4.6, 4.9

Table 9 Instrumentation Locations

3.4. Description of Tests

3.4.1. General

The fire in each experiment was initiated through the use of a number 7 crib positioned on the seat of the upholstered furniture. The crib was ignited with an electrical igniter and match head.

The following sections provide a summary of each of the tests considered within this report, as observed by Spearpoint (1996). The times of detector activation for each scenario is also stated.

3.4.2. CDT16

CDT16 involved the ignition of a fire on a single wooden framed armchair within the lounge. In this experiment the door between the lounge and the entry hall was closed, limiting the ventilation available for the combustion process. The chair consisted of CMHR foam with a FR cotton cover.

Spearpoint (1996) describes the test as follows:

'At 70 seconds (1:10) after the crib was ignited smoke was visible from the fire. The fire spread to the back cushion and at 150 seconds (2:30) flames had reached the top. Visibility began to deteriorate rapidly in the lounge at around 240 seconds (4:00). Twenty seconds later only the flames could be seen in the lounge whilst the first signs of smoke in the hall and rising up the stairwell were observed. The smoke in the hall and on the landing became more dense between 300 seconds (5:00) and 465 seconds (7:45) reducing the visibility during which time the temperature in the lounge began to decrease suggesting that the fire had ceased. At 620 seconds (10:20) a rise in the lounge temperature was recorded indicating that the fire may have started again. Visibility in the hall and on the landing became its worst at around 660s (11:00). Thereafter, visibility gradually improved and the test was terminated at 8,400 seconds (2:20:00).'

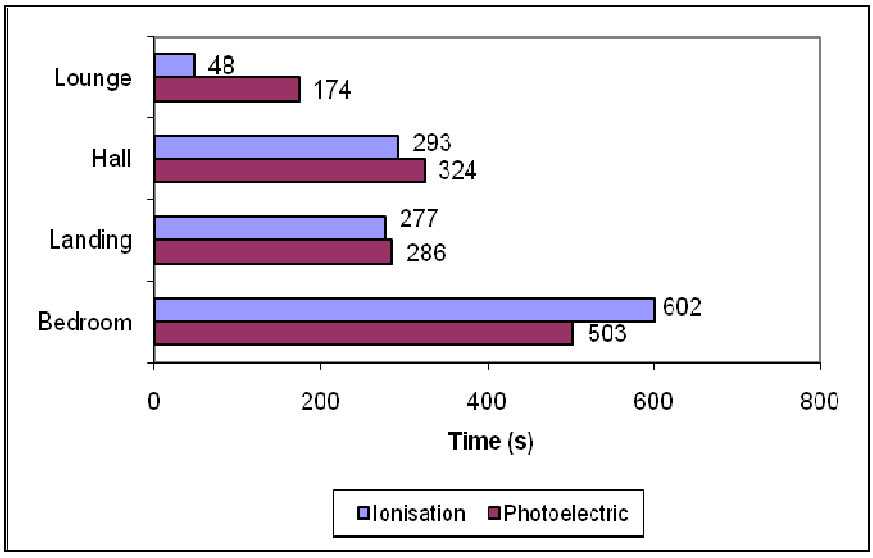

Figure 3 CDT16 Smoke Detector Activation Times: Test Data

The response times of the domestic smoke detectors are provided in Figure 3. The detectors on the First floor landing are noted as activating prior to those within the Hall at Ground level. It is also noted that there is a significant difference between the activation times for the ionisation and photoelectric detectors within the lounge. This is in accordance with the information provided by Spearpoint (1996), where the initial stages of the fire is assumed to only involve flaming combustion of the wooden crib. The photoelectric detector is not seen to activate until the fire has spread to the back of the couch and visible smoke is seen to be produced as a component of the combustion process.

3.4.3. CDT17

CDT17 involved the ignition of a fire on a wooden framed armchair within the lounge, also constructed of CMHR foam and FR cotton cover. The lounge door was open within this experiment, with the additional ventilation to the room of fire origin, allowing a greater degree of combustion of the armchair to occur, which results in a recorded mass loss of approximately 5.4kg in comparison to 3.5kg in CDT16.

Spearpoint (1996) describes the test as follows:

> 'At 99 seconds (1:39) the fire from the crib had spread to the back cushion of the chair. The fire spread over the back cushion and at 193 seconds (3:13) the first signs of smoke rising up the stairwell were observed. At 220 seconds (3:40) grey/brown smoke could be seen around the top of the kitchen door and the smoke rising up the stairwell was becoming more dense. At around 260 seconds (4:20) hazy smoke could be seen in the hall and on the landing. By 278 seconds (4:38) half of the back of the chair was alight and visibility on the landing was beginning to deteriorate. Total smoke obscuration occurred in the hall and landing at 336 seconds (5:36).'

The response times of the domestic smoke detectors are provided in Figure 4. As with CDT16, the landing ionisation detector activated before the hall ionisation detector and similarly for the photoelectric detectors.

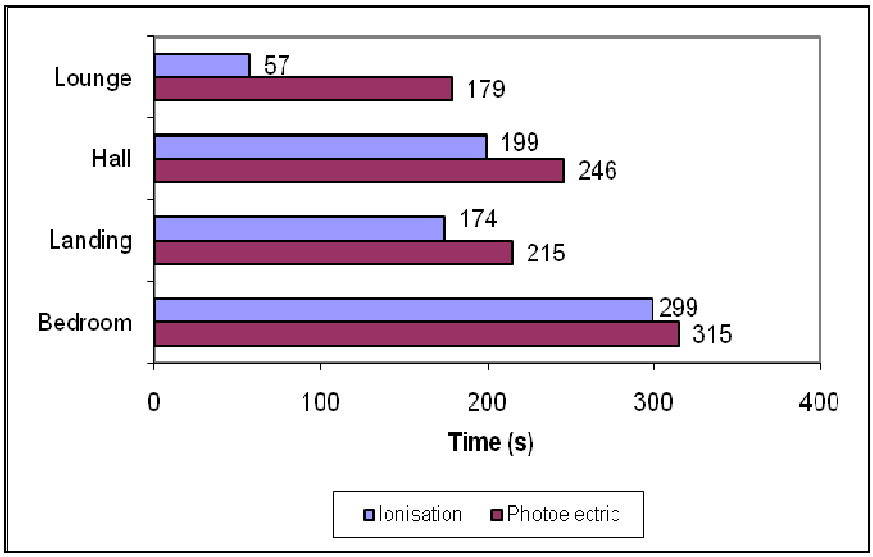

Figure 4 CDT17 Smoke Detector Activation Times: Test Data

There is again seen to be a large difference between the activation of the lounge ionisation and photoelectric detectors, with the photoelectric detector activating approximately two minutes later. As with CDT16, the lounge photoelectric detector does not activate until after it has been observed that the fire has spread to the back cushion of the couch.

3.4.4. CDT19

CDT19 involved the combustion of two chairs, each being of the same construction as those present in CDT16 and CDT17, i.e. CMHR foam and FR cotton cover. The chairs were positioned on the load cell adjacent to each other, and the lounge door was fully open during the experiment.

Spearpoint (1996) describes the test as follows:

> 'At 137 seconds (2:17) smoke was observed as the foam began to ignite and 10 seconds later the first signs of smoke rising up the stairwell were noted. The growth of the fire began to accelerate at 167 seconds (2:47) and flames were above the back of the chair. The volume of smoke rising up the stairwell increased at 207 seconds (3:27) and the landing started to become hazy. The smoke layer in the lounge had become lower than the top of the window at 217 seconds (3:37). At 227 seconds (3:47) the hall had started to become hazy and the visibility on the landing reduced such that the bedroom doors could not be seen from the upstairs camera. By 252 seconds (4:12) the front door to the house could not be seen from the landing and at 257 seconds (4:17) the lounge door was not visible from the hall. The fire had continued to grow and flames were within the smoke layer in the lounge. Visibility in the hall and landing deteriorated between 277 seconds (4:37) and 297 seconds (4:57) until it was no longer possible to see objects within these areas. At 327 seconds (5:27) the window in the lounge could not be seen and 20 seconds later the flames disappeared from the view. The test was terminated at (52:00).'

The response times of the domestic smoke detectors are provided in Figure 5. As in CDT16 and CDT17, the landing ionisation detector activated before the hall ionisation detector and similarly for the photoelectric detectors. The large difference between the activation of the lounge ionisation and photoelectric detectors is also again present, however in this instance the photoelectric detector activation prior to spread of the fire to the back of the chair.

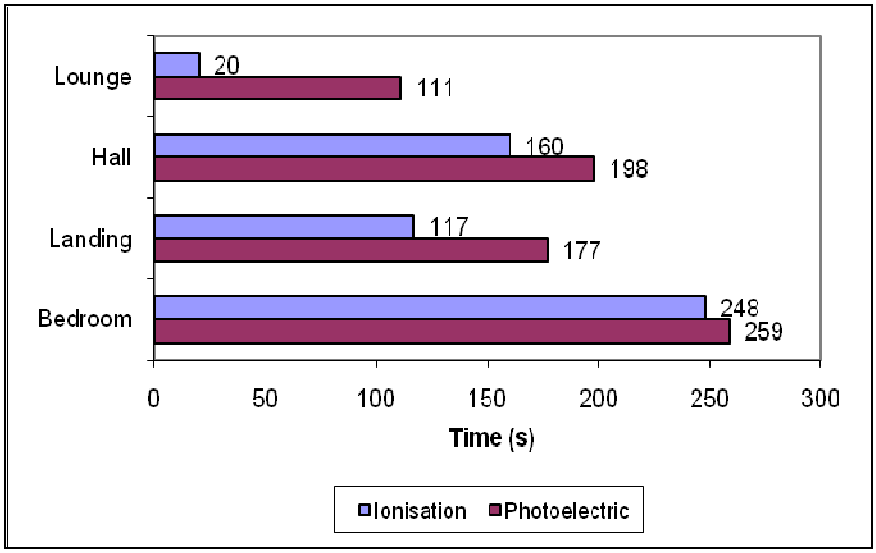

Figure 5 CDT19 Smoke Detection Activation Times

3.5. Brammer Research

3.5.1. Research Overview

Brammer's (2002) research had four objectives:

- Create an effective analysis model for the test house, placing emphasis on temperature and optical density.
- Investigate the effects of the physical features of the house.
- Compare the predicted with the actual test behaviour.
- Give recommendations as to parameters and methods of prediction for the behaviour of smoke detectors for use within current analysis software.

Brammer considered two of the Cardington tests; CDT17 and CDT20, both being experiments in which the lounge door was open. Using FDS version 2, both experiments were simulated and the smoke detector activation times derived using the temperature correlation method, pseudo-heat detector method and Heskestad's method.

3.5.2. FDS Model Development

The initial component of Brammer's research assessed various designs for the house within FDS and the relative grid size of the model, given the restrictions imposed by the rectilinear grid. Where sufficient information was available, the test model geometry adopted within this research is based on that presented by Brammer (2002), and thus was not reassessed. This includes the following parameters:

- *100mm grid dimension across all planes*: It is noted that Brammer undertook a grid size sensitivity analysis and thus this was not incorporated into the scope of the research presented in this project.

- *800mm open door widths*: Doors are noted to be 750mm, which does not align with the defined grid cell dimensions. Brammer assessed both 700mm and 800mm door openings and found there to be little effect on the environmental conditions.

- *The sloping stairway balustrades are modelled parallel to the stairs*: Brammer modelled a number of balustrade designs and found there to be little, if any, impact on the derived environmental conditions. It is noted that the balustrade within the experiments sloped parallel to the stairs.

- *The ceiling above the stairway is modelled in a step-wise fashion*: In addition to adopting the design defined by Brammer, the 'sawtooth' smoothing operation was also included within the modelling to reduce the impact on the airflow movement up the stairway and decrease the likelihood of eddies forming. This function is understood to have not been present within FDS Version 2.

- *Omission of radiators from within bedrooms 1 and 3*: Brammer undertook an analysis omitting these radiators from the model and found there to be little effect on the derived results.

3.5.3. Heat Release Rate Derivation

Brammer derived the heat release rate for each of the simulations by multiplying the experimental mass loss data by an effective heat of combustion and then formulating an 'idealised curve'. Simulations where run and the heat release rate adjusted until the resulting temperatures were comparable to that of the actual experiment within the lounge. Using this methodology the resulting effective heat of combustion for CDT17 was derived to be 30MJ/kg.

3.5.4. Soot Yield and Optical Density

For the simulations in which the optical density was assessed Brammer defined the soot yield to equal $0.10 kg_{soot}/kg_{fuel}$. Upon examining the results of the FDS simulations, the optical density values were however found to be significantly greater than those of the actual test data. As the trends in the optical density were considered comparable to that of the experiment Brammer (2002) subsequently halved the results 'as a means of attempting to draw some useful conclusions.'

3.5.5. Research Conclusions

Brammer (2002) made the following conclusions from his research:

- It was difficult to achieve good matches for temperature and optical density at the early stages of the fires.

- There was little difference between the temperature correlation and pseudo-heat detector methods for predicting smoke detector behaviour when a low RTI value is adopted.

- Activation times for both ionisation and optical detectors can be predicted by the use of the temperature correlation method with $T_{act} = 20°C$.

4. Modelling Parameters

4.1. Model Geometry

The FDS model of the Cardington house is based on the information presented by Spearpoint (1996) and Brammer (2002), as shown previously in Figure 1 and Figure 2. The model space is defined to be 8.0m by 6.4m by 5.0m high, comprising of 0.1m by 0.1m by 0.1m cells. As noted in Section 3.5.2, Brammer undertook a sensitivity analysis regarding cell dimensions as a part of his research and determined 0.1m to be appropriate. An additional sensitivity analysis on the grid dimensions was thus not included within the scope of this research work.

The house itself is defined to be constructed of concrete and gypsum board, with concrete being assumed to be adiabatic. The defined properties of the gypsum board are based on that presented by Quintiere (1998), as stated in Table 10. The external walls, ground floor, first floor and roof where defined to be concrete and the internal walls, stairway and balustrade gypsum board. It is noted that Brammer (2002) does not specify the properties of the walls, floors, etc defined within his FDS modelled, however it is not considered that any differences between his model and that detailed within this paper will have a significant impact on smoke movement within the simulations.

Property	Value
Conductivity	0.48W/m/K
Specific Heat	0.84kJ/kg/K
Density	1440kg/m^3

Table 10 Gypsum Board Properties

Restrictions imposed by the rectilinear grid requirements of FDS require that the sloping ceiling located above the stairway be modelled in a step-wise fashion. To lessen the impact of the 'stair-stepping' on fluid movement and flow pattern near the ceiling, the parameter 'SAWTOOTH=.FALSE.' is defined on each obstruction line making up the stepped ceiling. This inbuilt FDS parameter prevents vorticity from being generated at sharp corners, in effect smoothing out the jagged steps (McGrattan et al 2009a).

To ensure sufficient ventilation was available for the combustion processes to occur, and being representative of the natural level of leakage present within a building, openings within the external walls of the house are included in the model. Within the entry hall, an opening 0.1m wide by 2.0m high is defined at the location of the front door, and within an external lounge wall an opening 2.0m wide by 0.1m high is defined to outside. It is noted that Brammer (2002) did not provide any information regarding the inclusion of such openings within his modelling.

The open door present between the landing and bedroom has a width of 0.8m by 2.0m high, Within CDT17 and CDT19 an equivalent door opening is present between the lounge and entry hall. During experiment CDT16 the lounge door was closed, however leakage did occur through the gaps between the door and door frame. To enable sufficient oxygen to be present as required for the defined heat release rate, in lieu of the 0.8m by 2.0m high door opening a gap 0.1m wide by 1.0m high is defined. Further information is provided on this in Section 4.4.3.

Images of the defined house model, as produced by Smokeview, are provided in Figure 6, Figure 7 and Figure 8.

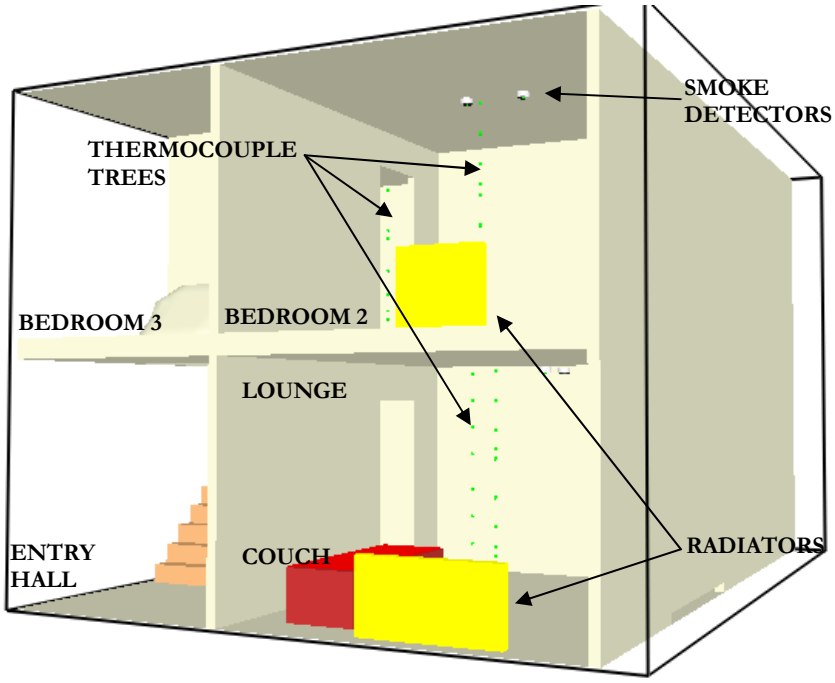

Figure 6 Smokeview House Model Image 1

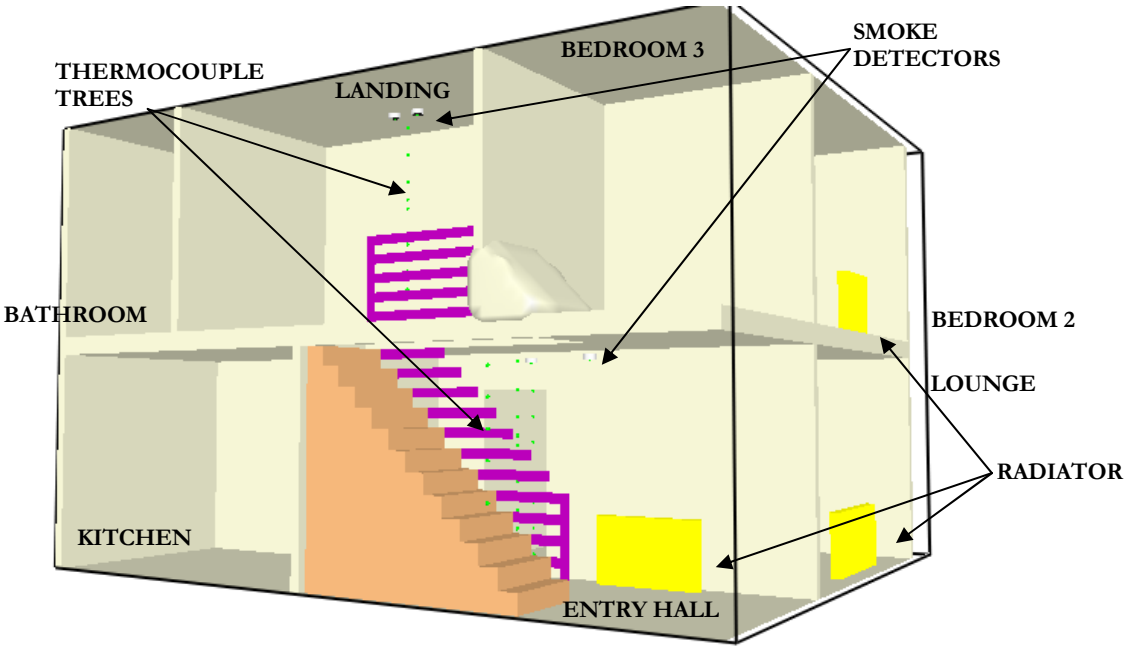

Figure 7 Smokeview House Model Image 2

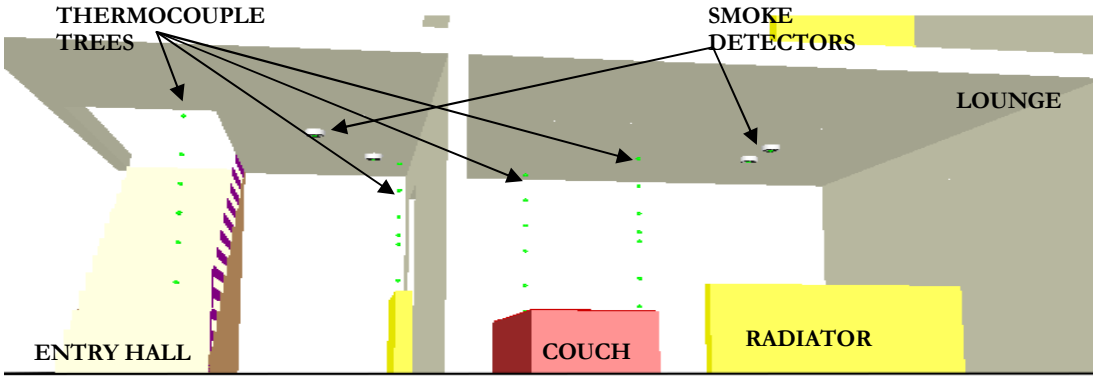

Figure 8 Smokeview House Model Image 3

4.2. Ambient Temperature

The presence of radiators within the house creates pre-existing air flow currents prior to ignition of the fire that may affect the early stages of smoke movement. They also create an uneven temperature distribution between and within the various rooms. The radiators are thus included within the simulations as objects of defined surface temperature. As justified within Brammer's (2002) research, only those radiators present in the lounge, entry hall and bedroom 2 are considered, the additional two radiators being located in rooms closed off from the remainder of the house.

Within Brammer's modelling, due to limitations present within FDS Version 2, the radiators where defined as steady state fires. For assessment of the smoke detector activation times utilising Heskestad's method, additional simulations were run excluding the radiators from the model, as they affected the optical density readings. In the simulations in which the radiators where present, Brammer defined them as fires with heat release rates equivalent to the radiator ratings. It is noted that Thomas's (2008) work utilising BRANZFIRE was unable to include the radiators within the assessment due to the limitations on the program.

As no information was found to be available on the size of the radiators, estimations were made based on that of comparable heaters in the market place today. The level of radiation emitted from an object is dependent on its temperature and surface area thus, assuming the ratings specified for the heaters to be representative of the thermal radiation emitted as assumed by Brammer, the defined temperature of the front surface of each of the objects were determined in accordance with Equation 11. Table 11 states the resulting dimensions of the three defined objects and their corresponding temperature.

$$\text{Radiation} = 5.67*10^{-8}*A_s*T^4 \qquad \text{[Equation 11]}$$

Location	Rating	Width	Depth	Height	Temperature
Lounge	2.0kW	1.4m	0.1m	0.7m	81ºC
Entry Hall	1.5kW	1.1m	0.1m	0.7m	76ºC
Bedroom 2	1.0kW	0.8m	0.1m	0.7m	66ºC

Table 11 Radiator Parameters

Six thermocouple trees where located throughout the house for comparison of temperature measurements between the experimental and computational results. Each tree consisted of eight thermocouples, their locations stated within Table 12, these being equivalent to that previously stated in Table 9.

Running an initial simulation of CDT16 in which the only heat sources were the three radiators, temperatures were found to stabilise within 600s. This is thus defined to be the time of ignition of the fires within the FDS simulations, which is noted as being equivalent to that defined in Brammer's research (2002). Figure 9, Figure 10 and Figure 11 show the recorded temperatures over the initial 600s time period for the

CDT16 FDS geometry within the lounge (central, T1), entry hall (T3) and on the stairway (T4) prior to ignition of the fire.

	T1 Lounge Central	T2 Lounge 2	T3 Entry Hall	T4 Stairs	T5 Landing	T6 Bedroom 2
(x,y)	(5.2, 3.9)	(4.3, 3.2)	(4.7, 2.2)	(5.3, 0.7)	(3.6, 1.7)	(6.0, 4.1)
z_1	0.1	0.1	0.1	0.9	2.7	2.7
z_2	0.4	0.4	0.4	1.3	3.0	3.0
z_3	0.7	0.7	0.7	1.6	3.3	3.3
z_4	1.0	1.0	1.0	1.9	3.7	3.7
z_5	1.4	1.4	1.4	2.2	4.0	4.0
z_6	1.7	1.7	1.7	2.6	4.3	4.3
z_7	2.0	2.0	2.0	2.9	4.6	4.6
z_8	2.3	2.3	2.3	3.2	4.9	4.9

Table 12 Temperature Thermocouple Locations

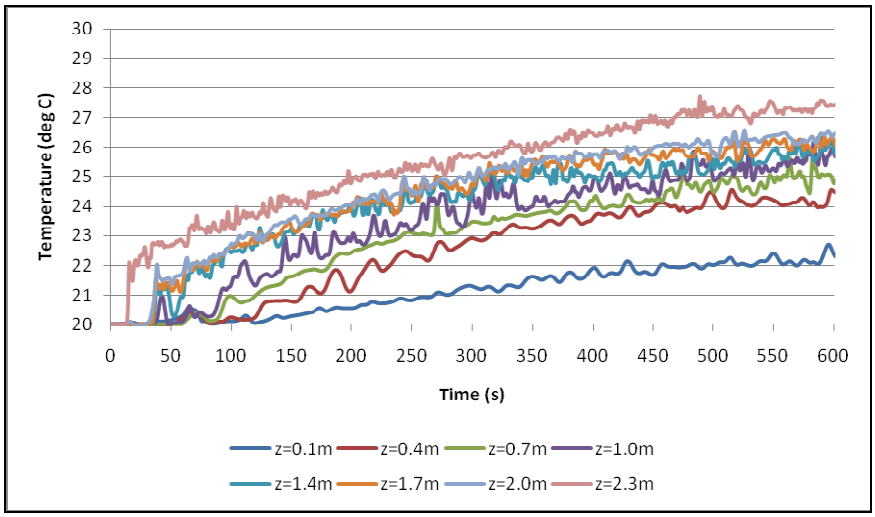

Figure 9 Lounge Central Temperatures (T1) Prior to Fire Ignition

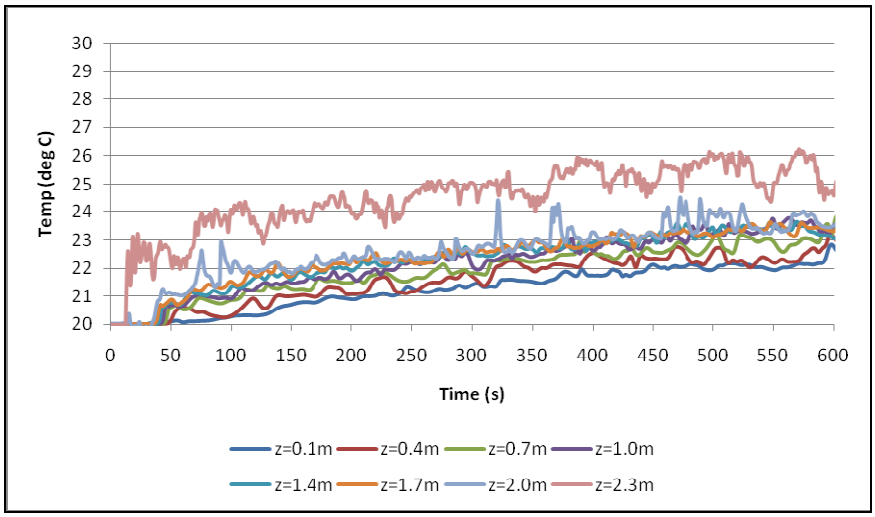

Figure 10 Entry Hall Temperatures (T3) Prior to Fire Ignition

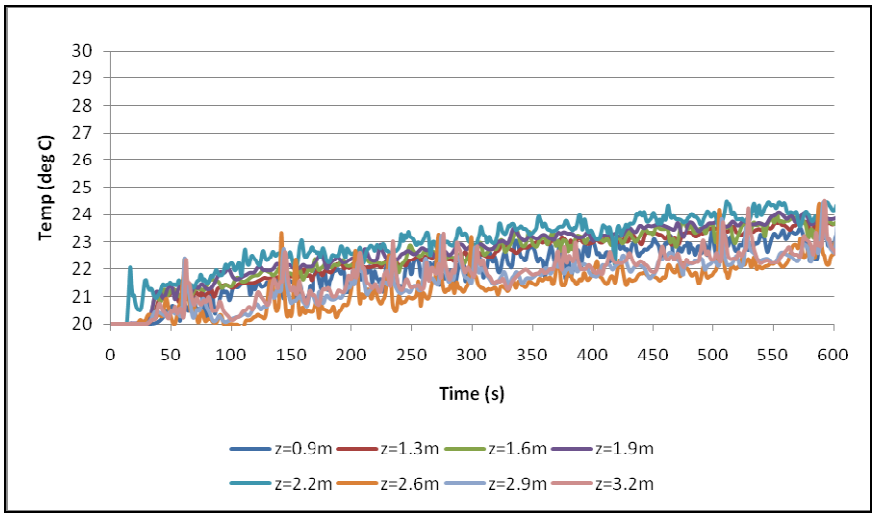

Figure 11 Stairway Temperatures (T4) Prior to Fire Ignition

Determination of the ambient temperatures is necessary for use within the temperature correlation algorithm for determining smoke detector activation times. Equating this to be the average temperature recorded in the minute prior to ignition, Table 13 states the resulting ambient temperatures at each of the smoke detector locations. As a component of the FDS program, at the start of each simulation a small degree of 'noise' is included within a model. As such variations may be seen between simulations of identical fire scenarios. By deriving the ambient temperature as the average of the temperatures recorded over a minute, it is assumed that any small variations in temperatures will be accounted for and thus the values stated in Table 13 are appropriate for use in the assessment of all simulations.

Detector	CDT16 (°C)	CDT17 (°C)	CDT19 (°C)
Ionisation			
Lounge	28	27	27
Entry Hall	26	27	27
Landing	23	23	23
Bedroom 2	24	25	25
Photoelectric			
Lounge	27	27	27
Entry Hall	25	26	26
Landing	23	23	23
Bedroom 2	25	25	25

Table 13 Ambient Temperatures at Smoke Detectors Prior to Fire Ignition

Whilst comparison cannot be made to temperatures at the detectors between the simulation and experimental data as this was not recorded during the Cardington house

tests, such comparison can be made at the thermocouple tree locations. Figure 12 and Figure 13 provide a comparison between derived ambient temperatures from CDT16 Simulation 1 results and the temperatures recorded at the time of ignition of the CDT16 experiment for the thermocouple trees located on the Ground and First floors. The temperature gradient created by the presence of the radiators is evident.

Comparing the results shown in the graphs, the ambient temperatures derived from the FDS simulation are shown to be higher than that recorded during the experiment on the Ground, whilst lower on the stairway and First floor. The temperatures derived on the First floor provide a closer approximation to the experimental results than those on Ground level, with the average difference in temperature at each thermocouple location being approximately 5°C.

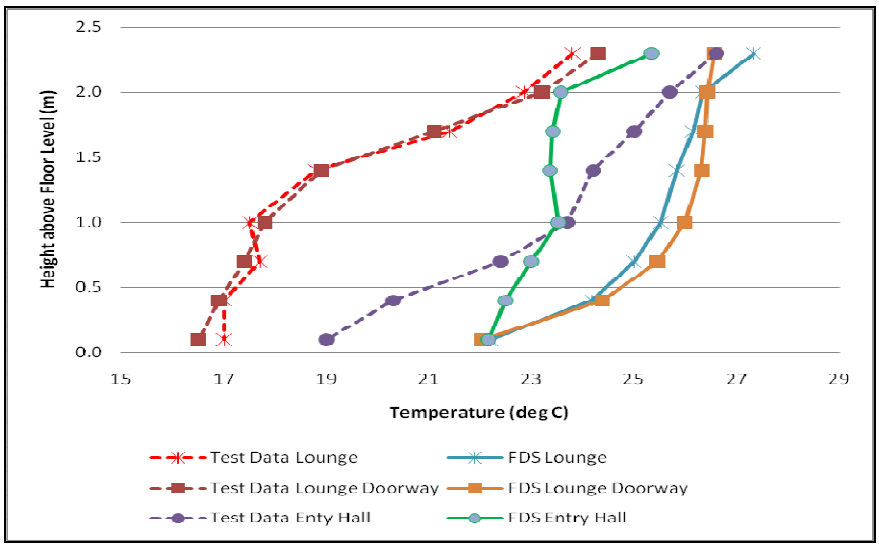

Figure 12 CDT16 Ambient Temperature Comparison: Ground Floor

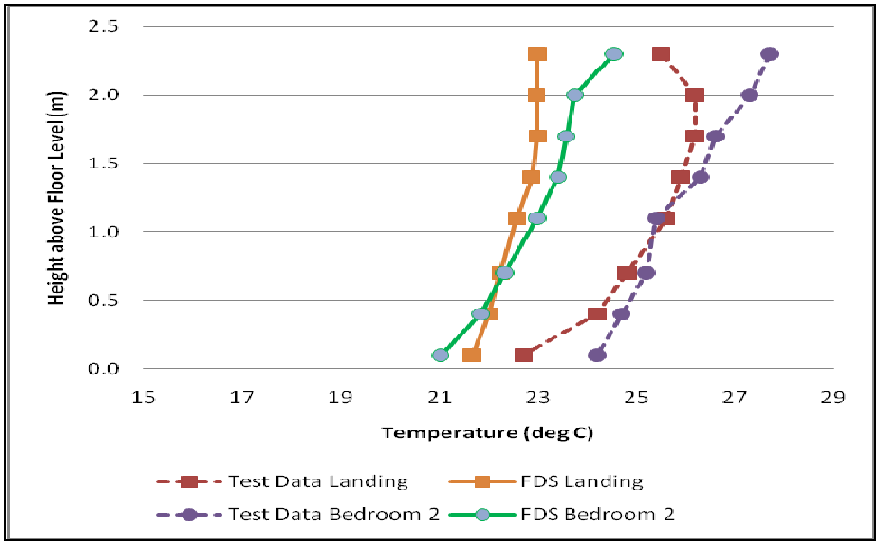

Figure 13 CDT16 Ambient Temperature Comparison: Upper Floor

Figure 14 and Figure 15 provide similar comparisons to temperatures from the CDT17 experiments. Comparable results are seen on the upper floor level, where the test temperatures are approximately 5°C higher. On the Ground level, with the open door between the lounge and entry hall, the experimental and derived temperatures are typically within a degree of each other, with a slightly larger variation seen at high level.

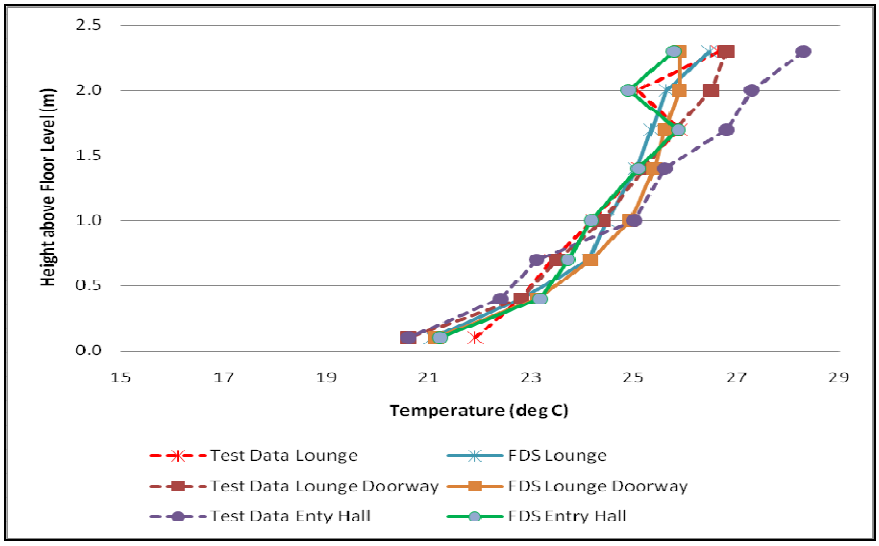

Figure 14 CDT17 Ambient Temperature Comparison: Ground Floor

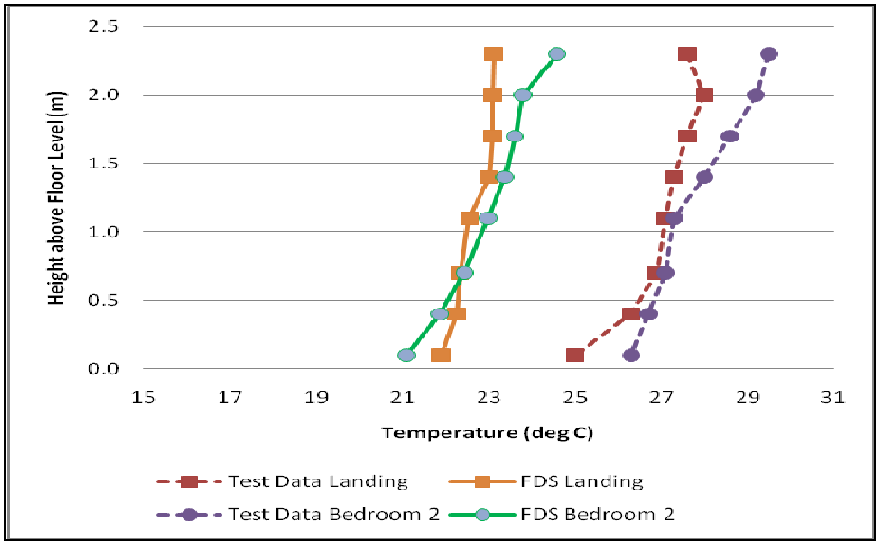

Figure 15 CDT17 Ambient Temperature Comparison: Upper Floor

It is noted that similar results to that shown for CDT17 are observed if the CDT19 experiment is assessed. This is as expected given that conditions prior to ignition are the same for the two experiments.

4.3. Derivation of Heat Release Rate Curves

The heat release rates defined within the FDS simulations are derived from the mass data recorded during the three subject experiments; Equation 12. Initially the raw mass data was utilised, which for CDT16 resulted in the mass loss rate shown in Figure 16.

$$\dot{Q} = \dot{m}\Delta H_{eff} \qquad \text{[Equation 12]}$$

This Figure indicates there to be is a significant degree of noise within the recorded mass data, which would affect the accuracy of the derived heat release rate profile. The presence of such noise is evident where there are seen to be increases in the recorded mass over a given time period, i.e. a negative mass loss rate.

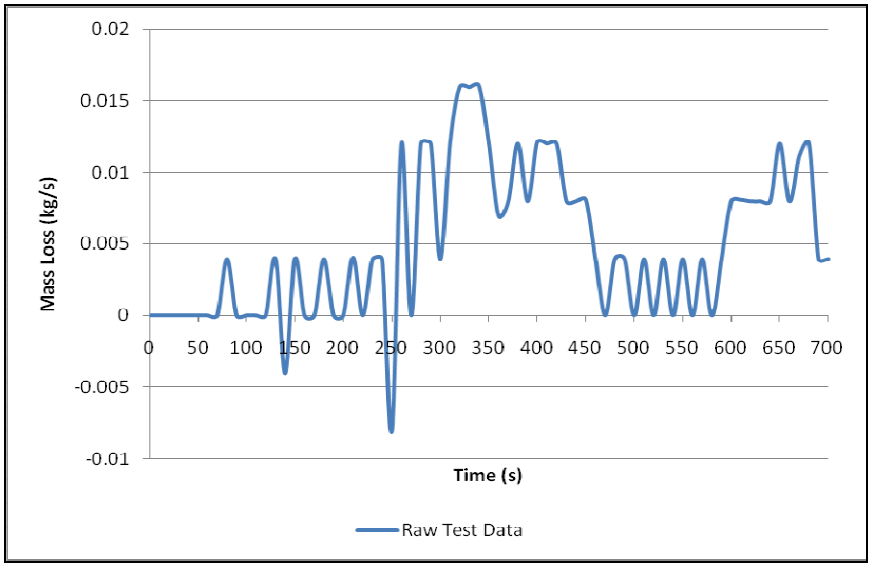

Figure 16 CDT16 Raw Mass Loss Data

To reduce the level of noise within the data such that accurate representations of the fire scenarios can be modelled, the Savitzky-Golay (SG) smoothing filter was utilised. Such a smoothing methodology is recommended by Tobeck (2007) for the derivation of heat release rates from mass loss data. Staggs (2005) also recommends this technique, stating,

> 'The Savitzky-Golay smoothing filter is applied to cone calorimeter mass data in order to obtain superior estimates of both sample mass and mass loss rate as functions of time, when compared with traditional numerical differentiation procedures.'

The basic concept of the SG filter is to fit a polynomial P of degree r to '$n_L + n_R + 1$' data points, obtained from n_L data points to the left and n_R data points to the right of a general data point (t_k, m_k). The smoothed data point is then obtained from the value of P at t_i.

The summary of the general process is provided as follows:

- Consider a general data set (t_i, m_i), $1 \leq i \leq n$, which is to be smoothed.
- Rescale the t values in the interval $[t_{i-n}L, t_{i+n}R]$ by the transformation

$$\tau_k = \tau_k - \frac{t_{i-n_L}}{t_{i+n_R} - t_{i-n_L}}\,;\; k = i - n_L, \ldots, i + n_R.$$

- Let the smoothing polynomial P be given by

$$P(\tau) = \sum_{j=0}^{r} p_j \tau^j$$

- The sum of squared deviations from the data set S, which is a function of the $r + 1$ unknown coefficients p_j, $j = 0, 1, \ldots, r$ is given by

$$S = \sum_{k=i-n_L}^{i+n_R} \left(P(\tau_k) - m_k\right)^2$$

- Unknown coefficients are then found by solving the $r + 1$ normal equations $\partial S/\partial p_j = 0$, $j = 0, 1, \ldots, r$. These equations in matrix form are $\mathbf{Ap} = \mathbf{b}$, where $\mathbf{p} = (p_0, p_1, \ldots, p_r)^T$ and the components of the coefficient matrix and right-hand-side vector are given respectively by

$$A_{jk} = \sum_{k=i-n_L}^{in_R} \tau_k^{l+j-1};\; j = 1,2,\ldots,r+1, l = 1,2,\ldots,r+1$$

$$b_j = \sum_{k=i-n_L}^{i+n_R} \tau_k^{j-1} m_k;\; j = 1,2,\ldots r, r+1$$

- The smoothed point at i is obtained by evaluating $P(\tau_i)$.

- To smooth the initial data points additional points are added at which the mass is equal to the starting mass as it can be assumed that no mass is lost prior to the experiment starting. That is for $i = 1\text{-}n_L, 2 - n_L, \ldots, 0$, define the additional points

$$t_i = t_1 + (i-1)(t_2 - t_1), m_i = m_1$$

Typically, at the other end of the data set n_R would decrease as the number of points available decreases, however in this instance the FDS simulations were only required to model the initial periods of the experiments, i.e. that during which smoke detection occurs, thus sufficient data points are available without having to decrease n_R.

In accordance with Tobeck (2007), r was defined equal to 2 and $n_R = n_L = 20$ for derivation of the smoothed mass loss values. Figure 17 provides a comparison between the raw mass loss data and the smoothed mass loss data for CDT19. CDT19 is provided as an example as the effect of the smoothing is more evident in this experiment than in CDT16 and CDT17.

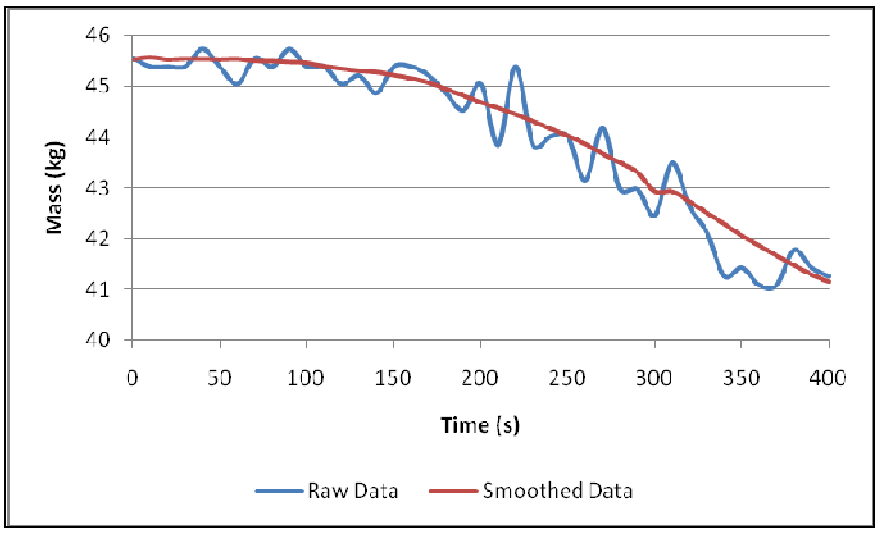

Figure 17 CDT19 Smoothed vs Raw Mass Data Comparison

Whilst it may not appear that the smoothing has had an extensive impact on the mass data, its full effect is evident through comparison of the derived heat release rate curve, where the difference in the peak heat release rates values is seen to be greater than a factor of ten; refer to Figure 18.

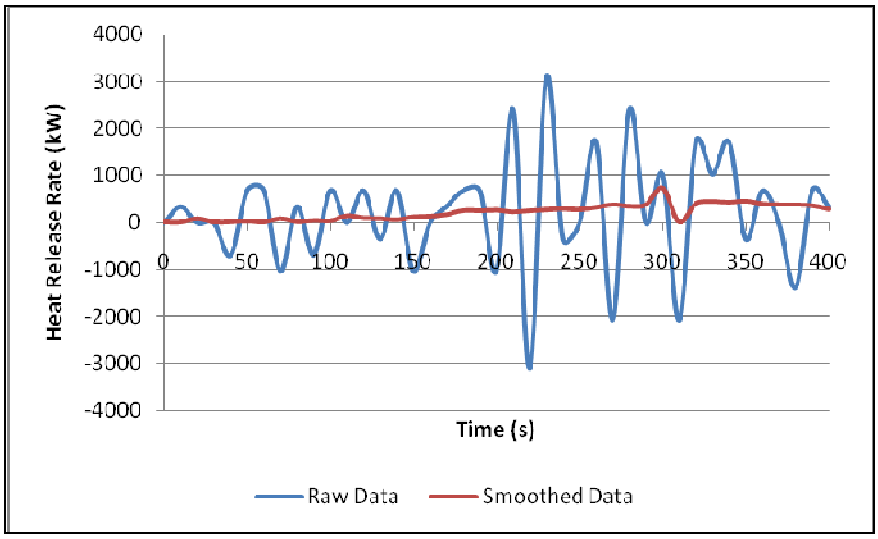

Figure 18 CDT19 Mass Data: Smoothed vs Raw Data Comparison

It is noted that whilst the smoothing of the data had a significant impact on the derived heat release rate curve, there is still some noise within the mass loss data, with small mass gains still present on occasion. In these instances, the heat release rate was defined to equal zero.

Figure 19 and Figure 20 show the comparative heat release rates for CDT16 and CDT17 respectively, assuming an effective heat of combustion of 20MJ/kg, as was assumed in the derivation of Figure 18. These smoothed heat release rates are that defined within the FDS models for the simulations undertaken.

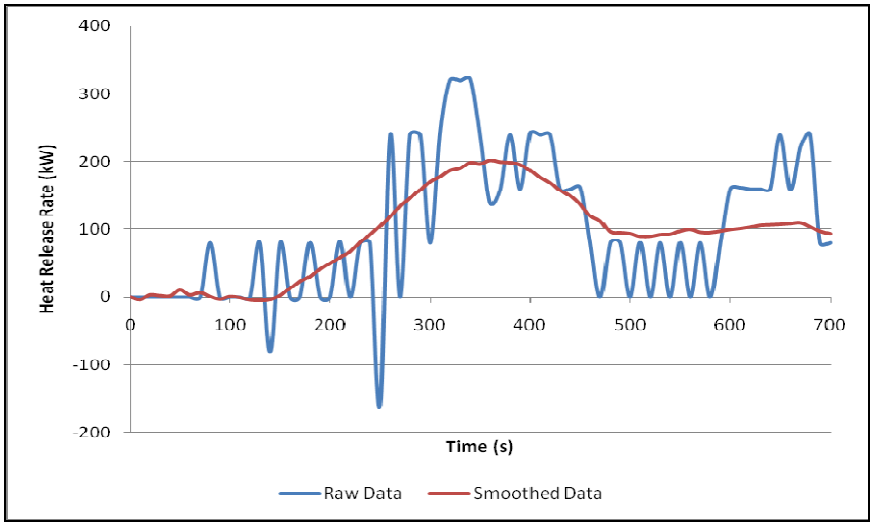

Figure 19 CDT16 Heat Release Rate: Smoothed vs Raw Data Comparison

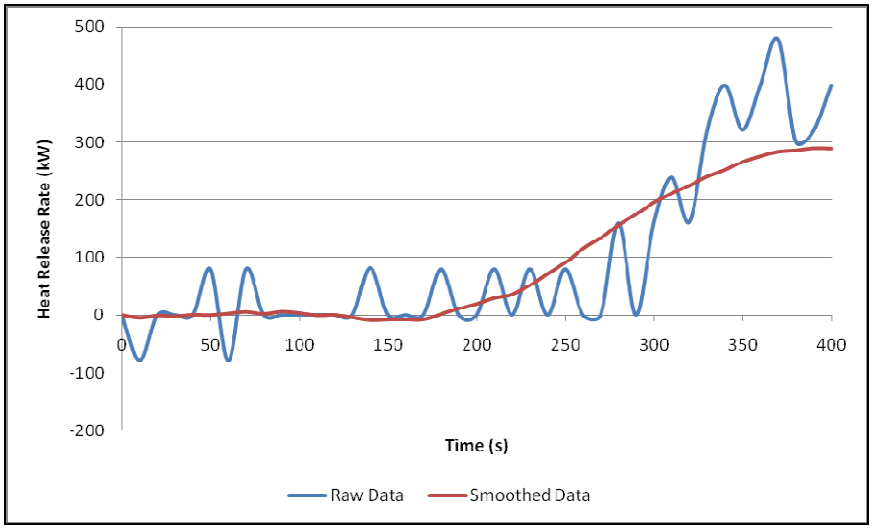

Figure 20 CDT17 Heat Release Rate: Smoothed vs Raw Data Comparison

4.4. Fuel Load

4.4.1. General

Various properties are able to be defined within FDS for representation of the fuel load, however given that fires typically involve more than one material as the source of fuel, it is difficult to accurately model a real fire scenario. For example, within the subject experiments the initial fuel source is the wood crib, with the upholstered furniture igniting after a given period of time. Excluding the burning of the wood crib, the furniture itself would also not have constant combustion properties throughout given the presence of the cotton cover over the foam.

FDS permits only a single gas phase reaction within a simulation, i.e. one 'reaction type'. Whilst the initial fuel is that of the wood crib, the primary fuel is the upholstered furniture and thus is defined to be the reaction within the simulation. As the exact properties of the armchair are unknown, as are its burning characteristics, the defined fuel parameters are representative of polyurethane, this being a typical material present within upholstered furniture. The defined material composition is based on the information presented by Babrauskas (2003) as stated in Table 14.

Property	Value
Number Carbon atoms in the fuel	6.3
Number Hydrogen atoms in the fuel	7.1

Table 14 Polyurethane Properties

4.4.2. Soot Yield

As detailed in Section 2.7 Robbins and Wade (2008) recommend that a defined soot yield be based on data from the flaming combustion of full sized items of furniture. Such information is not however available on the subject armchairs. The upholstered furniture assessed by Robbins and Wade, was stated to have a 95th percentile soot yield of 0.7kg_{soot}/kg_{fuel}. 0.05kg_{soot}/kg_{fuel} was found however to derive more comparable results within the analysis undertaken. Given Brammer (2002) found a soot yield of 0.10kg_{soot}/kg_{fuel} to significantly over predict the optical density the base soot yield value is defined to be 0.05kg_{soot}/kg_{fuel}.

Additional simulations were run of each experiment in which the defined soot yield was varied. In line with that stated above and the published references detailed in Section 2.4, soot yields of 0.10kg_{soot}/kg_{fuel} and 0.04kg_{soot}/kg_{fuel} were assessed.

4.4.3. Effective Heat of Combustion

Preliminary simulations of CDT16 were modelled to determine the effective heat of combustion of the fuel load. Comparison between the real test data and derived FDS temperatures at high level at each thermocouple tree locations were made. Such comparisons were made at high level, as this is the region in which smoke detectors are located and thus the area of concern for the research undertaken, i.e. z_8 as referenced in Table 12. Whilst the soot yield remained constant between the simulations, the effective heat of combustion and ventilation provisions were modified. Table 15 states the relevant parameters defined for a number of the initial trial simulations run for determination of the effective heat of combustion.

Ref.	Effective Heat of Combustion	Heat Release Rate Per Unit Area	Soot Yield	Lounge to Entry Hall Opening
	[MJ/kg]	[kW/m^2]	[kg_{soot}/kg_{fuel}]	[m]
A	30	481.49	0.05	0.1*0.1
B	14	224.70	0.05	0.1*0.1
C	20	320.99	0.05	0.1*0.5
D	20	320.99	0.05	0.1*1.0
E	20	320.99	0.05	0.1*1.8
F	25	401.24	0.05	0.1*1.0

Table 15 CDT16 Preliminary FDS Simulations

4.4.3.1. CDT16 Simulations A and B

The initial simulation assumed an effective heat of combustion of 30MJ/kg, this being equivalent to that utilised by Brammer and supported by the research presented by Grigis (Brammer 2002). As seen in Figure 21, insufficient ventilation was available for modelling of the defined heat release rate towards the end of the simulation.

Figure 22 and Figure 23 provide temperature comparisons between the FDS simulations and experimental results at high level for the thermocouple tree locations within the lounge, entry hall and stairway. Once significant growth of the fire begins approximately 150s after ignition, and prior to there being insufficient oxygen available for the defined combustion process, the temperatures within the lounge are seen to be greater than the test data, whilst those external to the room of fire origin are not seen to be significantly affected by the fire.

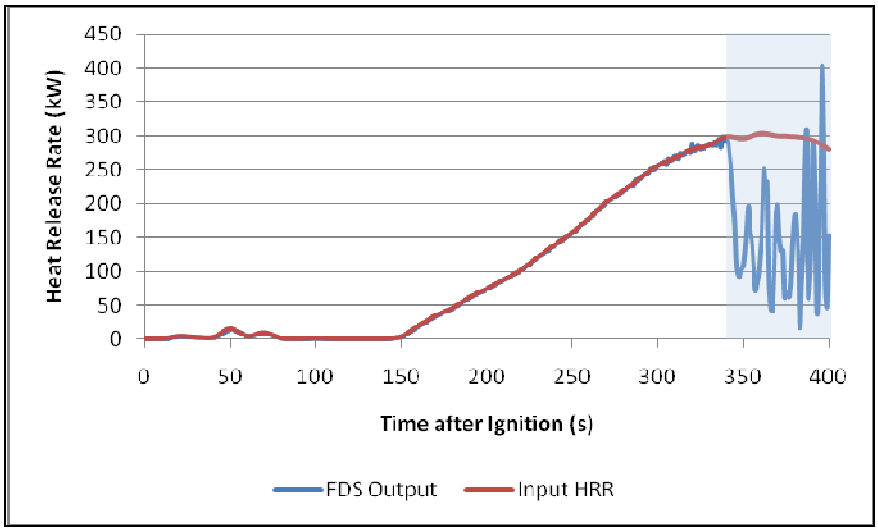

Figure 21 CDT16_A Heat Release Rate

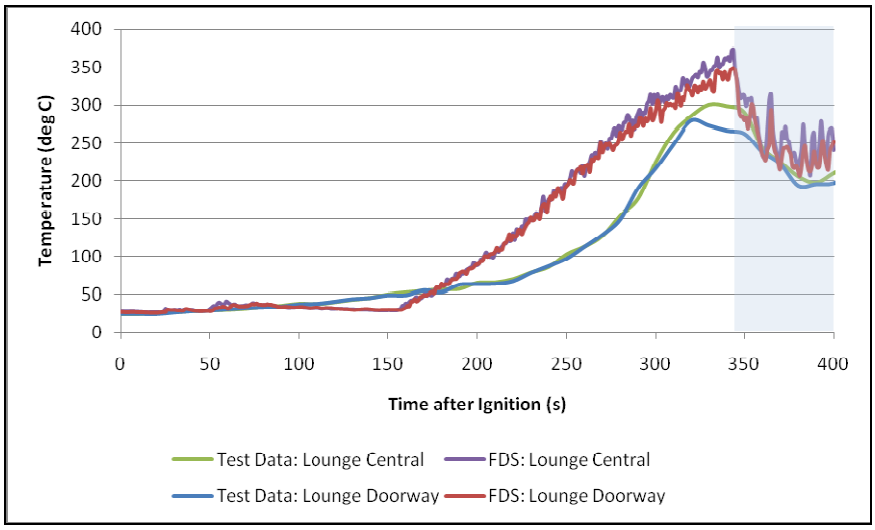

Figure 22 CDT 16_A Temperature Comparison: Lounge (T1 & T2)

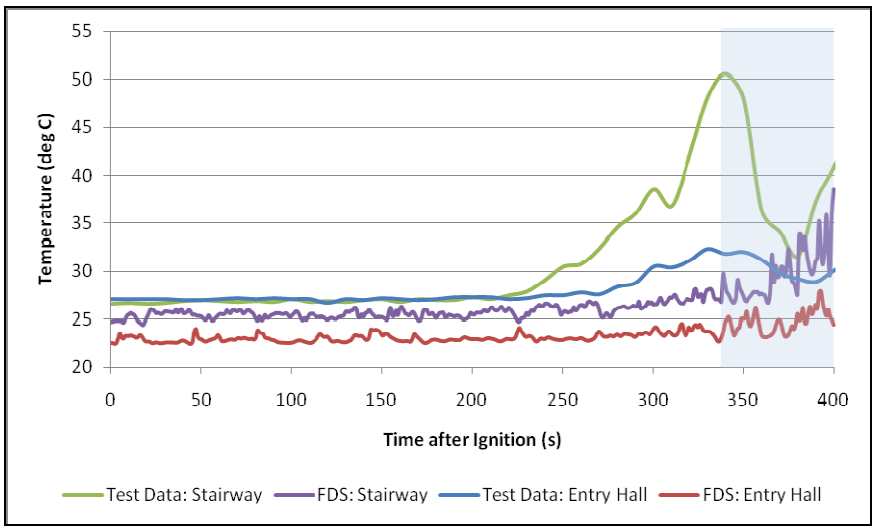

Figure 23 CDT16_A Temperature Comparison: Entry Hall (T3) and Stairway (T4)

Prior to increasing the extent of ventilation available from the lounge, Simulation 2 modelled a scenario with a significantly lower effective heat of combustion; 14MJ/kg. The heat release rate was able to be modelled as defined, however temperatures within the lounge where now less than the experimental results. As with the initial simulation, the fire had little effect on temperatures beyond the room of fire origin.

4.4.3.2. CDT16 Simulations C, D, E and F

Both the effective heat of combustion and the size of the opening between the lounge and the entry hall were modified for Simulation C. The effective heat of combustion was defined to be 20MJ/kg and the opening area was increased from 0.1m by 0.1m high to 0.1m by 0.5m high. It was again found that the extent of ventilation was

insufficient, with the heat release rate varying from the defined input values approximately 990s after ignition.

Simulations D and E where thus defined to be equivalent to Simulation C, however with increased opening areas of 0.1m by 1.0m high, and 0.1m by 1.8m high respectively. The derived temperature results and test data at high level at each thermocouple tree location are shown in Figure 24 to Figure 29 for the three simulations.

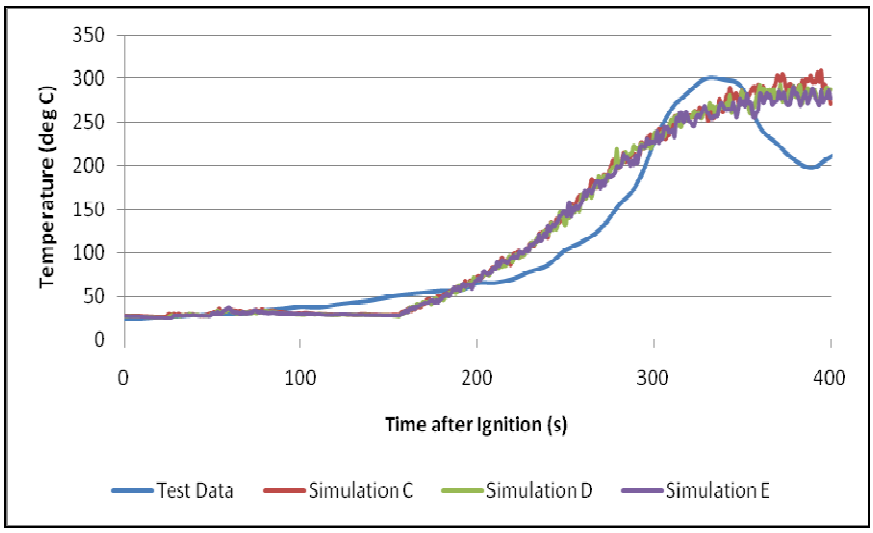

Figure 24 CDT16_C, D & E Temperature Comparison: Lounge Central (T1)

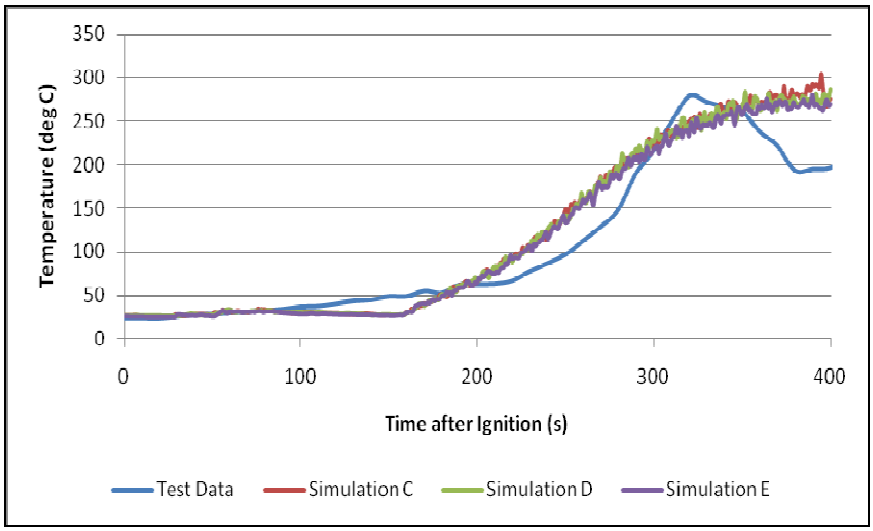

Figure 25 CDT16_C, D & E Temperature Comparison: Lounge Doorway (T2)

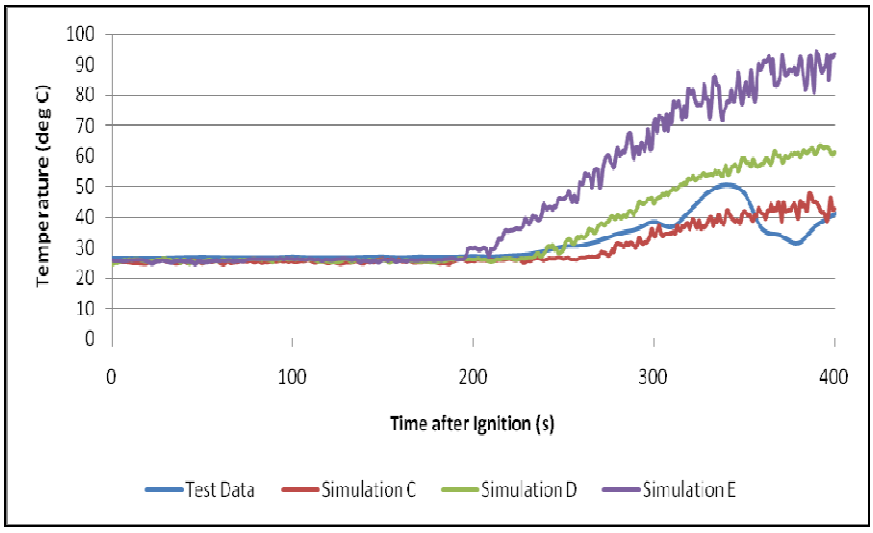

Figure 26 CDT16_ C, D & E Temperature Comparison: Entry Hall (T3)

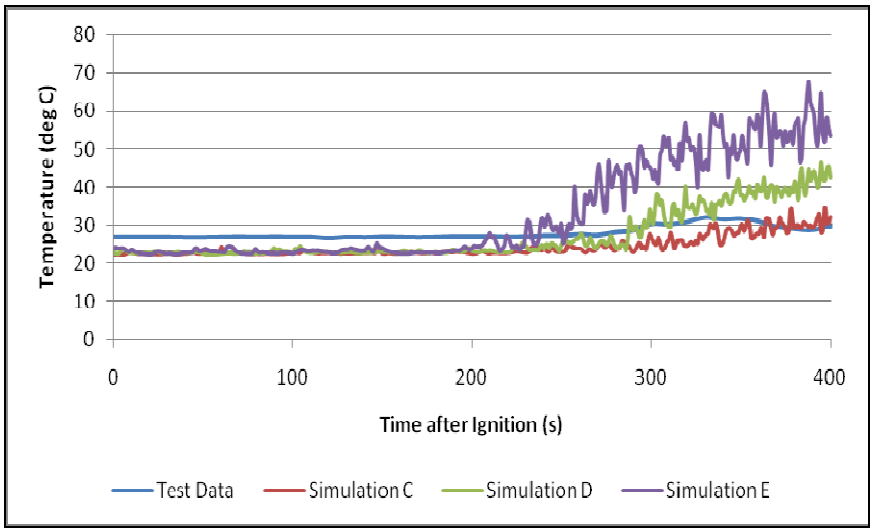

Figure 27 CDT16_C, D & E Temperature Comparison: Stairway (T4)

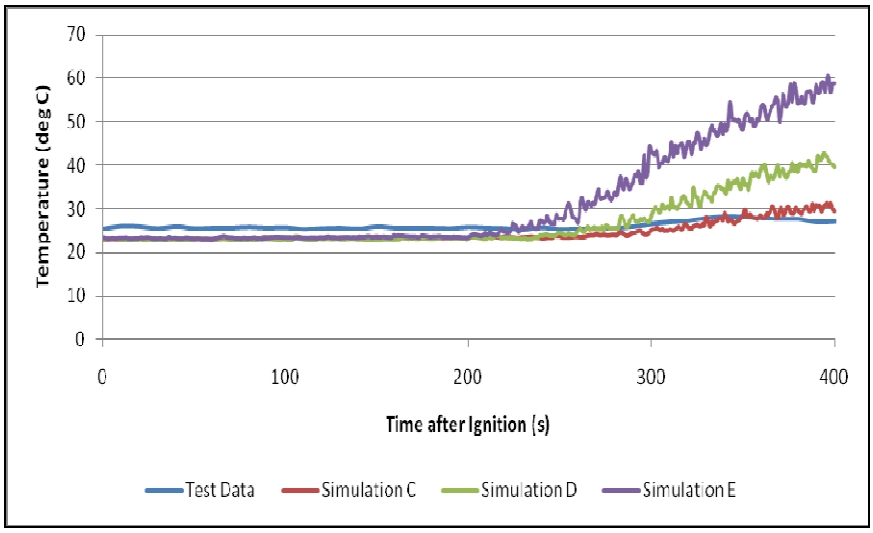

Figure 28 CDT16_C, D & E Temperature Comparison: Landing (T5)

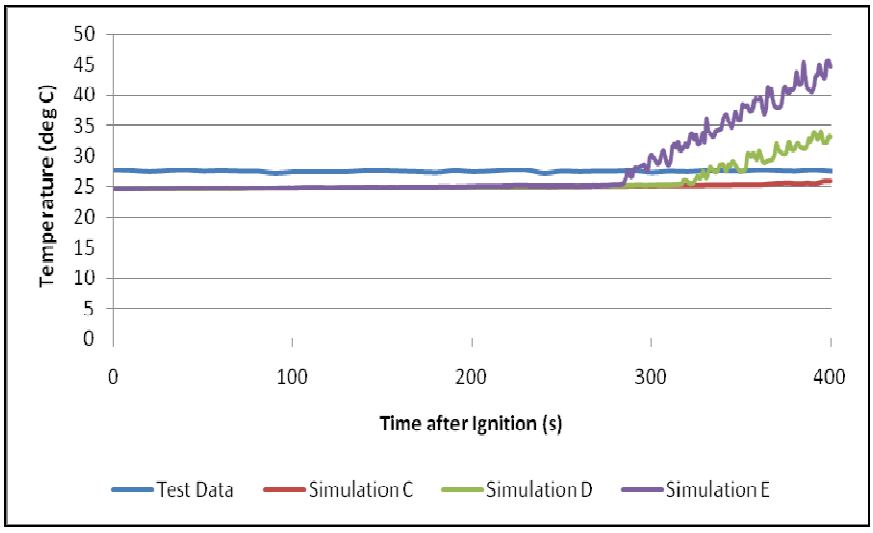

Figure 29 CDT16_C, D & E Temperature Comparison: Bedroom 2 (T6)

Whilst the size of the opening between the lounge and entry hall is seen to have minimal impact on the temperatures within the lounge, there is a significant difference between the derived temperatures beyond the room of fire origin. Increasing the area of the opening increases the extent which the fire affects conditions throughout the remainder of the house, with temperatures being seen to be significantly above the test data in Simulation 5.

The high temperatures throughout the remainder of the house may also be a result of reduced ventilation being provided from the house to outside. Prior to the experiments being undertaken however, testing indicated the house to be well sealed (Spearpoint 1996) and thus it was not considered desirable to increase the size of openings further.

The most comparable results are seen to be derived from Simulation D, with the smaller opening area, however given that insufficient oxygen was available for the defined heat release rate in this instance, an opening size of 0.1m by 1.0m was adopted.

To ensure that 20MJ/kg is an appropriate effective heat of combustion value, Simulation F replicated Simulation D with the exception of assuming 25MJ/kg. A comparison of the derived temperature profile to the test data and Simulation F is shown in Figure 30 to Figure 32.

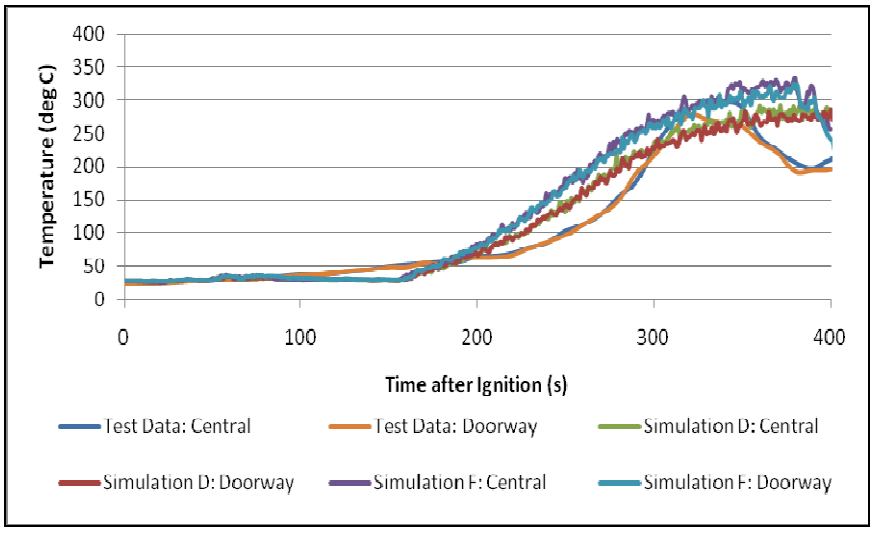

Figure 30 CDT16_D & F Temperature Comparison: Lounge (T1 & T2)

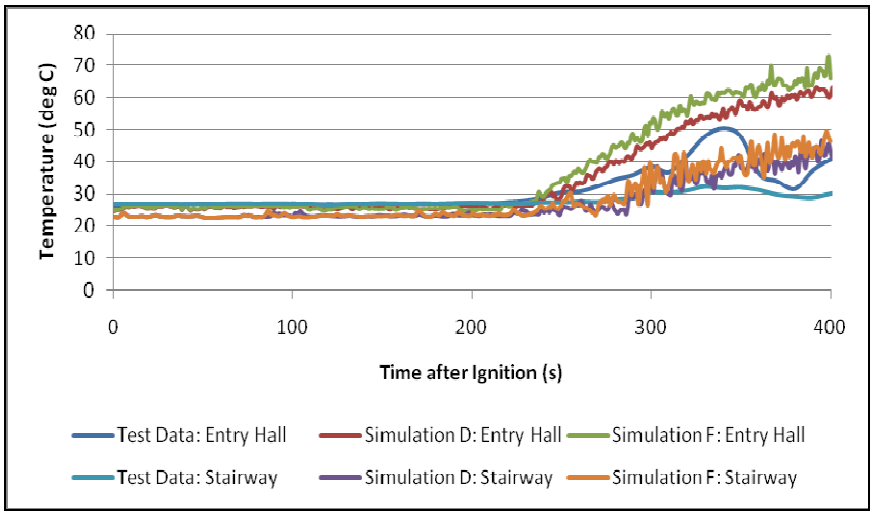

Figure 31 CDT16_D & F Temperature Comparison: Entry Hall (T3) & Stairway (T4)

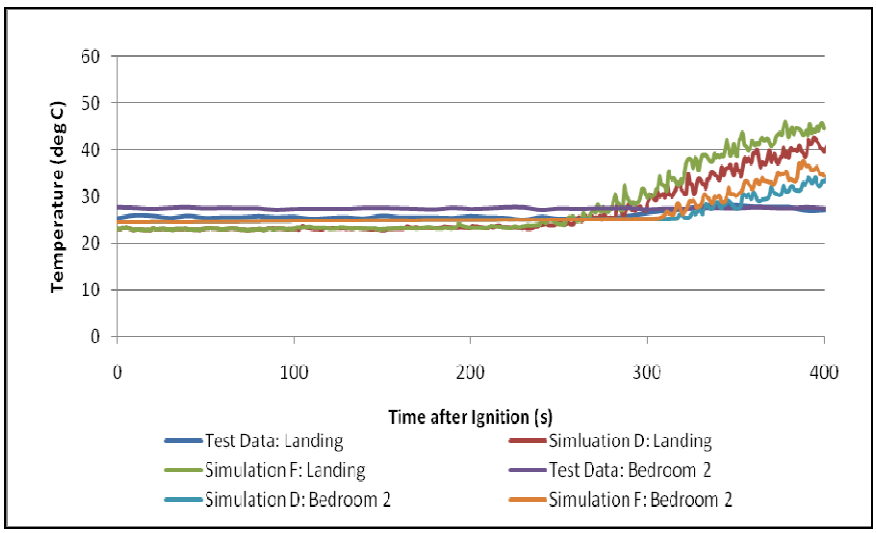

Figure 32 CDT16_D & F Temperature Comparison: Landing (T5) & Bedroom 2 (T6)

The peak temperatures recorded within the lounge for the first stage of Simulation F are comparable to the test data, however throughout the remainder of the house, the results were significantly higher. Insufficient ventilation was also found to be available for the defined heat release to be modelled approximately 1000s after ignition; refer to Figure 33.

In consideration of these results, the effective heat of combustion parameter is defined to be 20MJ/kg. This is noted as being comparable to the lower results stated in Table 7 and Table 8.

As the temperatures within the lounge provide a close approximation to the test data within Simulation F, and the lounge door within simulations CDT17 and CDT19 is open providing greater ventilation, sensitivity case scenarios for each soot yield value considered are modelled, based on an effective heat of combustion of 25MJ/kg.

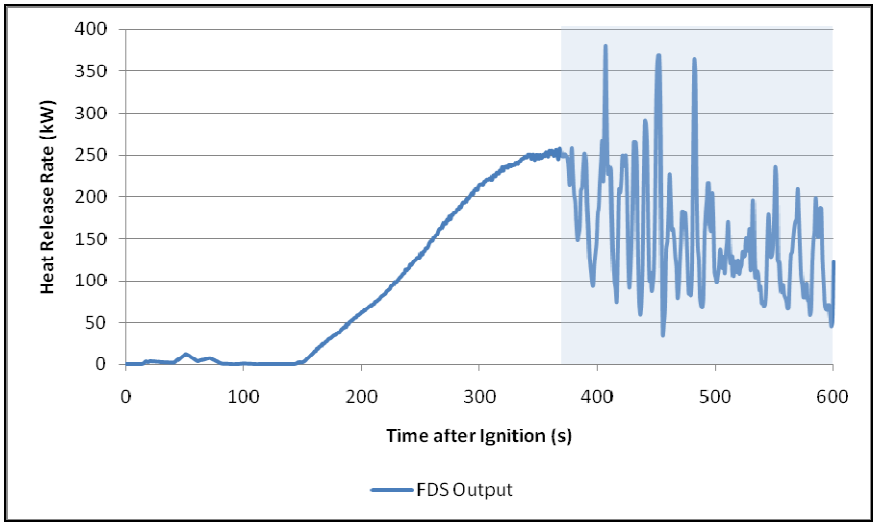

Figure 33 CDT16_F Heat Release Rate

4.5. Smoke Detection Assessment

4.5.1. Smoke Detection Derivation

To derive the smoke detector activation times in accordance with the temperature correlation method, temperature thermocouples are defined at each of the smoke detector locations, as shown in Figure 1 and Figure 2, and stated in Table 16. Activation times are determined for rise in temperature activation criterions of 4°C,

13°C and 20°C above ambient, these values being adopted by Brammer within his research and being comparable to that stated within the literature, as detailed in Section 2.3.

FDS Version 5 includes an inbuilt smoke detector algorithm to enable the time of smoke detector activation to be automatically derived during a simulation. The defined prediction algorithm is based on the two parameter algorithm proposed by Cleary et al, as detailed in Section 2.5. The user is required to input the values of the empirical constants α_e, β_e, α_c and β_c; refer to Equation 8 and Equation 9.

Location	x co-ordinate	y co-ordinate	z co-ordinate
Ionisation Detectors			
Lounge	5.8	4.7	2.3
Entry Hall	5.9	1.6	2.3
Landing	3.8	1.2	4.9
Bedroom 2	6.1	4.6	4.9
Photoelectric Detectors			
Lounge	5.3	4.7	2.3
Hall	5.0	2.0	2.3
Landing	4.1	1.2	4.9
Primary Bedroom	6.1	4.0	4.9

Table 16 Smoke Detector Locations

The Fire Dynamics Simulator (Version 5) User's Guide (McGrattan et al. 2009) recommends that α_e, β_e, α_c and β_c, be defined as stated in Table 17 for derivation of accurate activation times for unidentified ionisation and photoelectric detectors. As noted in Section 2.5 by equating α_e equal to zero, β_c and β_e to minus one, the algorithm is equivalent to Heskestad's method. For each FDS simulation, smoke detector activation times were derived for each of the parameter recommendations stated in Table 17 for the respective detector type locations.

Detector	α_e	β_e	α_c, L	β_c
Cleary Ionisation (CI1)	2.5	-0.7	0.8	-0.9
Cleary Ionisation (CI2)	1.8	-1.1	1.0	-0.8
Cleary Photoelectric (CP1)	1.8	-1.0	1.0	-0.8
Cleary Photoelectric (CP2)	1.8	-0.8	0.8	-0.8
Heskestad Ionisation	-	-	1.8	-

Table 17 Recommended Empirical Constants for use within Cleary's Two Parameter Prediction Algorithm (McGrattan and Forney 2005)

4.5.2. FDS Simulations

Having established the input parameters for the FDS models, the simulations modelled for derivation and assessment of smoke detector activation times are as summarised in Table 18. It is noted that simulations CDT16_1 and 4 are equivalent to models D and F previously detailed in Section 4.4.3. Appendix B provides the input file for CDT16, Simulation 1.

Simulation No.	Effective Heat Combustion	Soot Yield
	[MJ/kg]	[kg_{soot}/kg_{fuel}]
CDT16		
1	20	0.05
2	20	0.10
3	20	0.04
4	25	0.05
5	25	0.10
6	25	0.04
CDT17		
1	20	0.05
2	20	0.10
3	20	0.04
4	25	0.05
5	25	0.10
6	25	0.04
CDT19		
1	20	0.05
2	20	0.10
3	20	0.04
4	25	0.05
5	25	0.10
6	25	0.04

Table 18 FDS Simulations

5. Smoke Detector Activation Prediction Modelling

5.1. Introduction

This section of the report provides the results of the FDS modelling undertaken with respect to the derived smoke detector activation times, as detailed in the preceding sections and summarised in Table 18. Whilst conditions fluctuate over time as shown in the previous temperature comparison Figures, it is noted that activation is assumed to occur when the defined activation criterion is initially reached within a simulation. The temperature correlation method is noted to assess temperatures rounded to the nearest whole number.

5.2. CDT16 Results

5.2.1. Temperature Correlation Method

Figure 34 and Figure 35 show the derived activation times using the temperature correlation prediction method when assessing conditions at the ionisation and photoelectric detector locations for Simulations 1, 2 and 3; i.e. where the effective heat of combustion is 20MJ/kg and soot yields $0.05kg_{soot}/kg_{fuel}$, $0.10kg_{soot}/kg_{fuel}$ and $0.04kg_{soot}/kg_{fuel}$ respectively. Whilst the experimental data is provided for 1200s (20 minutes), the CDT16 simulations are only run for 700s after ignition of the fire (a total simulation time of 1300s). This period is more than a minute and a half longer than the time at which the last detector was recorded to activate within the experiments. During this time, derived temperatures within the bedroom did not however reach 20°C above ambient and thus no activation time is shown in the Figures for this acceptance criterion. Given the difference that would have been present from the derived results to the experimental activation times had the simulation been re-run for a longer period of time, i.e. greater than 90s, it was not considered necessary that further analysis be undertaken. Furthermore it is stated that whilst there is little change in the recorded mass for the second half of the experiment, the overall trend of these values is to increase rather than decrease, i.e. a mass gain. Modelling of this time period would have therefore included a significantly high degree of error within the defined heat release rate.

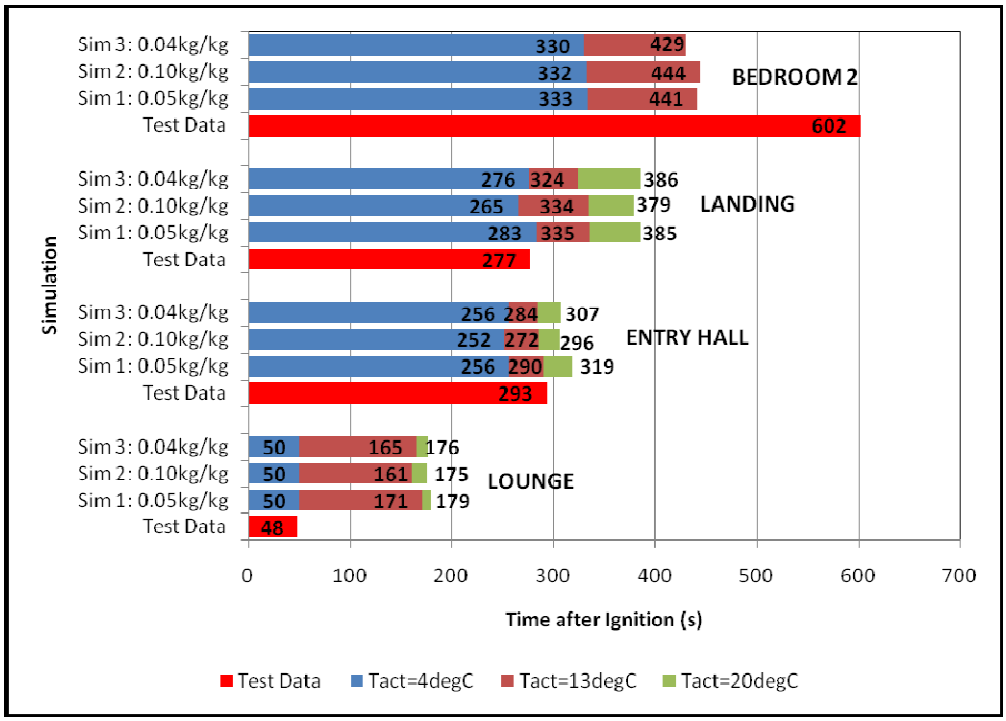

Figure 34 Temperature Correlation: CDT16_1, 2 & 3 Ionisation Detectors

Typically the derived activation times are found to be comparable to each other at a given detector location for the different soot yields considered. This is as expected given the predication algorithm assesses temperature directly. The variations that are present between the derived results for each detector location is a result of the FDS simulations being independent from each other and initiated from time step '0'. FDS initialises the flow field with a very small amount of "noise" to prevent the development of perfectly symmetric flow (McGrattan et al 2009c). Whilst the effect on the derived fluid flow is minimal as seen, it does result in small variations between the derived environmental conditions of the simulations. This consequently produces the variations seen between the derived activation times.

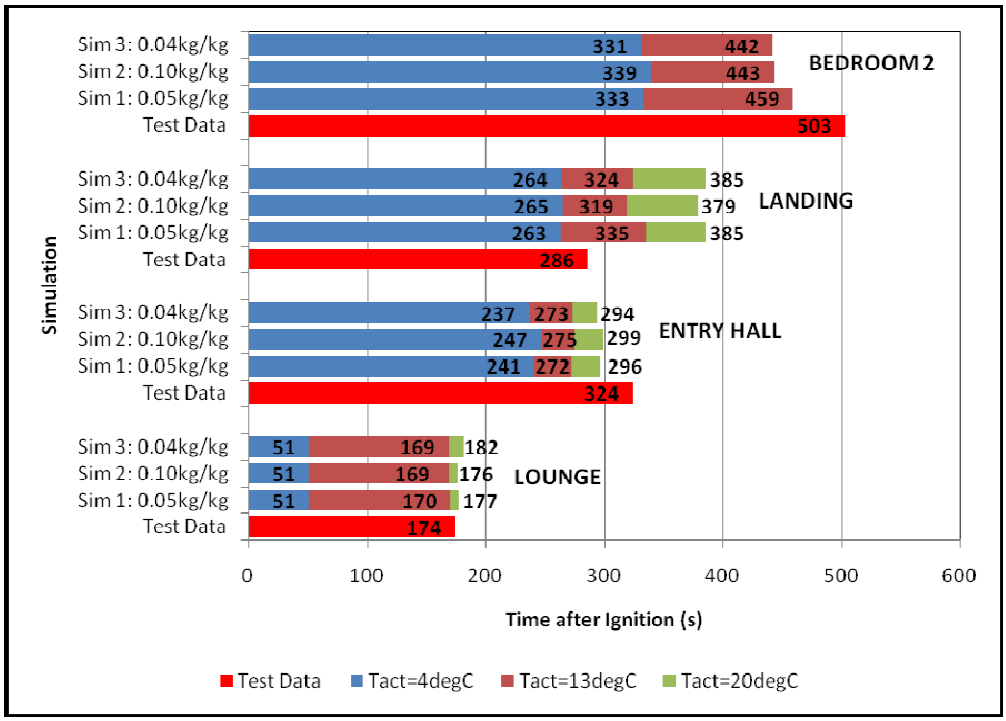

Figure 35 Temperature Correlation: CDT16_1, 2 & 3 Photoelectric Detectors

For the ionisation detectors within the lounge, an activation criterion of 4°C accurately derives the experimental detector activation time. For the lounge photoelectric detectors a similar result is not seen, with an activation criterion of 20°C providing a more accurate comparison. This difference is considered to be due to the different operating mechanisms of the two types of detectors and the fire scenario being assessed, as discussed further in Section 6.

Ionisation detector activation times derived on the landing are also seen to be comparable to the test data when assuming an activation criterion of 4°C. The entry hall results are comparable for an activation criterion of 13°C, however the entry hall detectors are derived to activate prior to those on the landing, which did not occur during the experiment. It is noted this was also found to occur within both Brammer's (2002) and Thomas's (2008) analysis. The reason for this difference may be due to an inaccurate recording of the location of the smoke detectors within the entry, and/or inaccurate modelling of the radiators within the FDS simulation. As seen and discussed further later within this report, the location of the detectors within the entry hall appear to be on the cusp of the smoke flow path at the early stages of the fire from the lounge

up to the landing through the stairway void. Slight errors within the locations of these detectors could thus have a significant impact on the derived activation times.

The purpose of including of the radiators within the model prior to the ignition of the fire was to establish fluid currents throughout the house, similar to that which would have been present within the experimental tests. Errors within the representation of these models would thus modify the initial air movement currents derived, which may subsequently affect smoke movement during the early stages of the fire. If this was to occur the environmental conditions would be affected and thus the derived smoke detector activation times influenced.

Regardless that insufficient ventilation was provided for Simulations 4, 5 and 6, where the heat of combustion is defined to be 25MJ/kg (refer to Section 4), similar results are shown in Figure 36 and Figure 37 were derived to that shown in Figure 34 and Figure 35. This is a result of the detectors activating prior to the level of available oxygen within the lounge influencing the heat release rate and conditions throughout the house. The only detector for which this did not occur was the photoelectric detector within the bedroom during Simulation 5, where the soot yield is defined to be $0.10kg_{soot}/kg_{fuel}$. Prior to the impact of the low oxygen levels being seen, temperatures at the detector are oscillating between 18°C and 19°C above ambient, however the activation criterion of 20°C is not reached in this time period. It is noted that activation of this detector was not derived from the results of Simulation 1, 2 or 3, as commented previously.

Figure 38 and Figure 39 provide comparison between the derived activation results from Simulations 1 and 4, to examine the extent of the effect of change in heat of combustion from 20MJ/kg to 25MJ/kg. It is noted that with the increased temperatures resulting from the larger heat of combustion, with the temperature correlation methodology activation times are now derived for the smoke detectors within the bedroom for Simulation 4, as is evident in Figure 36 and Figure 37.

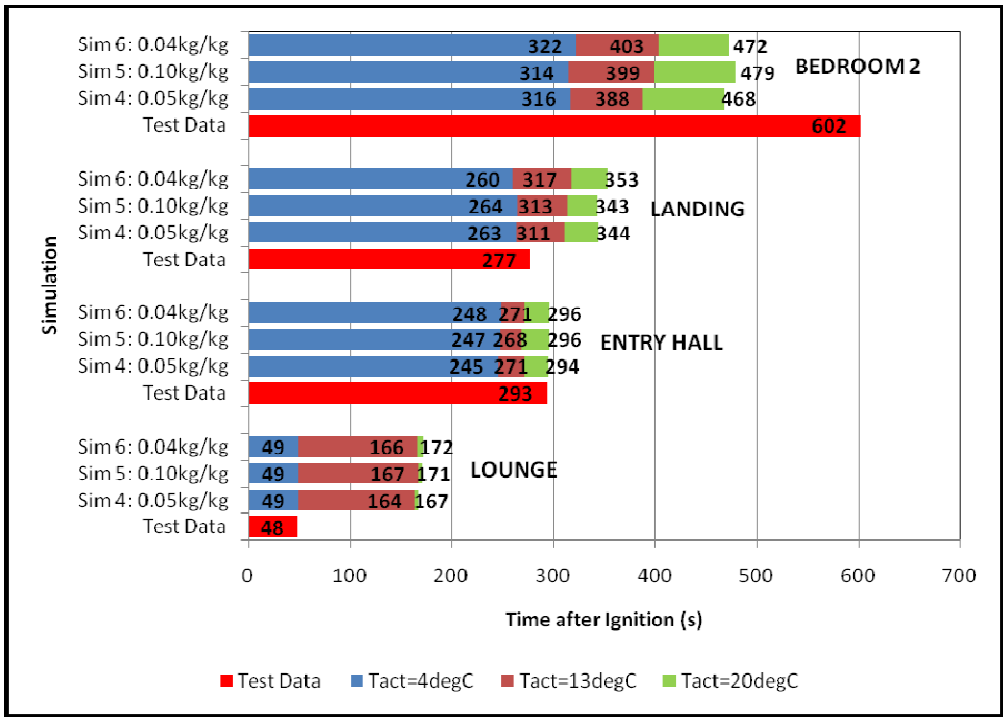

Figure 36 Temperature Correlation: CDT16_4, 5 & 6 Ionisation Detectors

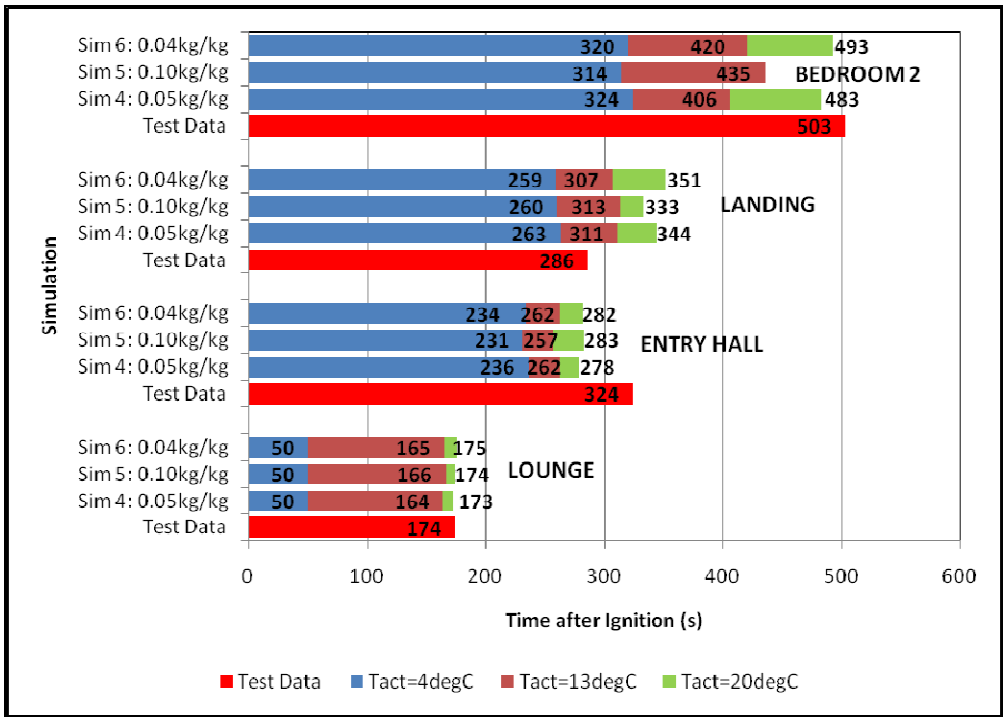

Figure 37 Temperature Correlation: CDT16_4, 5 & 6 Photoelectric Detectors

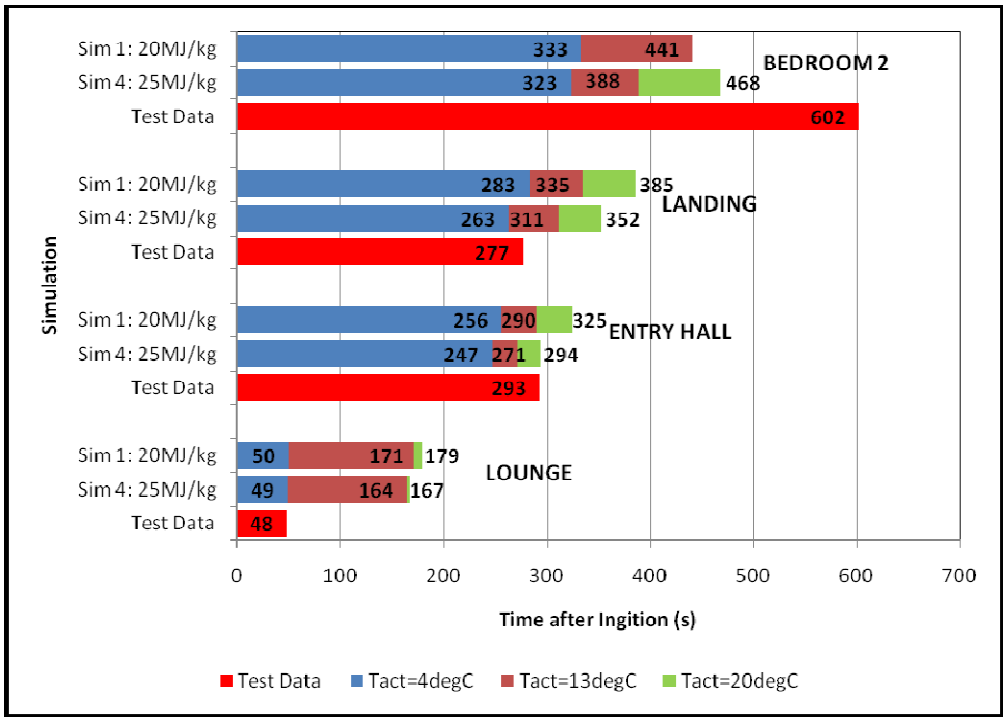

Figure 38 Temperature Correlation: CDT16_1 & 4 Ionisation Detectors

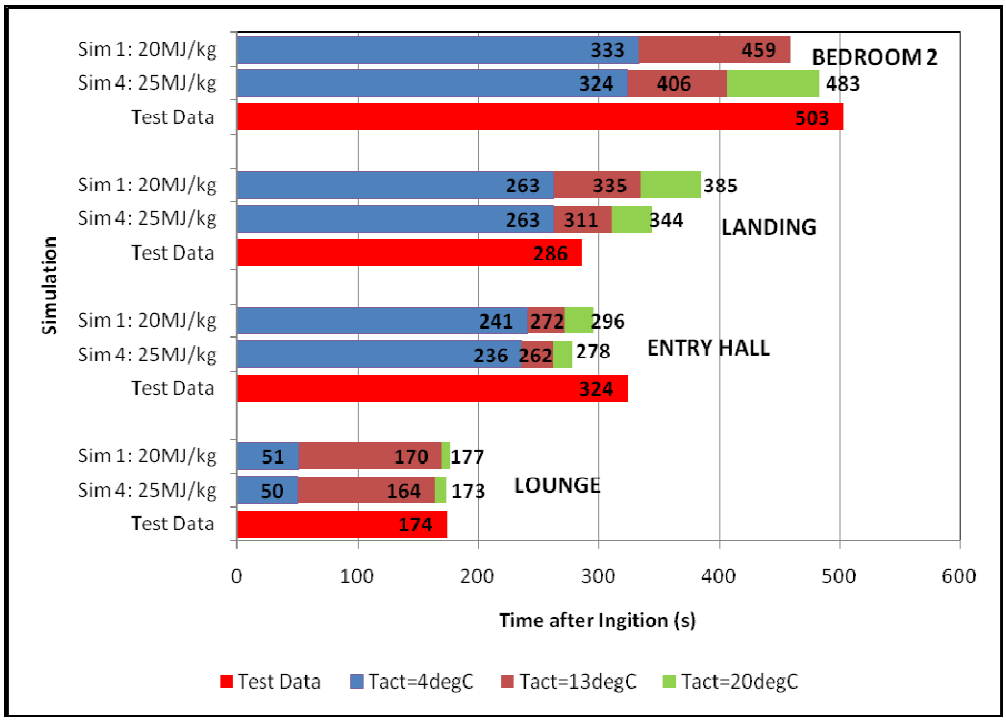

Figure 39 Temperature Correlation: CDT16_1 & 4 Photoelectric Detectors

In addition to determining the times at which the smoke detectors activate using the temperature correlation method, the derived FDS temperatures at the time of actual detector activation is considered. Figure 40 to Figure 43 present this information by

highlighting the difference in the temperature to ambient of the FDS results at the time of the detector's recorded activation during the experiment.

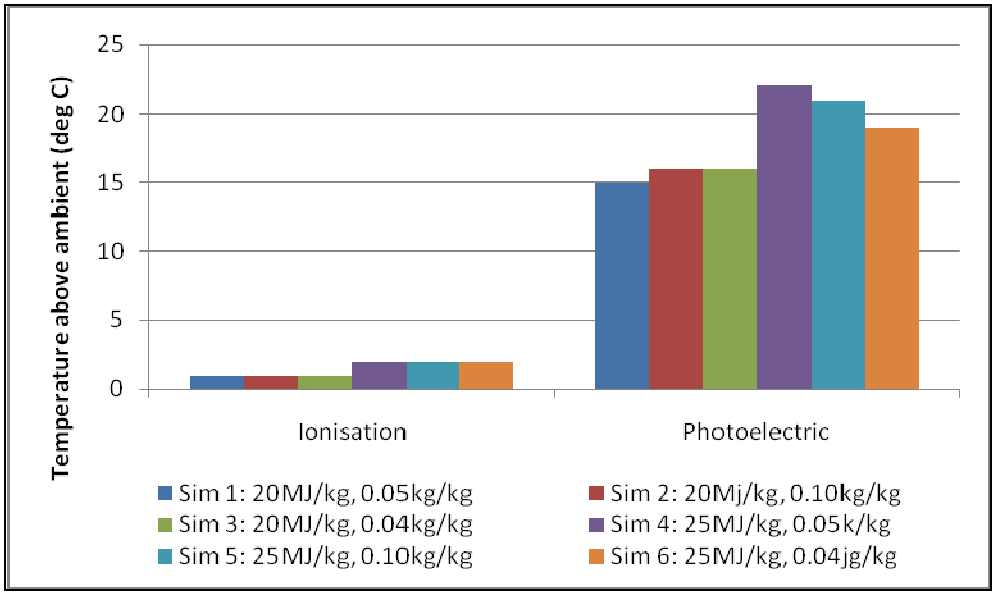

Figure 40 CDT16 Temperature Conditions at Experiment Activation Time: Lounge

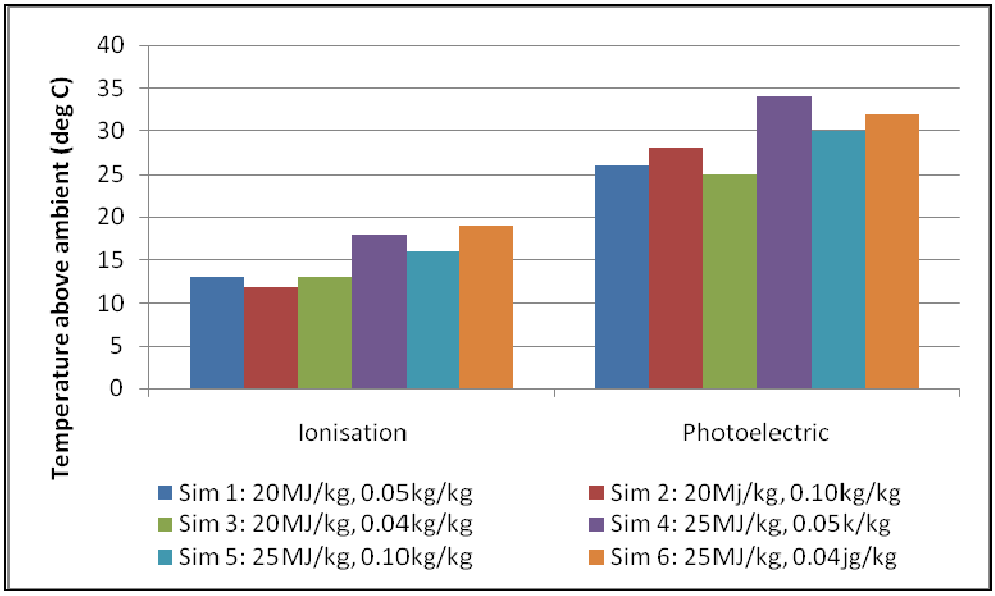

Figure 41 CDT16 Temperature Conditions at Experiment Activation Time: Entry Hall

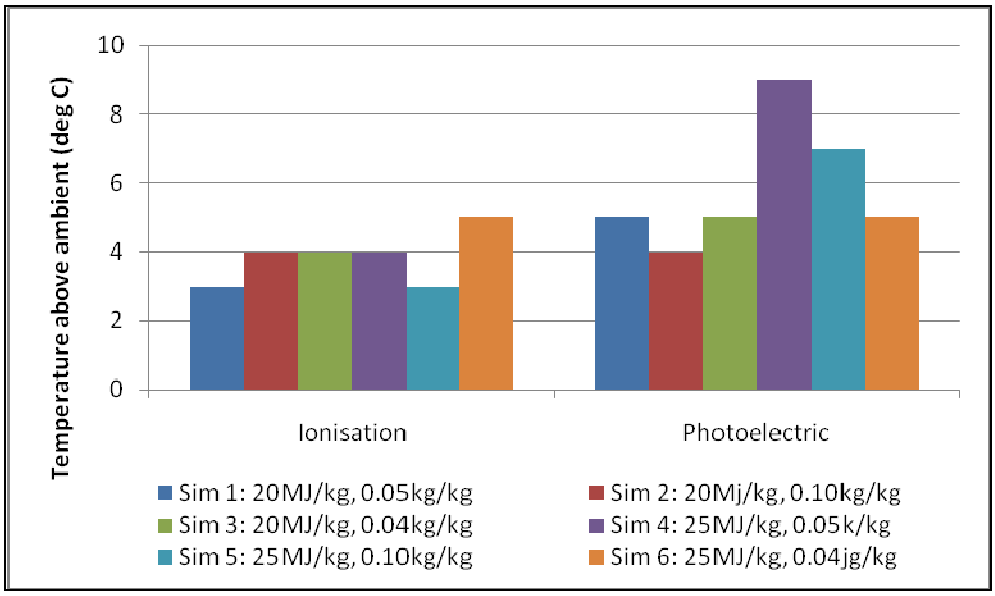

Figure 42 CDT16 Temperature Conditions at Experiment Activation Time: Landing

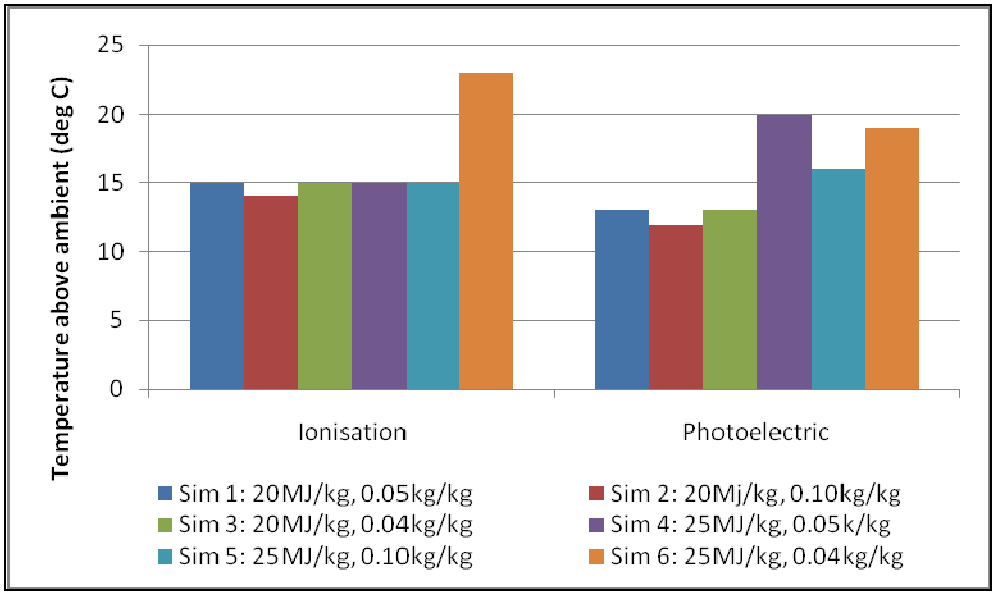

Figure 43 CDT16 Temperature Conditions at Experiment Activation Time: Bedroom 2

It is evident from these graphs that there is no constant activation criteria that can be defined for an accurate assessment of the smoke detector activation time across the board, even if considering each detector type separately. For the ionisation detectors, an activation criterion of 4°C above ambient would appear to be appropriate within the lounge and landing, whilst in the entry hall and bedroom, 15°C above ambient would provide a closer comparison to the test data. For the photoelectric detectors, with the exception of the bedroom, a higher rise in temperature is typically required at each

location for the fire scenario being assessed. Within the lounge and bedroom, 15°C would appear to be appropriate in comparison to 27°C in the entry hall.

Whilst these results could be used for recommendations of activation criterion, the temperatures noted may have been exceeded prior to the experimental detector activation time. For example, within the bedroom, the ionisation detector activated 602s after ignition during the experiment. As stated above, and shown in Figure 43, an appropriate activation criterion is 15°C above ambient, i.e. a temperature of 39°C. This temperature is initially reached 502s after activation in Simulation 1, resulting in a derived activation time over 90s earlier than occurred during the experiment; refer to Figure 44.

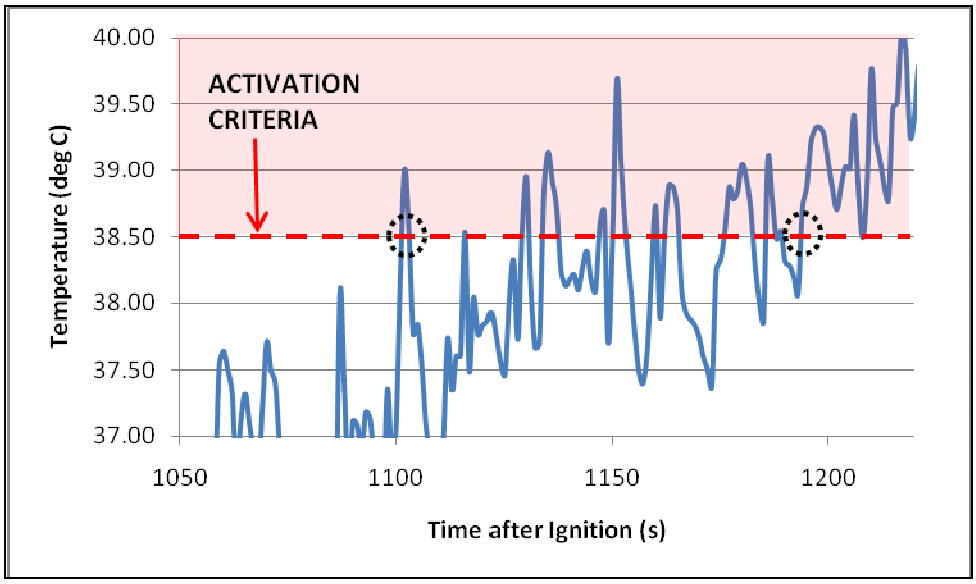

Figure 44 CDT16 Temperature Conditions: Bedroom Ionisation Detector

As is evident in Figure 44, a temperature of 39°C is not sustained after 502s, but rather drops back down and continues to fluctuate whilst continuing its upwards progression. If activation was instead considered to occur at the point in which the activation criterion was reached and sustained, the resultant time would be 602s, which is equivalent to the actual test activation time.

Applying the additional criterion that temperatures must be sustained for at least 5s for activation to be determined to occur, Table 19 provides a comparison between the

newly derived activation times and those shown in the previous Figures for Simulation 1.

	Lounge			Entry Hall			Landing			Bedroom		
Activation Criterion	**4°C**	**13°C**	**20°C**	**4°C**	**13°C**	**20°C**	**4°C**	**13°C**	**20°C**	**4°C**	**13°C**	**20°C**
Original	52s	171s	179s	255s	290s	319s	283s	343s	425s	342s	458s	N/A
Modified	50s	171s	179s	256s	290s	319s	283s	335s	385s	333	441s	N/A
Experiment	48s			293s			277s			602s		

Table 19 CDT16 Temperature Correlation: Comparison between derived Activation Times

It is apparent that the modified acceptance criterion typically does not result in the derivation of a different activation. In the instances where this is seen to occur, the new activation times are actually seen to be less comparable to the experimental data. As such, for CDT17 and CDT19, the original consideration that activation occurs once the temperature criterion is reached is maintained. This is also understood to be adopted by Brammer in his research.

5.2.2. Heskestad Method

The derived detector activation times using the Heskestad prediction algorithm are shown in Figure 45 to Figure 48. The change in heat of combustion from 20MJ/kg to 25MJ/kg is seen to have little influence on the derived activation times, with the higher heat release rate (i.e. greater heat of combustion) deriving only slightly earlier activation times. The extent of this difference does however increase with distance from the fire.

Whilst the simulations with the higher soot yield are shown to derive the earliest activation times, the difference between the simulation results is not significant. With the soot yield defined in Simulations 2 and 5 at least double that defined within alternative Simulations, the derived activation times within the lounge vary by only 6s, on the landing 15s and within the bedroom, 21s. Excluding the results for the entry hall, the magnitude of the difference between these derived activation times for the various scenarios is seen to increase with distance from the fire. The results derived within the entry hall have a greater range than the other locations, this range being 52s, due to the locations of the two detectors relative to the lounge door opening and the stairway void. This is discussed further at a later stage of this report.

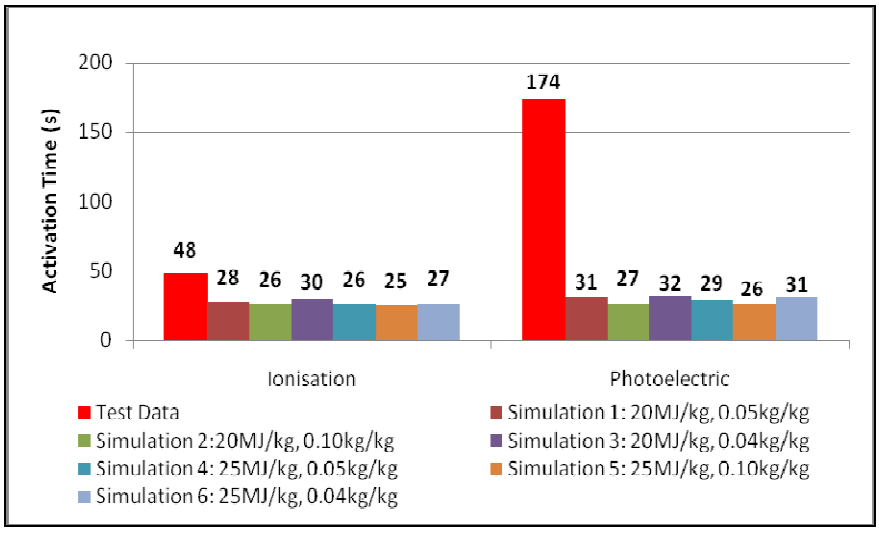

Figure 45 CDT16 Heskestad Method: Lounge

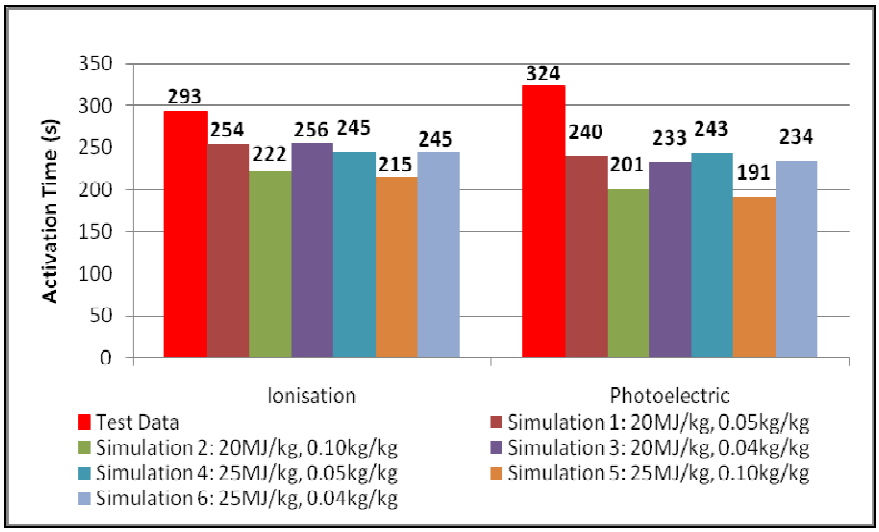

Figure 46 CDT16 Heskestad Method: Entry Hall

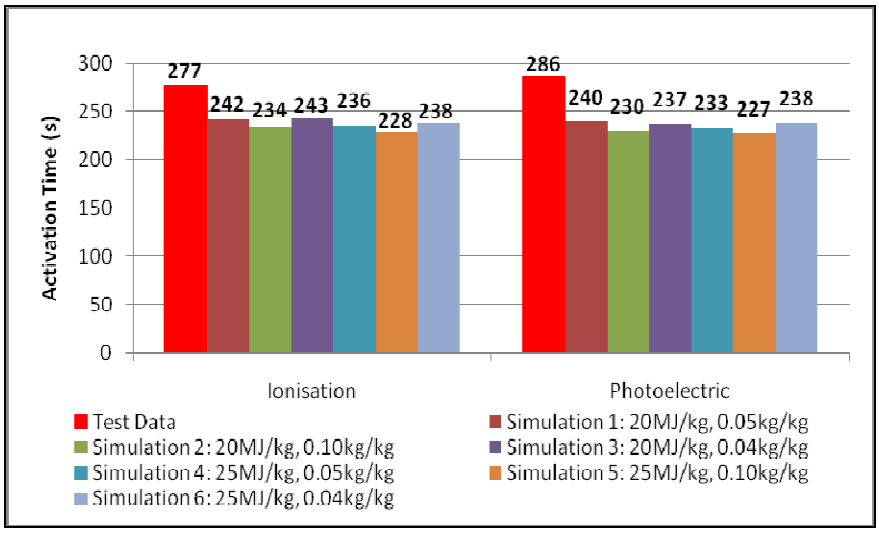

Figure 47 CDT16 Heskestad Method: Landing

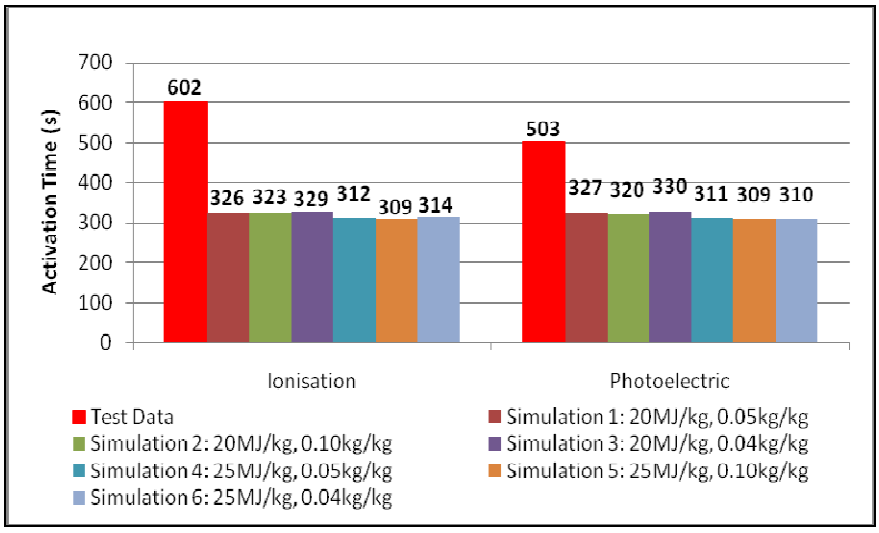

Figure 48 CDT16 Heskestad Method: Bedroom 2

As with the temperature correlation method, the Heskestad method does not provide any consideration of the mode of combustion relative to the operation mechanism of the subject detector, thus deriving comparable activation times for the ionisation and photoelectric detectors. The small difference between the results shown is simply due to the different locations of the detectors both within the experiment and in the FDS model.

Figure 45 also highlights the impact of defining a single fuel source within a simulation of a fire scenario. Whilst the initial stages of combustion within the experiment produced comparatively little visible smoke, within FDS simulations a constant soot yield was defined, this value being representative of that for the combustion of the armchair. The over prediction of soot yield during the early stages of the fire results in the significant under prediction of the activation time of the lounge photoelectric smoke detector. Such differences are not seen within the entry hall and landing as the detectors in these locations activate after the fire has begun to grow and the fire spread to the armchair. Whilst some degree of error may still be present in the derived activation times due to this initial over prediction of the soot yield, the effect on the results is not as significant.

Assessing the derived results against the experimental detector activation times, there is not seen to be a close resemblance. With all detector activation times being underestimated, simulations with the lower soot yield of 0.04kg_{soot}/kg_{fuel} provide the

most comparable results. Within the landing and entry hall results range from 73% to 87% of the actual activation times, and in the lounge (considering only the ionisation detector) and bedroom, the derived times are approximately half that which occurred during the experiment.

Whilst the derived activation times are approximately half the test data within both the lounge and bedroom, the magnitude of this difference is significantly less within the lounge. The magnitude of this variance between the derived and test data is in fact greater within the bedroom than in all other locations. This is a result of the over prediction of hazardous conditions within the bedroom derived towards the end of the simulation, as highlighted in Figure 32, where the temperature comparisons are provided between the FDS and experimental test data.

The temperature comparison graph is referred to in this instance as the optical density readings at the detector locations cannot be compared; this not being a measurement that was recorded during the experiments. The difference in optical density reading within the bedroom between experimental and derived activation times can be assessed, however only at heights of 0.5m and 1.5m above floor level. A similar situation also applies for the other detector locations. As shown in Figure 49, low level optical density results were recorded during the experiment within the bedroom at 1.5m above floor level, however after approximately 300s FDS derived values are seen to constantly increase during the simulations. Subsequently, the derived activation times from the FDS simulations range between 309s and 329s for the two detector locations, i.e. detection is determined to occur shortly after the continual increase in optical density begins.

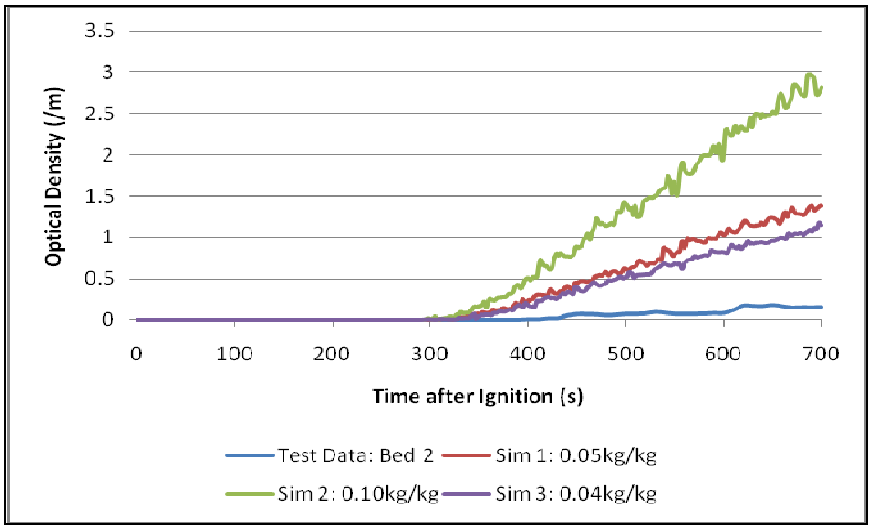

Figure 49 CDT16 Optical Density: Bedroom, 1.5m above floor level

5.2.3. Cleary Method

The derived results using the parameter combinations stated in Table 17 within the Cleary prediction algorithm provide comparable results at each detector location within a simulation. Typically, results between the two parameter combinations for each detector type vary by only a couple of degrees, as shown in Figure 50 for the lounge ionisation detector. The largest range between two activation times within a simulation is 9s, derived from Simulation 6, on the landing for the photoelectric detector; Figure 51. The results are also noted as being comparable to that derived using the Heskestad algorithm, thus many of the comments provided in the previous Section are also applicable in this instance.

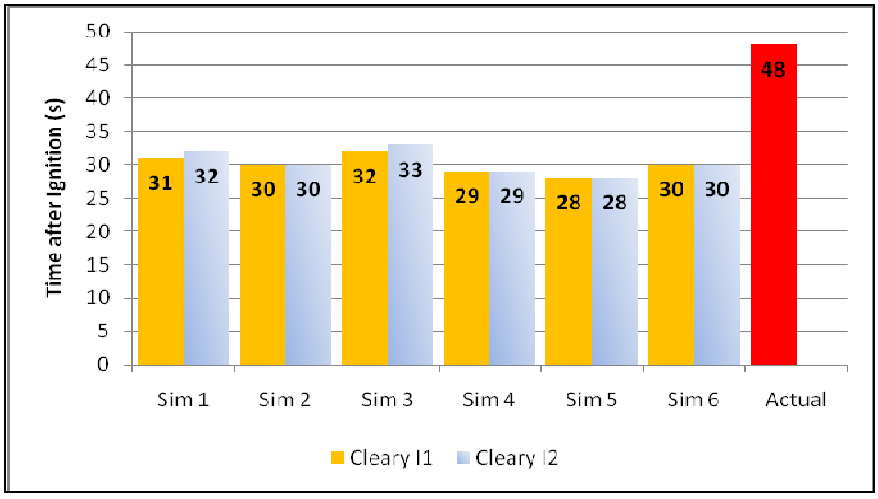

Figure 50 CDT16 Cleary Method: Lounge Ionisation

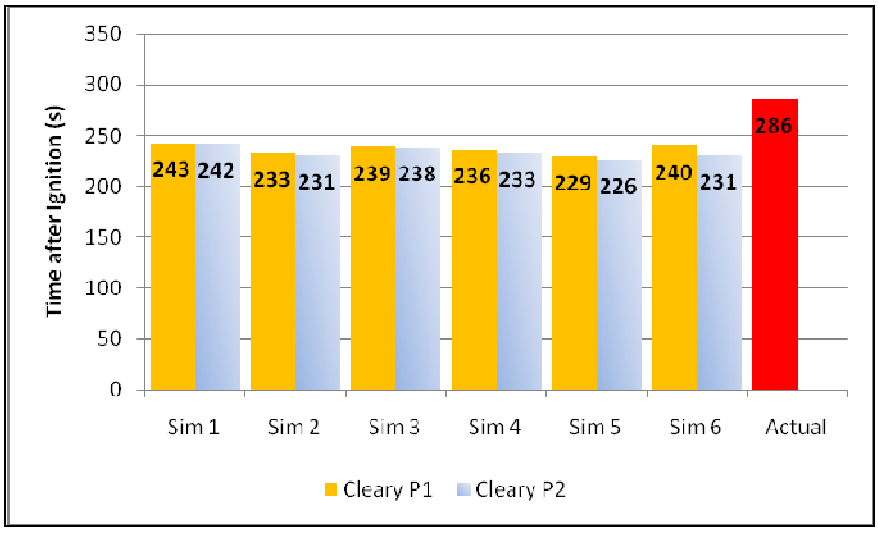

Figure 51 CDT16 Cleary Method: Lounge Photoelectric

The two Figures above highlight the similarity between the derived activation times for a given detector. As detailed with regards to the Heskestad algorithm results, assessment of the simulations with the higher effective heat of combustion (Simulations 4, 5 and 6) derive earlier activation times than their counterpart simulation in which an equivalent soot yield is defined (Simulations 1, 2 and 3 respectively). The range between these activation times is however not significant. Within the lounge, activation times vary by up to 3s, whilst further from the fire within the bedroom, the variance between the derived times from Simulations 3 and 6 is 23s for the photoelectric detector, as shown in Figure 52.

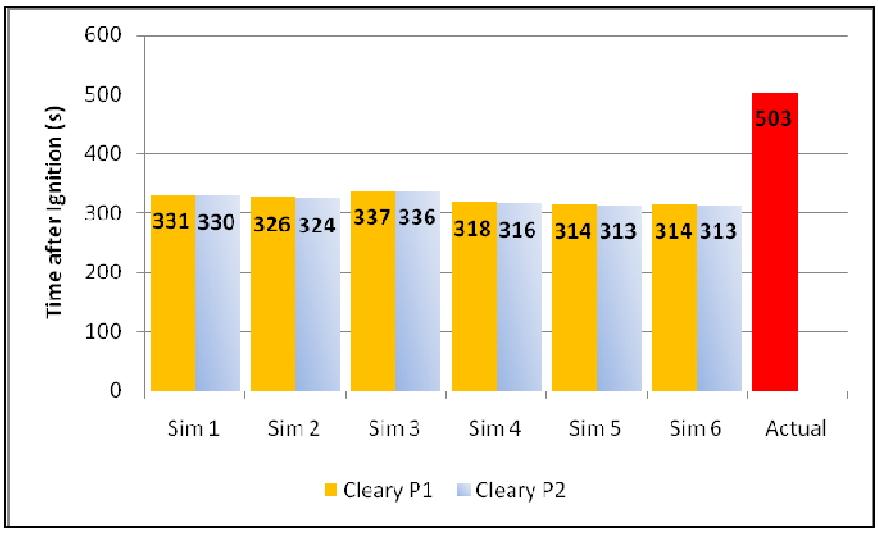

Figure 52 CDT16 Cleary Method: Bedroom Photoelectric

The largest variance in derived activation times at a given detector location occurs within the entry hall. As shown in Figure 53 and Figure 54, the activation times derived in Simulation 5 and 3 vary by 44s (25MJ/kg, 0.10kg_{soot}/kg_{fuel}; 20MJ/kg, 0.04kg_{soot}/kg_{fuel} respectively) at the photoelectric detector, and 40s at the ionisation. Within the bedroom the largest difference is 27s at the ionisation detector, on the landing 17s at the photoelectric, and 5s at the lounge ionisation detector.

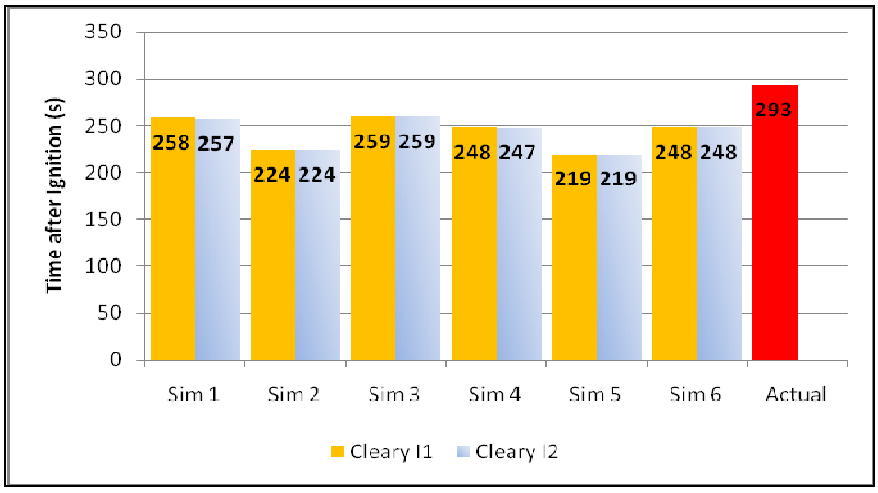

Figure 53 CDT16 Cleary Method: Entry Hall Ionisation

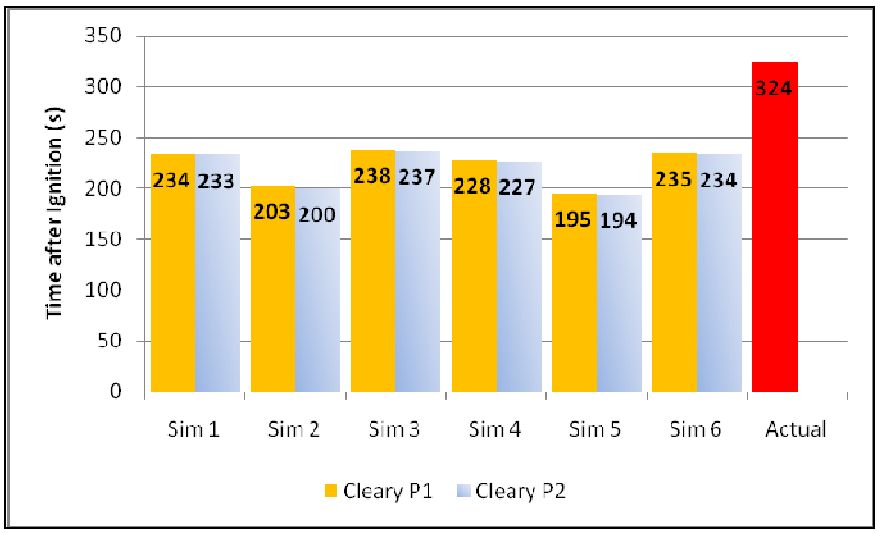

Figure 54 CDT16 Cleary Method: Entry Hall Photoelectric

Whilst different variables are used to assess the ionisation and photoelectric detectors, and noting that the experiment activation times of the two detector types differ, the derived activation times for the two detectors were found to be comparable at each location. This was apparent both near to the fire and at a distance, as shown in Figure

55 and Figure 56, which provide comparison between the lounge and bedroom ionisation and photoelectric results respectively. The only exception to this occurs in the entry hall where a larger range is seen, as shown in Figure 57.

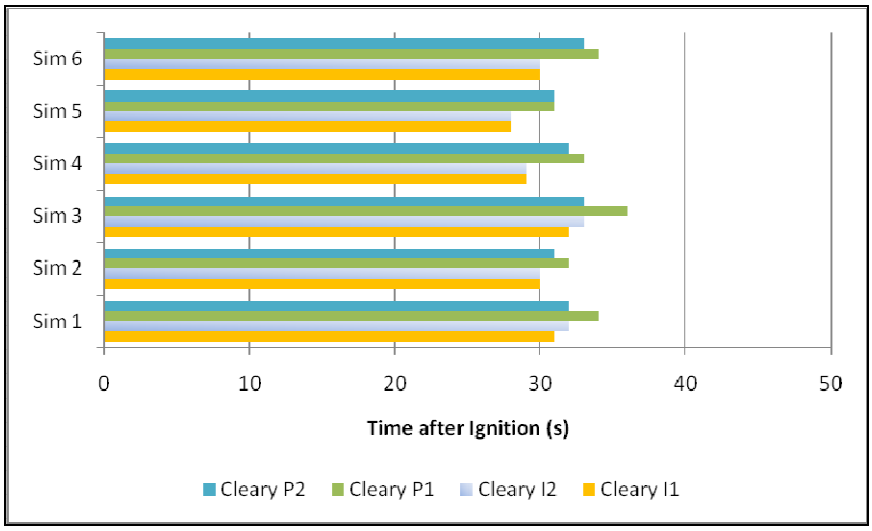

Figure 55 CDT16 Cleary Method: Lounge Ionisation and Photoelectric

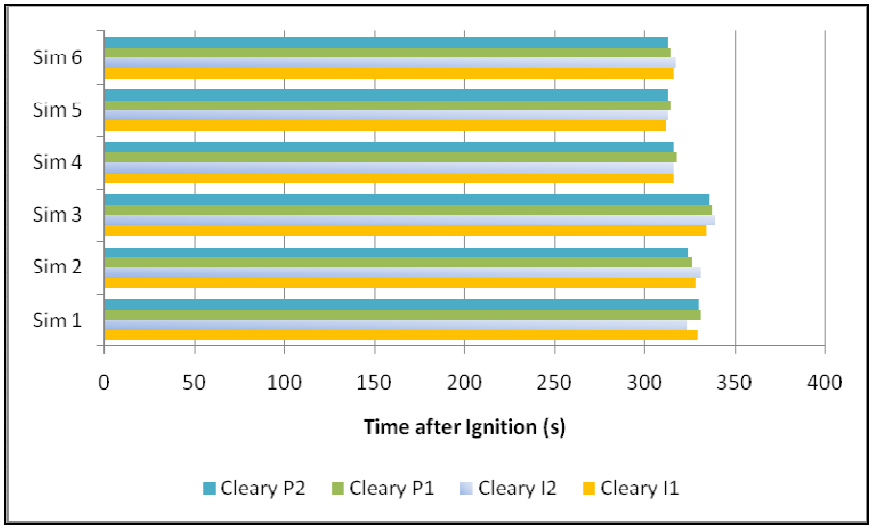

Figure 56 CDT16 Cleary Method: Bedroom Ionisation and Photoelectric

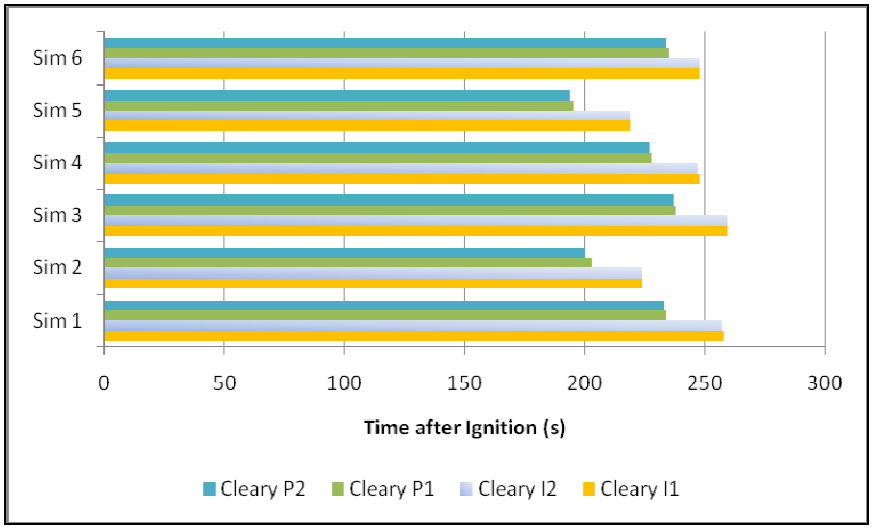

Figure 57 CDT16 Cleary Method: Entry Hall Ionisation and Photoelectric

Assessing the derived results against the experimental detector activation times, there is not seen to be a close resemblance. This was similarly stated when comparing the derived Heskestad results. All detector activation times are underestimated, thus simulations with the lower soot yield of $0.04kg_{soot}/kg_{fuel}$ provide the most comparable results.

The magnitude of the difference between the derived and test activation times is greatest within the bedroom, resulting from the over prediction of hazardous conditions in this location towards the end of the simulation. This has already been discussed in Section 5.2.2 and the reader is referred back to this location for further details.

5.3. CDT17

5.3.1. Temperature Correlation Method

Figure 58 and Figure 59 provide the derived activation times when applying the temperature correlation method to the temperature results of the CDT17 FDS simulations with an effective heat of combustion is 20 MJ/kg; i.e. Simulations 1, 2 and 3. In this fire scenario, where the lounge door is open, the results are seen to be comparable to each other at each given detector location, with derived activation times varying by only a few degrees between the simulations. As noted in Section 5.3, this

variance is a result of the small degree of noise included within FDS simulations at their initiation.

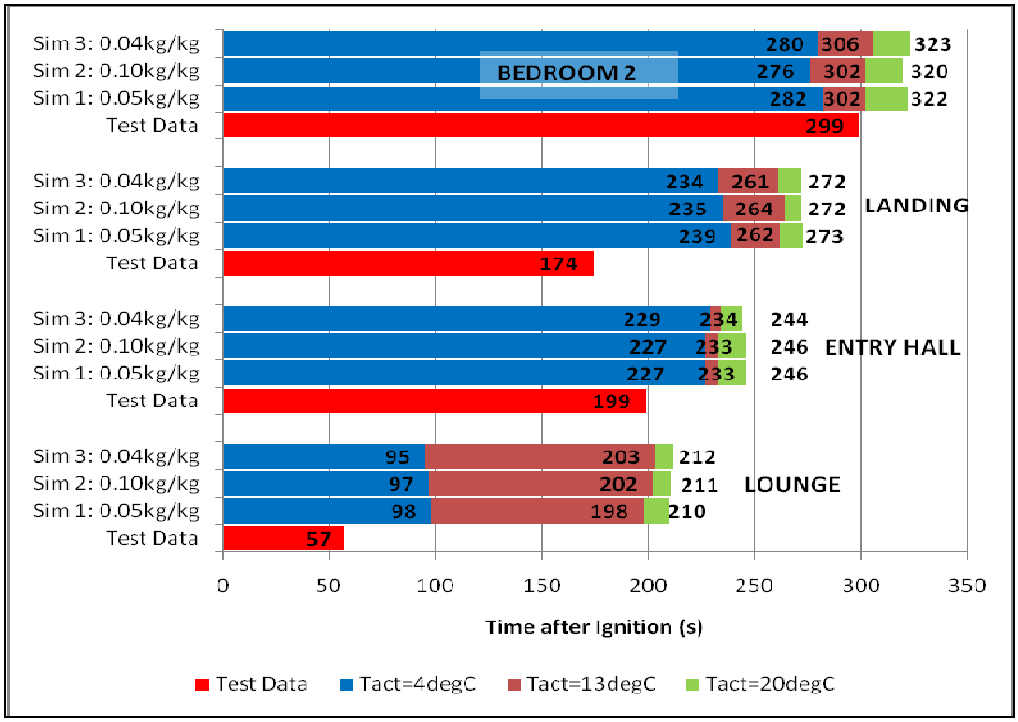

Figure 58 Temperature Correlation: CDT17_1, 2 & 3 Ionisation Detectors

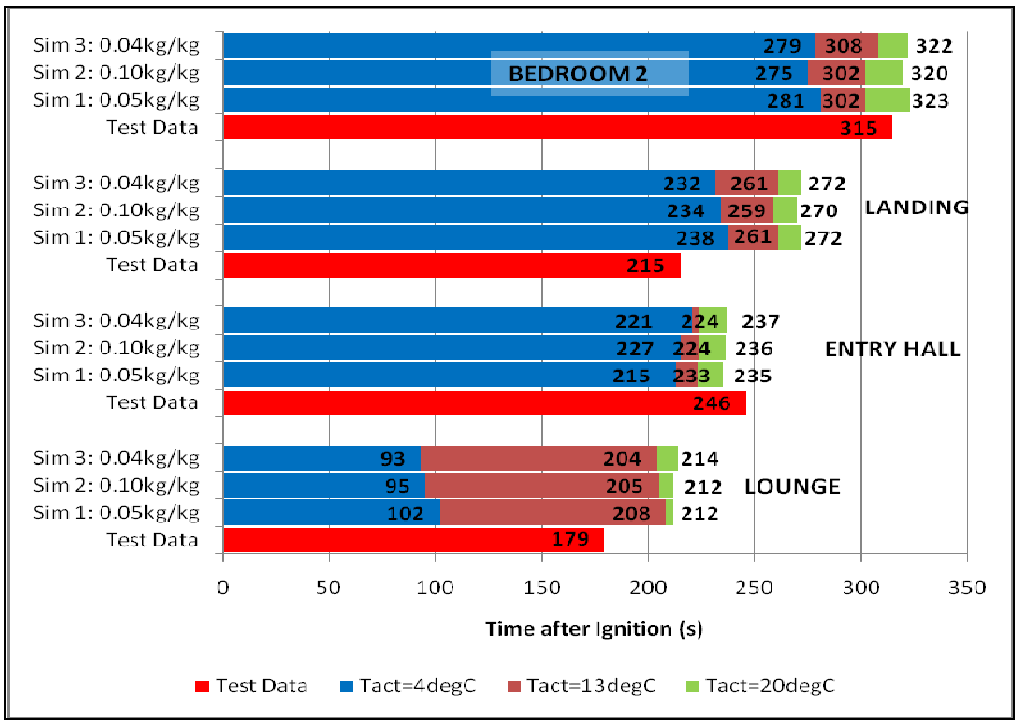

Figure 59 Temperature Correlation: CDT17_1, 2 & 3 Photoelectric Detectors

In this fire scenario, the temperature correlation method typically overpredicts the activation time for the ionisation detector. Considering an activation criterion of 4°C above ambient at the ionisation detector locations, the activation times are overpredicted by approximately 40s, 29s and 61s within the lounge, entry hall and landing respectively. Within the bedroom this activation criterion underpredicts the experimental activation time by approxiamtely 19s, with the activation criterion of 13°C deriving results within 3s of the actual test activation time.

Whilst the ionisation detector activation times are typically overpredicted this is not seen for the photoelectric detectors. Rather, the dervied conditions produce early activation times within the lounge, entry hall and bedroom when assessing with an activation criterion of 4°C. The difference to the test data is approxiametely 77s, 31s and 34s respectively. Within the entry hall even an activation criterion of 20°C still derives an activation time approximately 10s earlier than that of the test data. The only location where an overprediction of the test data results for an activation criterion of 4°C above ambient is on the landing, where the difference in times is approxiametly 19s.

Figure 60 and Figure 61 provide the derived activation times at the various detector locations for Simulations 4, 5 and 6. Comparing Figure 58 to Figure 60 and Figure 59 to Figure 61 it is evident that simulations 4, 5 and 6, provide earlier activation times than Simulations 1, 2 and 3, as expected given the higher heat of combustion defined. This difference is however not extensive, with 19s being the greatest range, as occurs within the lounge at the photoelectric detector.

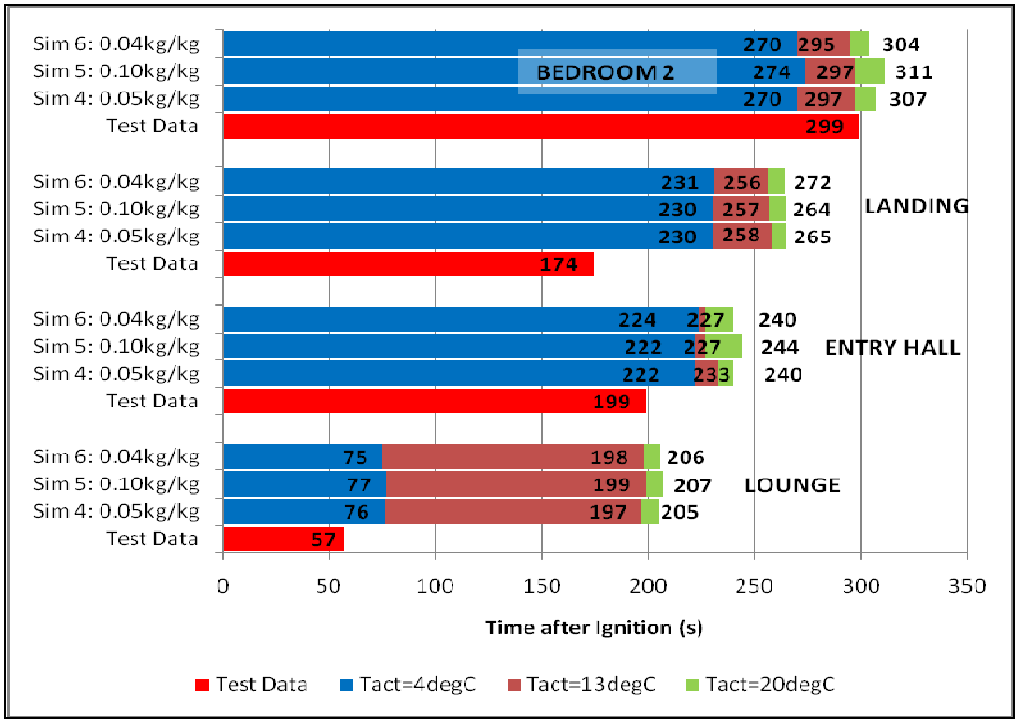

Figure 60 Temperature Correlation: CDT17_4, 5 & 6 Ionisation Detectors

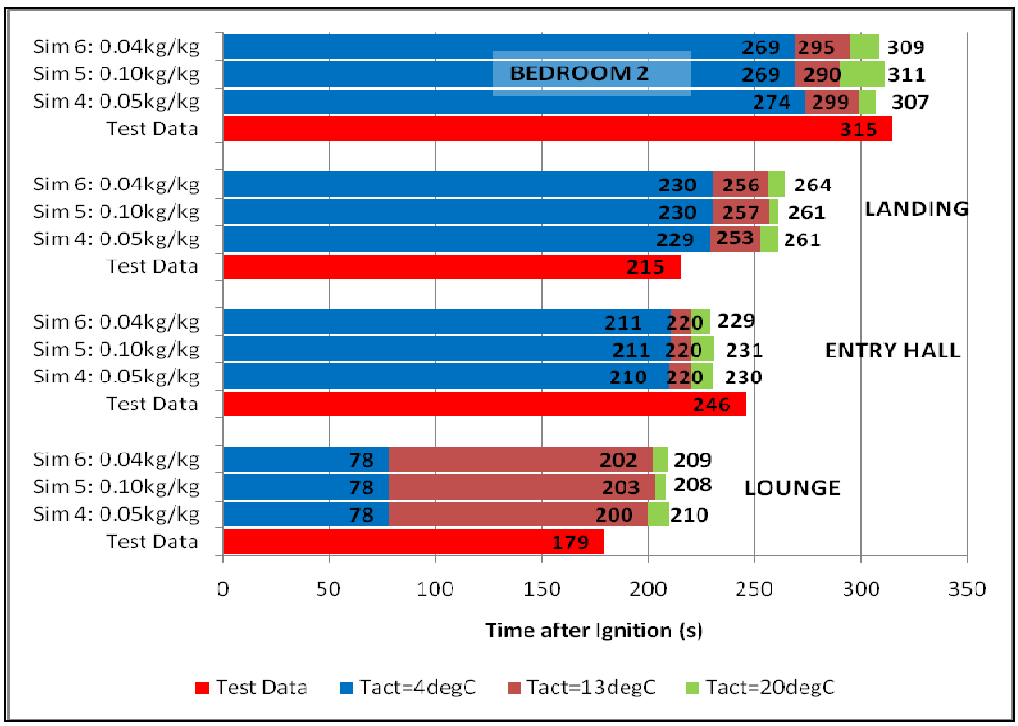

Figure 61 Temperature Correlation: CDT17_4, 5 & 6 Photoelectric Detectors

For each detector type and location, the derived results are seen to be most comparable to the real test data for the same activation criterion when comparing equivalent soot yield simulations for the two effective heats of combustion. Table 20 states the

criterion that derives an activation time most comparable to that of test data at each detector location.

Detector Type	Activation Criterion			
	Lounge	Entry Hall	Landing	Bedroom
Ionisation	4°C	4°C	4°C	13°C
Photoelectric	13°C	20°C	4°C	20°C

Table 20 CDT17 Activation Criterion Comparable to Experimental Detector Activation Times

At each of the detector locations the difference in derived temperature to ambient, as defined in Table 13, at the time of detector activation during the experiments, is stated in Table 21 and Table 22 for the ionisation and photoelectric detectors respectively.

Location	Ambient Temperature (°C)	Sim 1 (°C)	Sim 2 (°C)	Sim 3 (°C)	Sim 4 (°C)	Sim 5 (°C)	Sim 6 (°C)
Effective Heat Combustion (MJ/kg)		**20**	**20**	**20**	**25**	**25**	**25**
Soot Yield (kg/kg)		**0.05**	**0.10**	**0.04**	**0.05**	**0.10**	**0.04**
Lounge	**27**	-2	-2	-2	-2	-2	-2
Entry Hall	**27**	0	0	0	0	0	0
Landing	**23**	0	1	1	1	1	1
Bedroom 2	**25**	2	10	10	16	15	13

Table 21 CDT17 Temperature Difference to Ambient at Experimental Activation: Ionisation Detectors

Location	Ambient Temperature (°C)	Sim 1 (°C)	Sim 2 (°C)	Sim 3 (°C)	Sim 4 (°C)	Sim 5 (°C)	Sim 6 (°C)
Effective Heat Combustion (MJ/kg)		**20**	**20**	**20**	**25**	**25**	**25**
Soot Yield (kg/kg)		**0.05**	**0.10**	**0.04**	**0.05**	**0.10**	**0.04**
Lounge	**27**	-1	-1	-1	0	0	0
Entry Hall	**26**	28	19	26	34	33	37
Landing	**23**	0	1	1	1	1	1
Bedroom 2	**25**	12	14	14	20	22	21

Table 22 CDT17 Temperature Difference to Ambient at Experimental Activation: Photoelectric Detectors

With the exception of within the bedroom and the photoelectric detector within the entry hall, the temperatures at the time of smoke detector acitvation within the experiment are seen to be approximately equivalent to ambient. The temperatures within the lounge are infact below that of the derived ambient temperatures. Comparing experimental and derived temperatures at high level within the lounge after igntion, as shown in Figure 62 for Simulation 1, it can be seen that there is a lag in the

time unitl temperature rises occur within the FDS simulation. Highlighting the time period shortly after ignition within Figure 63, the extent of the effect of this is evident.

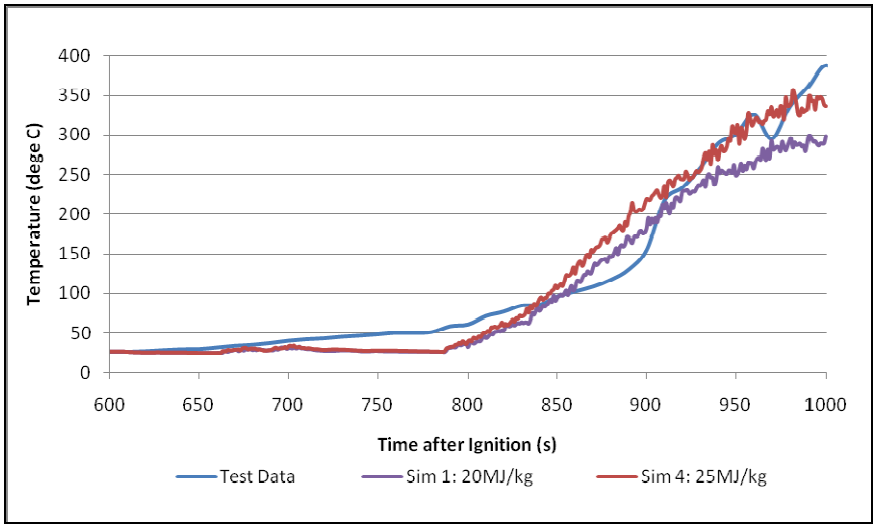

Figure 62 CDT17_1 Temperature Profile: Lounge Thermocouple; z_8

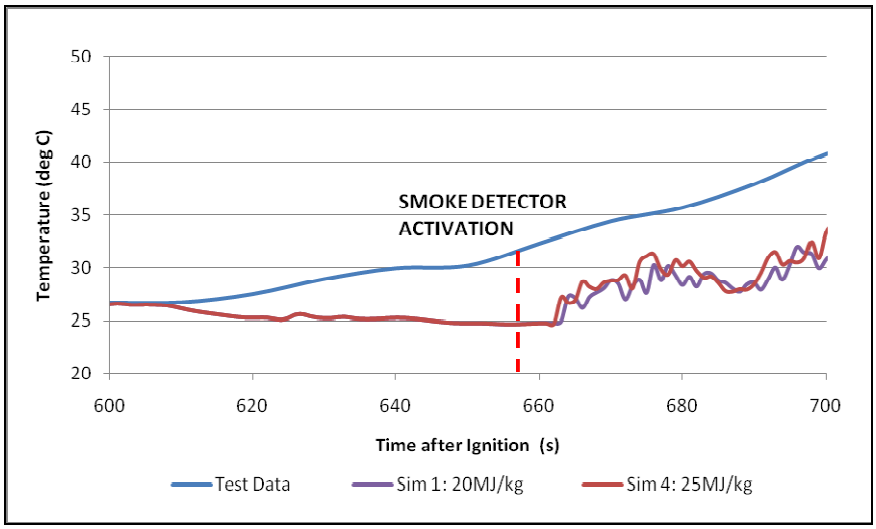

Figure 63 CDT17_1 Temperature Profile Section: Lounge Thermocouple; z_8

This difference in temperature at the early stages of the fire is considered to be a result of errors within the heat release rate profile after the smoothing of the mass data. Smoothing of the mass data was necessary given the degree of noise present, which saw the mass of the chair increase on occassions, however it has resulted in the removal of small perturbation within the heat release rate profile that occured shortly after igntion. With the removal of the radiatior from the lounge at the time of ignition and the delay until fire growth begin, temperatures are thus seen to drop.

5.3.2. Heskestad Method

The derived detector activation times using Heskestad's prediction algorithm are shown in Figure 64 to Figure 67. The results derived within the lounge and bedroom are comparable across the simulations, whilst there is a greater range between the activation times derived on the landing and within the entry hall. This is a result of the fluid flow patterns through the house. For the initial time period after ignition, conditions throughout the house are comparable between the simulations as the differences between the input parameters are not yet evident. Given that the lounge detectors activate during this early stage the derived results are similar.

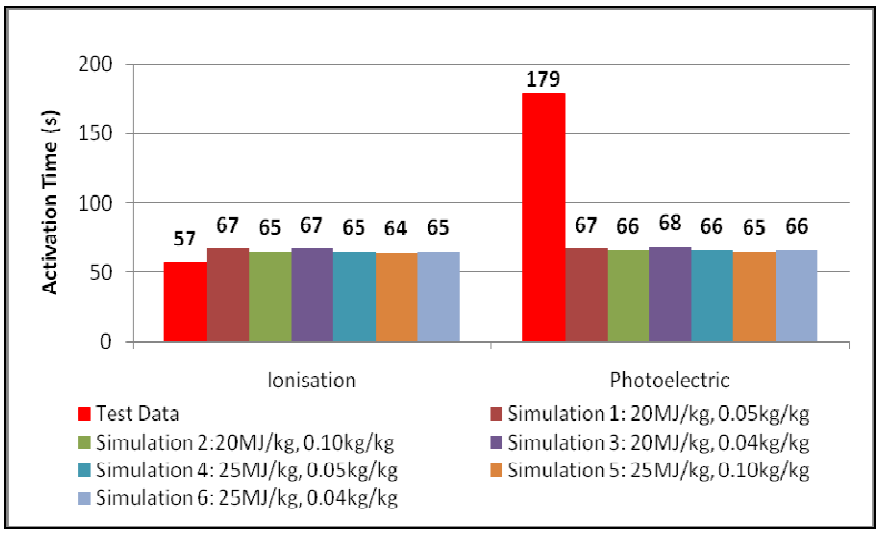

Figure 64 CDT17 Heskestad Method: Lounge

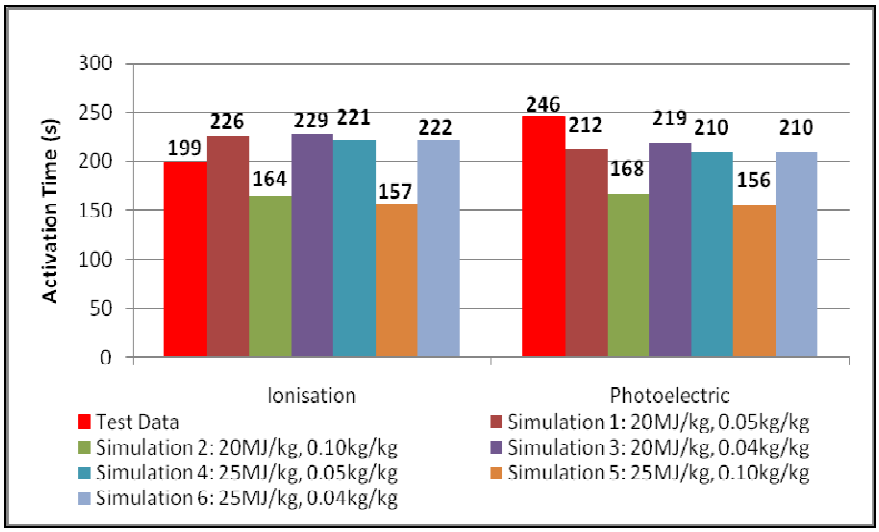

Figure 65 CDT17 Heskestad Method: Entry Hall

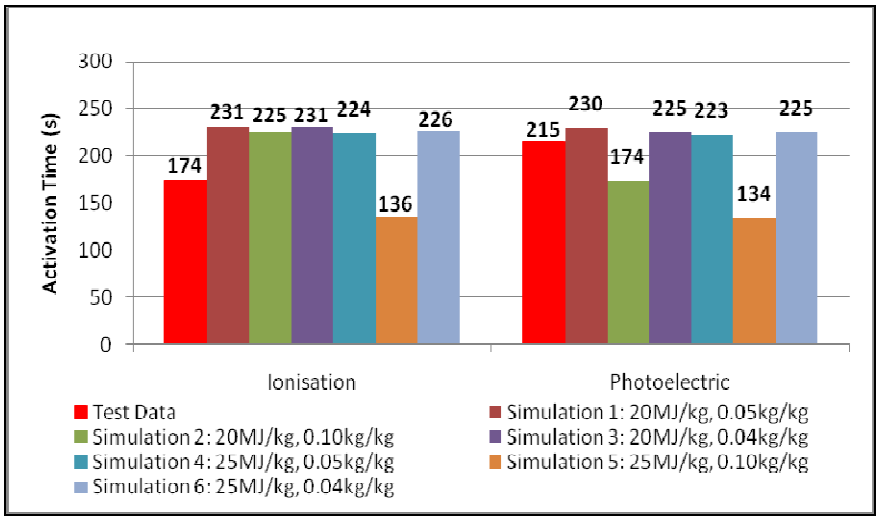

Figure 66 CDT17 Heskestad Method: Landing

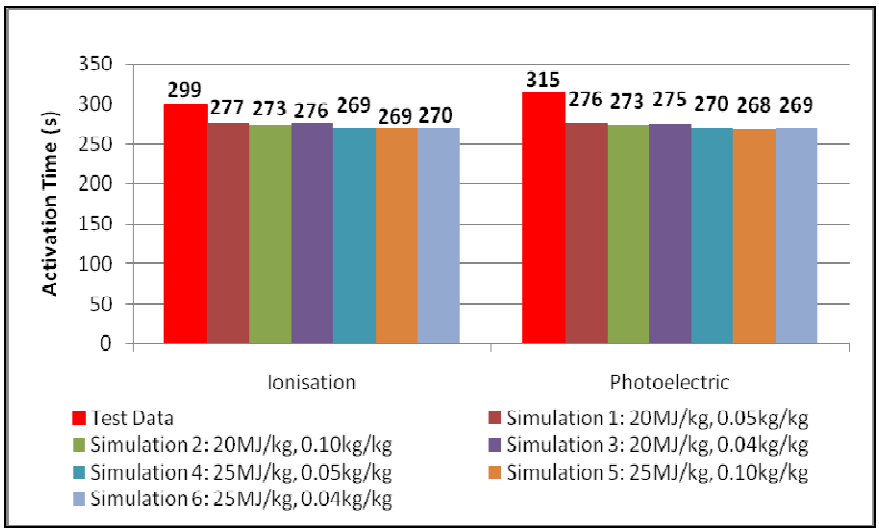

Figure 67 CDT17 Heskestad Method: Bedroom

Being the room of fire origin, a well defined smoke layer forms within the lounge. During the initial stages of its development a small volume of the rising smoke continuously flows through the doorway into the entry hall. Due to natural buoyancy effects this smoke rises, flowing through the stairway void to the First floor landing. The location of a detector relative to the flow paths of this smoke and its density, will determine as to when activation occurs, resulting in the greater variance in results seen at these locations. This is the reason for the large difference in activation times within Simulation 2 on the landing between the ionisation and photoelectric detectors in comparison to the other simulations.

Simulations 2 and 5 have soot yields of $0.10kg_{soot}/kg_{fuel}$ and thus a larger volume of smoke is produced during the combustion process than in the other simulations. Whilst the separation distance between the ionisation and photoelectric detectors is not significant, it is of sufficient length that enough smoke is recorded at the photoelectric detector location for activation but not at the ionisation detector as a result of transport effects including agglomeration, deposition and loss of buoyancy, as referred to in Section 1.1.1. Activation is therefore not seen to occur until the fire is more developed and a larger volume of smoke is flowing through the stairway void into the landing. In Simulation 5, where the effective heat of combustion is greater, higher temperatures result and thus more buoyant smoke particles. A greater density of smoke therefore reaches the ionisation detector location during the earlier time period, resulting in activation.

This large range in activation times is not seen within the result derived for the detectors within the bedroom as sufficient smoke does not flow into this room until a significant volume of smoke has developed within the landing, and the developing layer dropped below the height of the door frame. It is noted that the smoke layer within the landing is not as well defined as that within the lounge due to the constant ejection of fluid through the stairway void creating turbulence. Smokeview images are provided over a period of time during the simulation as Figure 68 to Figure 73, highlighting this movement of smoke.

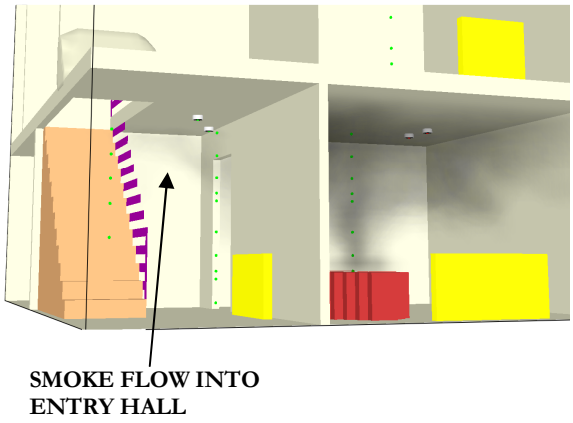

Figure 68 CDT17 100s after Ignition

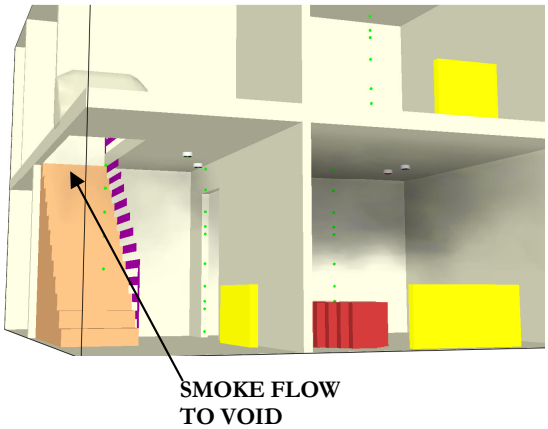

Figure 69 CDT17 117s after Ignition

Figure 70 CDT17 173s after Ignition

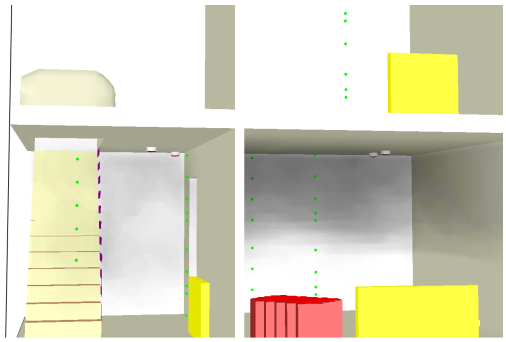

Figure 71 CDT17 176s after Ignition

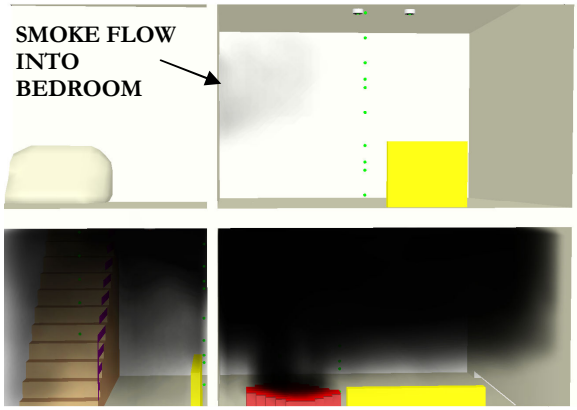

Figure 72 CDT17 249s after Ignition

Figure 73 CDT17 249s after Ignition

Assessing the derived results against the actual test data there is not seen to be any consistency as to when or where they are comparable or rather if activation times are over predicted or under predicted. For the ionisation detectors, derived activation times are within approximately 10s for all simulations. In the entry hall and landing the lower soot yields are found to results in activation times greater than the test data, whilst the larger soot yield of 0.10kg_{soot}/kg_{fuel} typically derive activation times earlier than the test data. All simulations are seen to derive activation times 20 to 30s earlier than the test data within the bedroom.

Considering the photoelectric detectors, the lounge predictions are significantly less than the actual activation time during the experiment for all scenarios. In the entry hall and bedroom earlier activation times were also derived, however on the landing earlier activation times where derived for the higher soot yield simulations but not those with the lower defined value.

5.3.3. Cleary Method

As occurred with the assessment of CDT16, the derived activation times utilising the Cleary algorithm are comparable both to each other, and to the results derived using the Heskestad algorithm, within the lounge and bedroom. Examples of this are shown in Figure 74 and Figure 75, which present the derived activation times within the lounge for the ionisation detector, and within the bedroom for the photoelectric detector respectively.

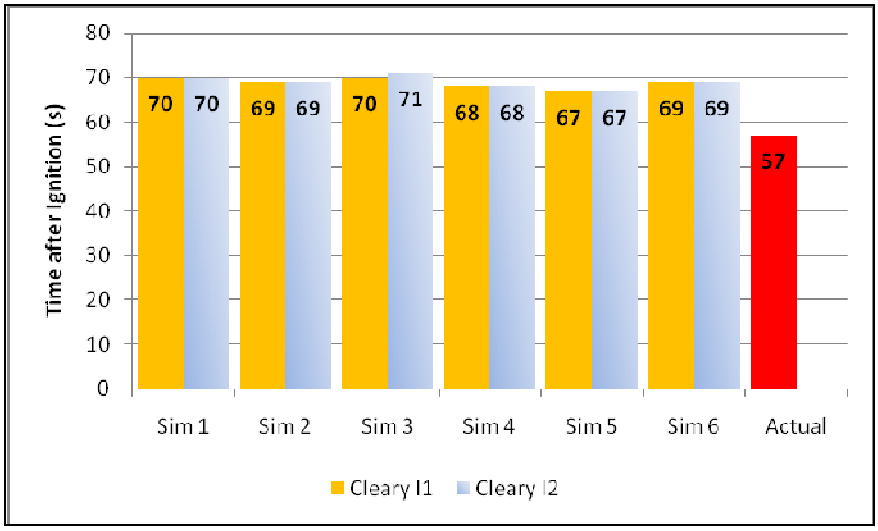

Figure 74 CDT17 Cleary Method: Lounge Ionisation

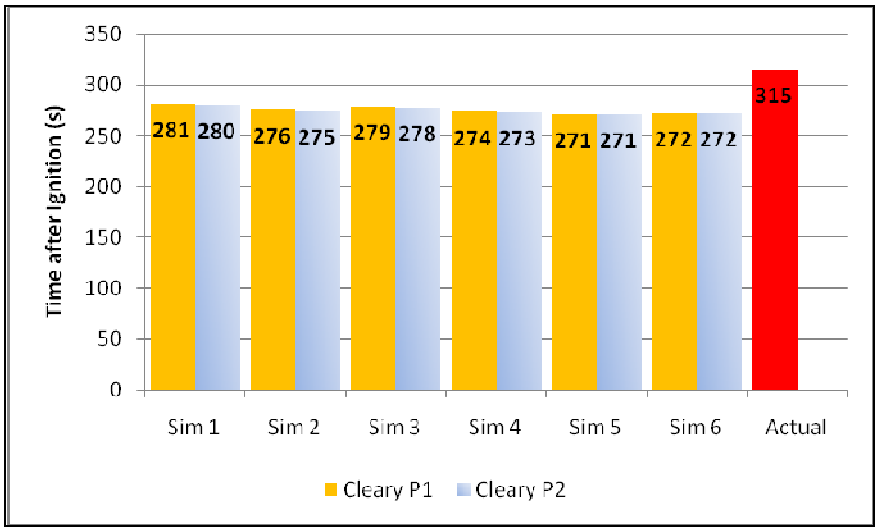

Figure 75 CDT17 Cleary Method: Bedroom Photoelectric

Within the entry hall, however Simulations 2 and 5, with the higher soot yield values, derive significantly earlier activation times. This is shown in Figure 76 and Figure 77.

At the ionisation detector location the derived activation times in Simulations 2 and 5 are approximately 35s earlier than the test data, whilst the remaining simulations derive times approximately 30s later that the test data. At the photoelectric detector, all simulations derive an activation time prior to that which occurred during the experiment, this being approximately 70s for the higher soot yield simulations and 30s for those with the lower soot yield defined. This variation is a result of the location of the detectors relative to the lounge and the path of travel of the smoke from the lounge through the stairway void to the landing, as discussed previously.

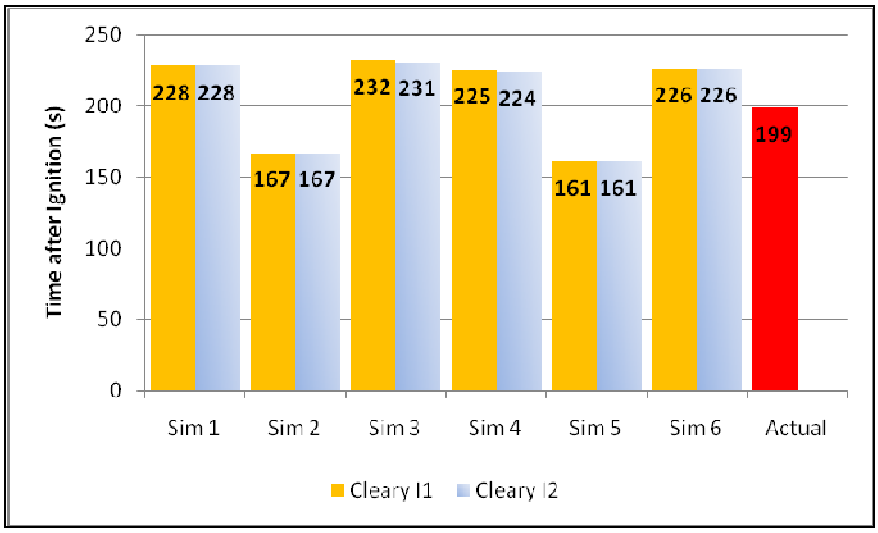

Figure 76 CDT17 Cleary Method: Entry Hall Ionisation

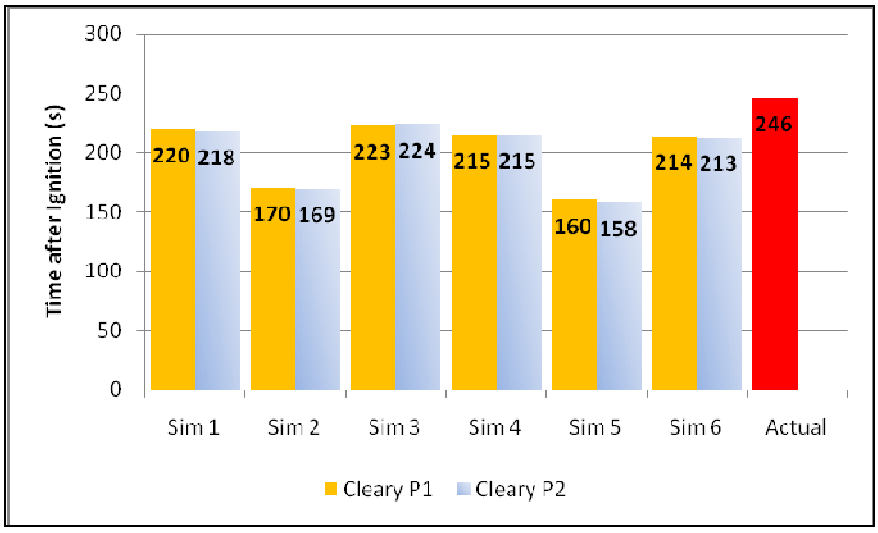

Figure 77 CDT17 Cleary Method: Entry Hall Photoelectric

Activation times for the detectors located on the landing show similar results to that for the entry hall, with the exception of the result derived using the second parameter

combination within the Cleary method at the ionisation detector; refer to Figure 78 and Figure 79. Again, the earlier activation times seen are a result of the location of the detectors relative to the lounge and the path of travel of the smoke to reach this location. The density of smoke present at the ionisation detector location is seen to be sufficient for activation when considering one of the parameter combinations within the prediction algorithm, but not the second. At the photoelectric detector, both parameter combinations derive earlier activation that the simulations with lower soot yields, however one is still found to predict activation 18s earlier than the other.

It is noted that these derived activation times on the landing in Simulation 2 is the only instance where the Cleary results are not comparable to that derived within the Heskestad assessment. On all other occasions the results derived by the two methods are within one to two seconds of each other. The Heskestad prediction algorithm derived activation times to be 225s at the ionisation detector and 174s at the photoelectric. For both detector types Heskestad's activation times are between the two derived Cleary results, being a closer resemblance to the second ionisation and photoelectric algorithm parameters shown in Table 17 respectively.

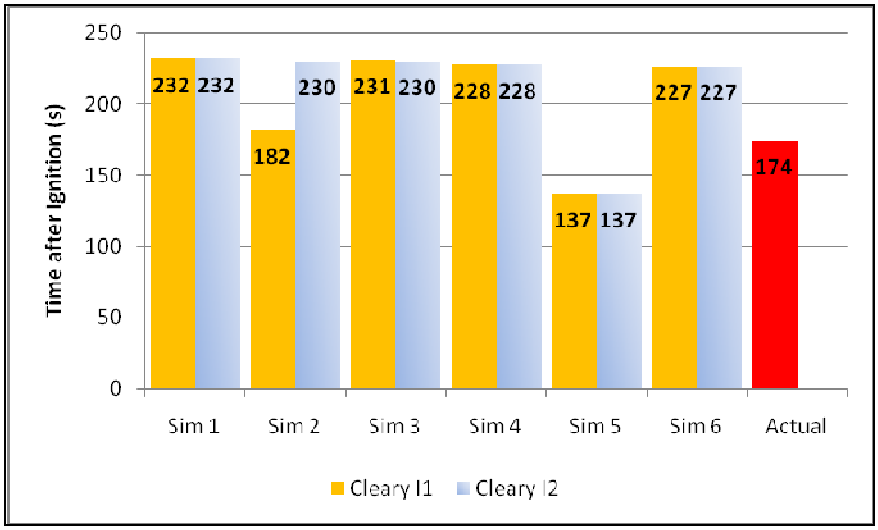

Figure 78 CDT17 Cleary Method: Landing Ionisation

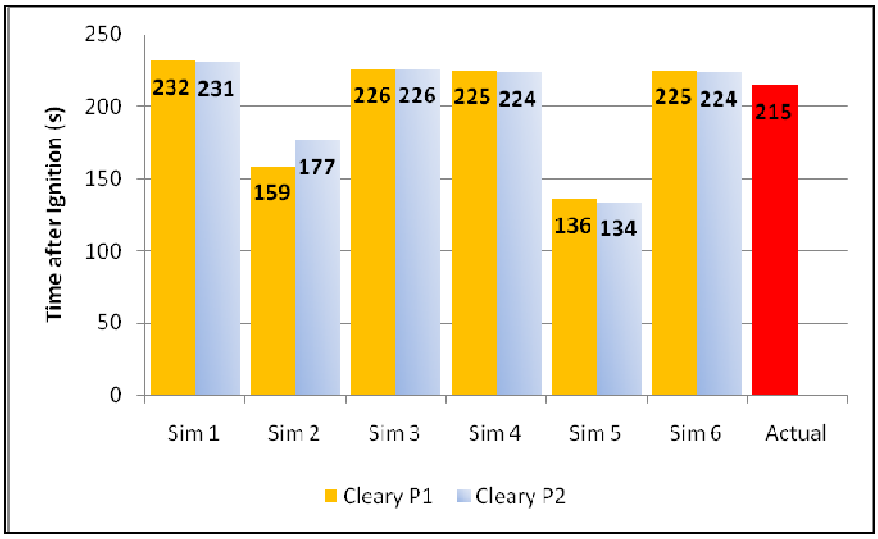

Figure 79 CDT17 Cleary Method: Landing Photoelectric

Assessing the results against the experimental smoke detector activation times, with the exception of within the bedroom the ionisation detector activation times are over predicted with the lower soot yield values and also over predicted within the lounge for the higher soot yield value. Under predictions occur on the landing and entry hall. Within the bedroom, all derived activation times are under predicted.

Considering the photoelectric detectors, all activation times under predict the test data within the lounge, entry hall and bedroom. On the landing the higher soot yield simulations derive an earlier prediction time, whilst the lower soot yields derive activation times delayed by up to 30s after that within the experiment.

5.4. CDT19 Results

5.4.1. Temperature Correlation Method

Figure 81 and Figure 82 provide the derived activation times when applying the temperature correlation method to the results of the CDT19 FDS simulations in which an effective heat of combustion of 20MJ/kg is defined; i.e. Simulations 1, 2 and 3. As with the previous fire scenarios assessed, the derived activation times are comparable at each detector location, with the largest range being 7s, which occurs within the bedroom. In contrast to CDT17 were initial perturbations where seen to be removed by the smoothing of the mass data, within CDT19 the smoothing process finds such

perturbations to occur shortly after ignition. The derived heat release rate profile defined within the CDT19 simulations is shown in Figure 80, with Figure 18 previously providing a comparison of the experimental versus smoothed mass loss history.

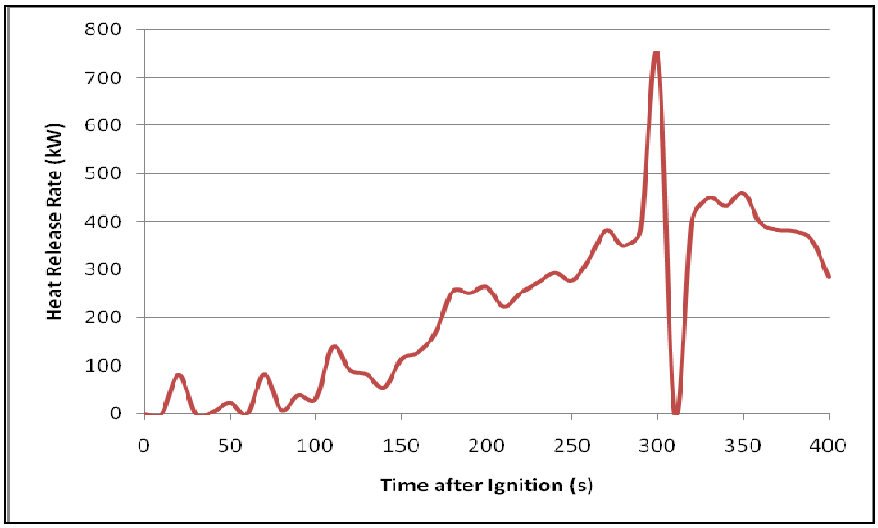

Figure 80 Heat Release Rate: CDT19

These initial perturbations result in an early peak in the derived temperatures of large enough magnitude to result in the derivation of early activation times within the lounge. The size of this initial peak is sufficient to derive equivalent activation times for the activation criterion of 4°C and 13°C. A criterion of 20°C derives activation to occur only 4s later. Similarly within the entry hall the 4°C and 13°C activation criteria derived similar results, however temperatures are seen to take longer to rise 20°C above ambient beyond the room of fire origin.

As expected, the derived activation times at the ionisation and photoelectric detectors are found to be comparable. The variance seen between these results is due to the smoke flow patterns throughout the house and the relative locations of the detectors. The photoelectric detector in the entry hall is located closer to the centre of the smoke flow path fromteh lounge to hte landing than the ionisation and as a result there is a slight lag between the temperatures at the two locations during the early stages of the fires development. A similar situation applies on the landing as has been discussed in Section 5.3.2, where the flow path of the smoke up through the stair void passes the photoelectric detector prior to the ionisation detector.

In this fire scenario, the temperature correlation approach derives smoke detector activation to occur both prior to that within the experiment and after, dependent on the location and the activation criteria being considered. Within the lounge and landing, as activation criterion of 13°C provides a close comparison to the test data, the times being within 5s. In the entry hall and bedroom however, an activation criterion of 20°C predicts activation to occur approxiamtely 70s and 50s respectively, prior to that which occurs during the experiment.

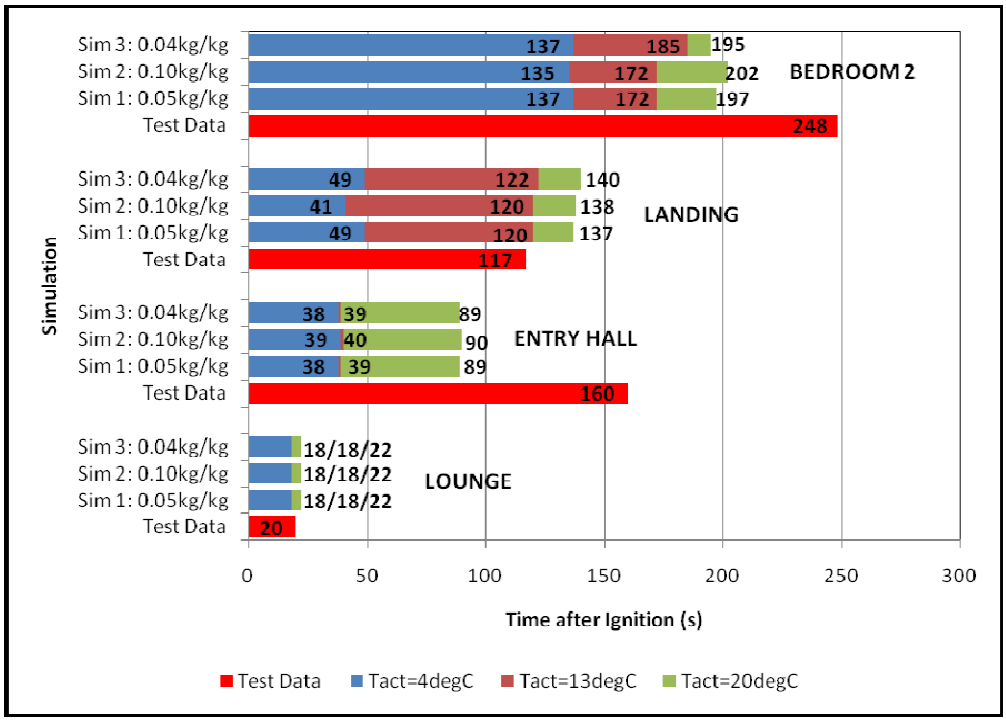

Figure 81 Temperature Correlation: CDT19_1, 2 & 3 Ionisation Detectors

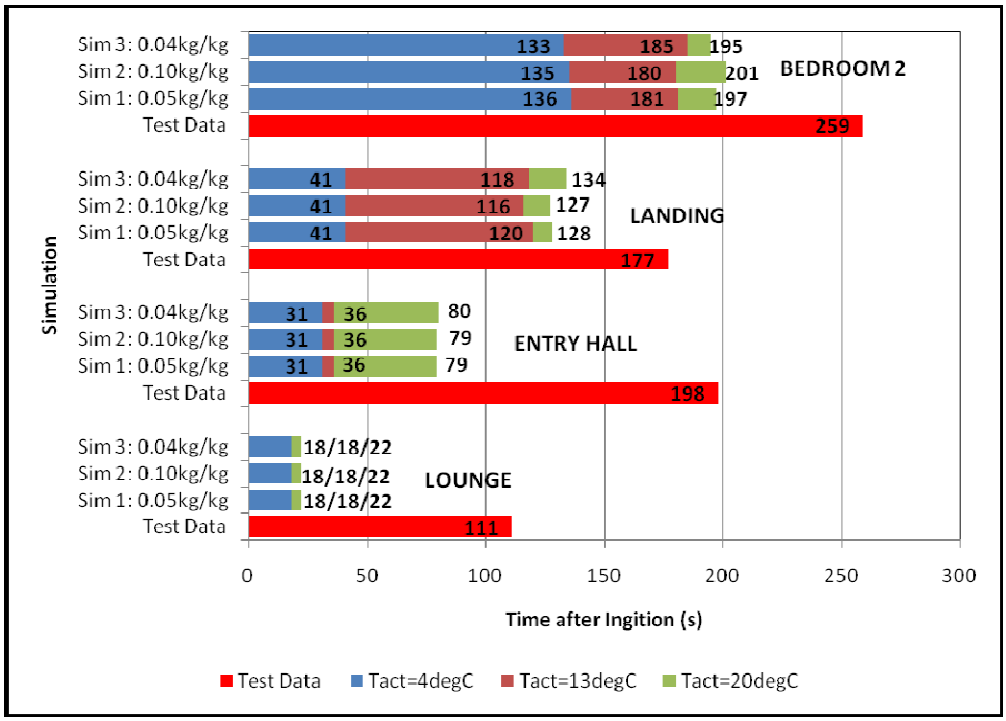

Figure 82 Temperature Correlation: CDT19_1, 2 & 3 Photoelectric Detectors

A different scenario is seen with the photoelectric detectors, where the temperature correlation method predicts activation significantly earlier than the test data. The most comparable result is derived within the lounge, where the activation times differ by approxiametly 50s.

Overall, result are not found to be comparable to the experimental smoke detector activation times. In accordance with Spearpoint (2002), the growth of the fire was not seen to accelerate until 167s, when flames spread to the back of the chair. From the smoothed mass data, growth of the fire is however derived to begin approximately 80s after ignition, as seen in the heat release rate profile shown in Figure 18.

Comparing the temperatures derived at the highest thermocouple locations of the thermocouple tree located within the lounge to the experimental data, as shown in Figure 83, it is seen that whilst the initial and final temperature results within the lounge are comparable, there is a significant difference between the temperatures in between these time periods. Similar results are seen within the entry hall and on the stairway as shown in Figure 84 and Figure 85. The impact on temperature of early

growth of the fire, and the initial perturbations defined in the heat release rate profile are clearly seen within these Figures.

Whilst the heat release rate curve could have been modified, removing the initial perturbations and delaying the time at which growth of the fire began to occur, given the objectives and scope of the research it was desirable to maintain the assessment method that had been adopted within the analysis of CDT16 and CDT17. This enables comparisons to be made regarding the ability of the various prediction algorithms and modelling techniques to be adopted within typical engineering practice. As such each of the FDS simulations were undertaken as detailed in Table 18 and the results assessed.

By modelling the fire scenario with a higher effective heat of combustion value, as occurred in Simulations 4, 5 and 6, the derived results were comparable to that shown in Figure 81 and Figure 82, with activation occuring slightly early with the greater heat heat of combustion and hence greater environmental temperatures were derived to that seen in the above figures.

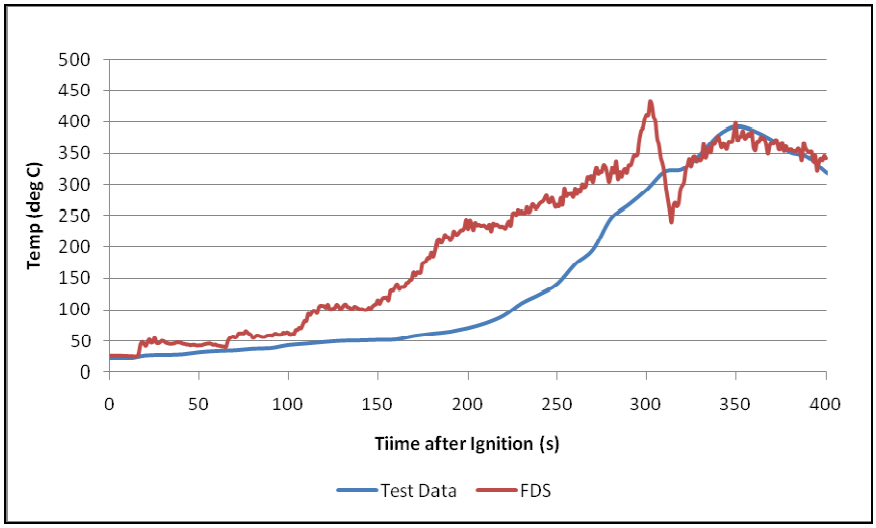

Figure 83 CDT19 Lounge Thermocouple: Temperature at 2.3m above floor level

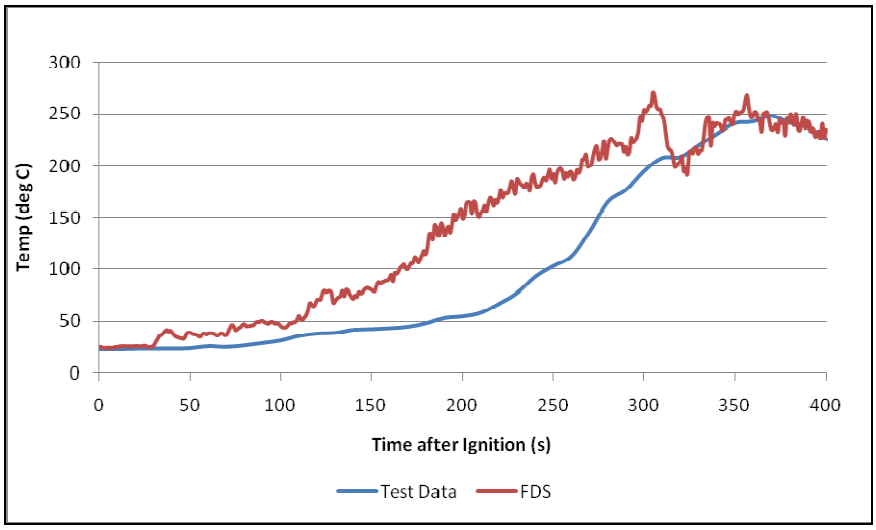

Figure 84 CDT19 Entry Hall Thermocouple: Temperature at 2.3m above floor level

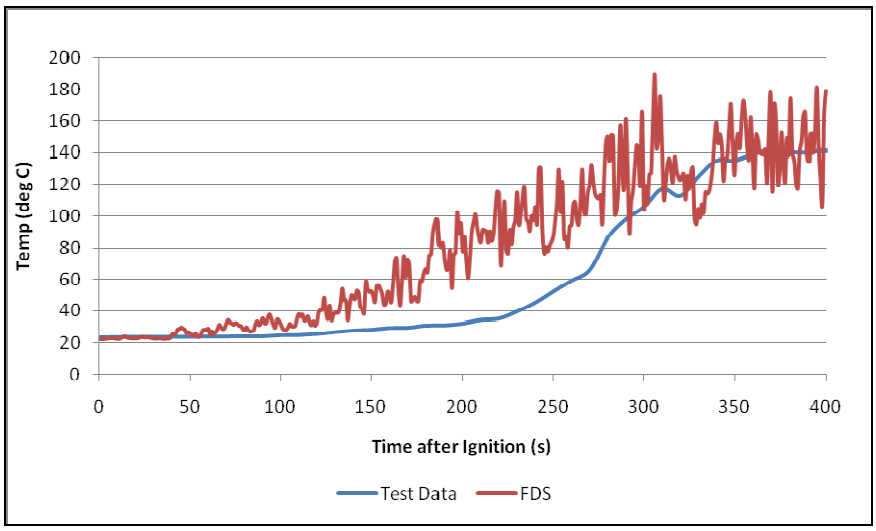

Figure 85 CDT19 Stairway Thermocouple: Temperature at 3.2m above floor level

Whilst the results are not comparable to the experimental data, the extent of the impact which the location of a detector can have on the derived activation time is evident in these simulations. Within the entry hall, the derived activation time at the ionisation detector, which is not as centrally located between the lounge door and the stairway void in comparison to the photoelectric detector, is approximaetly 80s for an activation criterion of 20°C above ambient. The derived photoelectric detector activation time under the same assessment criteria is 37s; refer to Figure 86 and Figure 87. Figure 88 provides a comparison of the tempertures at the two detector locations over this time period from Simulation 5; lag in the temperature rise at the ionisation detector behind that at the photoelectric detector is clearly evident.

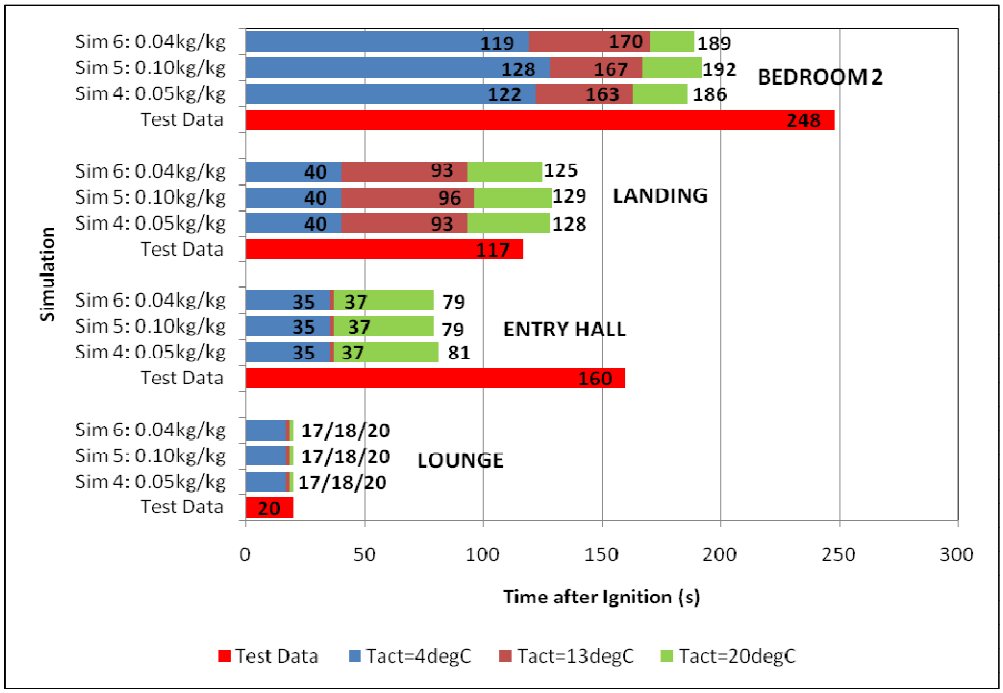

Figure 86 Temperature Correlation: CDT19_4, 5 & 6 Ionisation Detectors

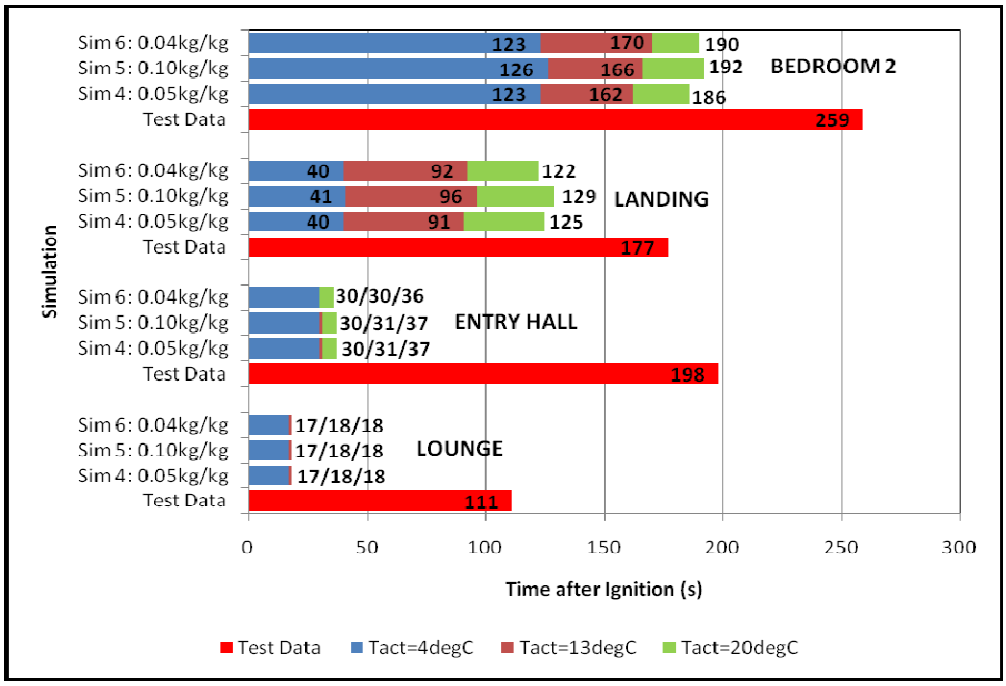

Figure 87 Temperature Correlation: CDT19_4, 5 & 6 Photoelectric Detectors

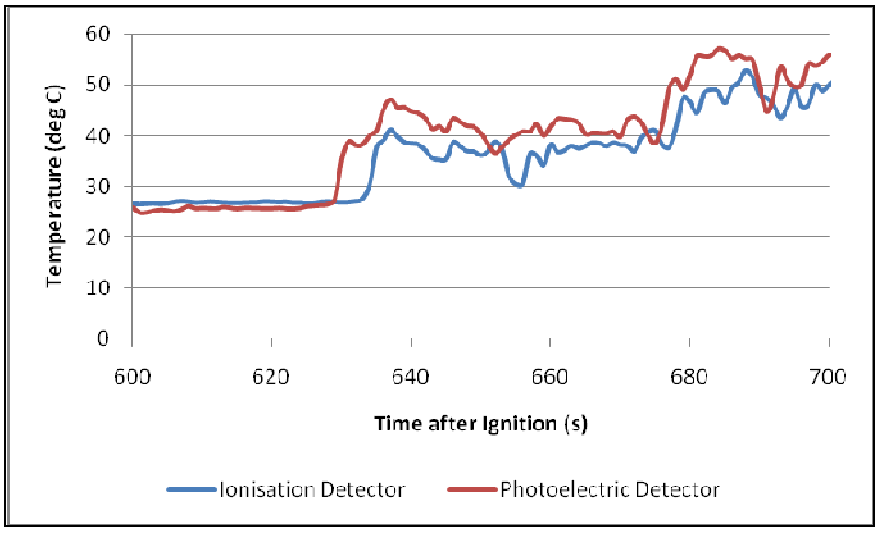

Figure 88 CDT19_5 Entry Hall Detector Location Temperature Profiles

At each of the detector locations the difference in derived temperature to ambient, as defined in Table 13, at the time of detector activation during the experiments, is shown in Figure 89 to Figure 92. With the faster growth rate in this experiment than CDT16 and CDT17, for each detector type and location a larger range in temperatures is seen. With the exception of the bedroom, where the ranges are comparable for the ionisation and photoelectric detctor locations, the ionisation detectors are seen to have a smaller range.

Whilst is does not appear that a given value is appropriate as an acceptance criterion for each of the detectors, given the large range this is not the case. Rather the results highlight that the actual value of the acceptance criterion adopted is not as significant in this instance, as a larger band of temperatures will be derived within a short time period around activation than would occur for a lower growth rate.

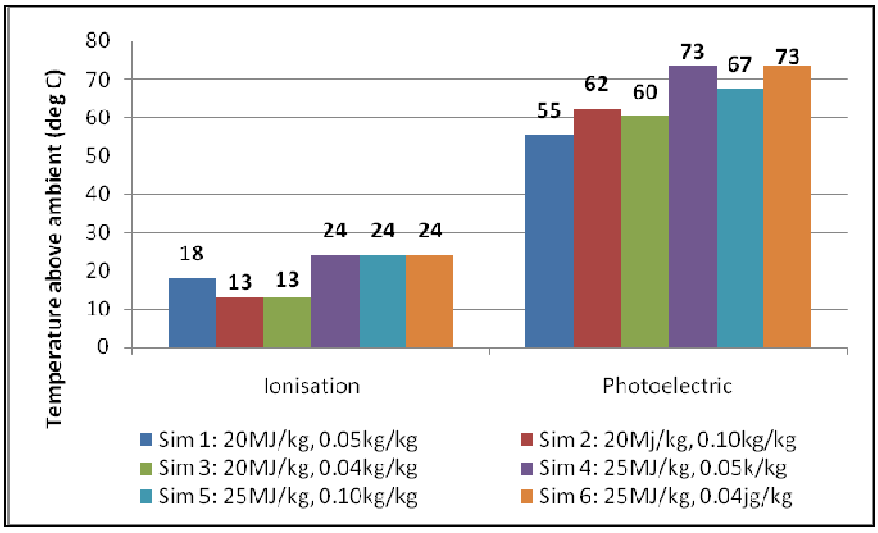

Figure 89 CDT19 Temperature Difference to Ambient at Experimental Activation: Lounge Detectors

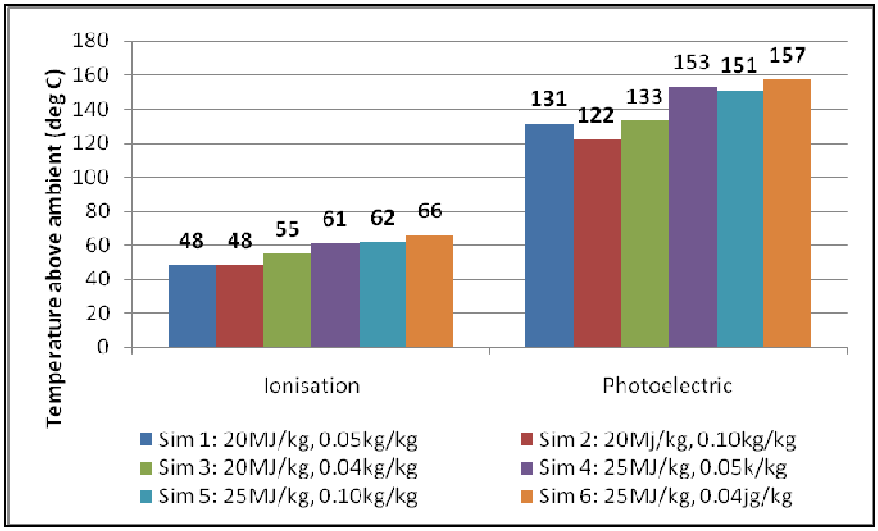

Figure 90 CDT19 Temperature Difference to Ambient at Experimental Activation: Entry Hall Detectors

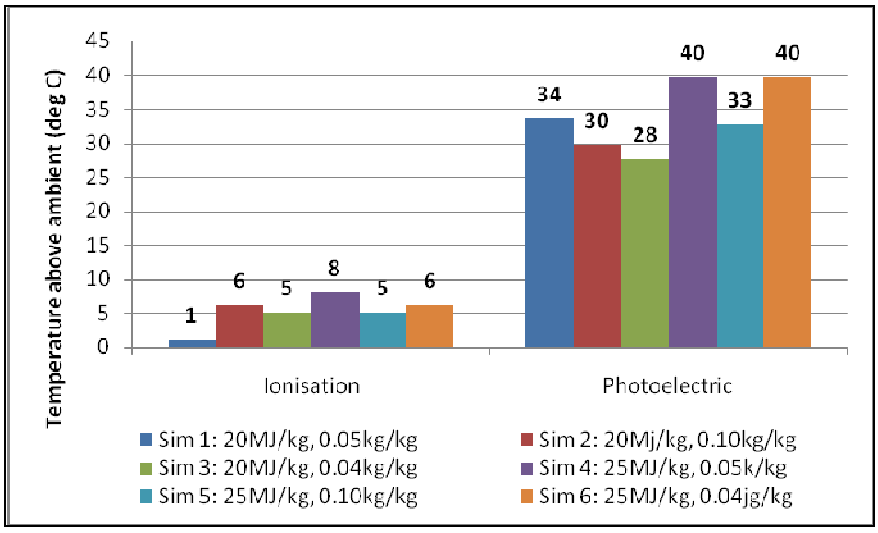

Figure 91 CDT19 Temperature Difference to Ambient at Experimental Activation: Landing Detectors

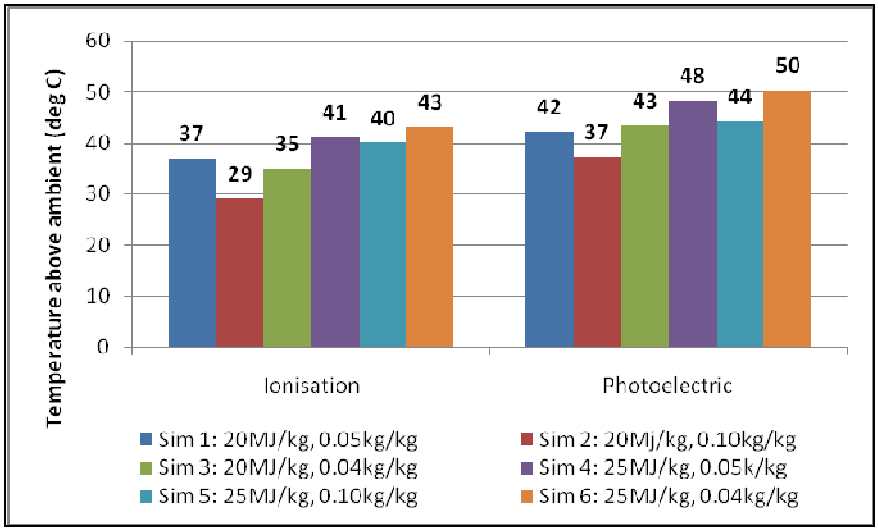

Figure 92 CDT19 Temperature Difference to Ambient at Experimental Activation: Bedroom Detectors

5.4.2. Heskestad Method

The derived activation times for each of the simulations when Heskestad's prediction algorithm is adopted are shown in Figure 93 to Figure 96. At each detector type and location the derived results are comparable across the simulations, with the range in activation times typically being only a few seconds. The largest range occurs within the bedroom, which is 18s.

The only location at which the results are comparable to the experimental data is within the lounge, for the ionisation detector. In accordance with Spearpoint (2002), smoke was not observed until 137s after ignition, when the foam began to ignite. Whilst some smoke must have been present to activate the lounge ionisation detector, just prior to this its volume and density would have been minimal. With a constant soot yield defined throughout a simulation and the initial perturbations defined within the heat release rate as detailed in the previous Section, the smoke detectors are derived to activate within a short period of time after ignition. The detectors within the bedroom are noted as not being derived to activate until approximately two minutes after ignition, however this is still significantly sooner than that within the experiment.

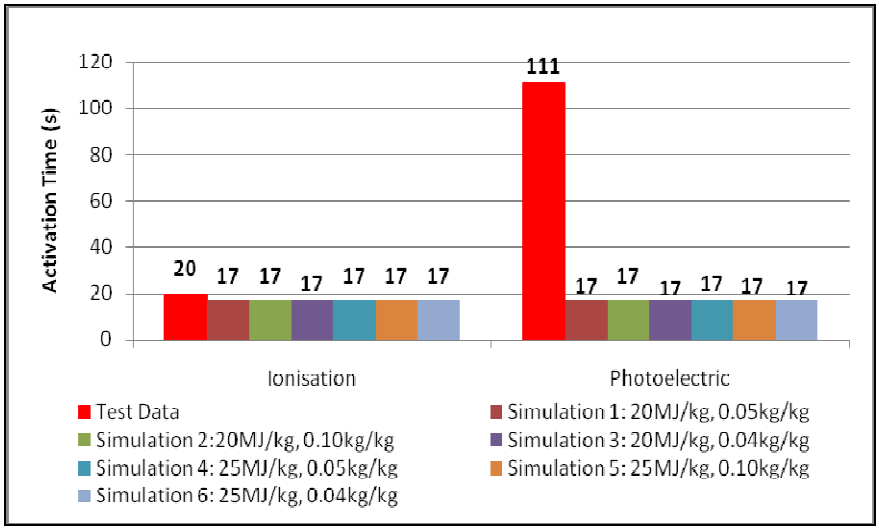

Figure 93 CDT19 Heskestad Method: Lounge

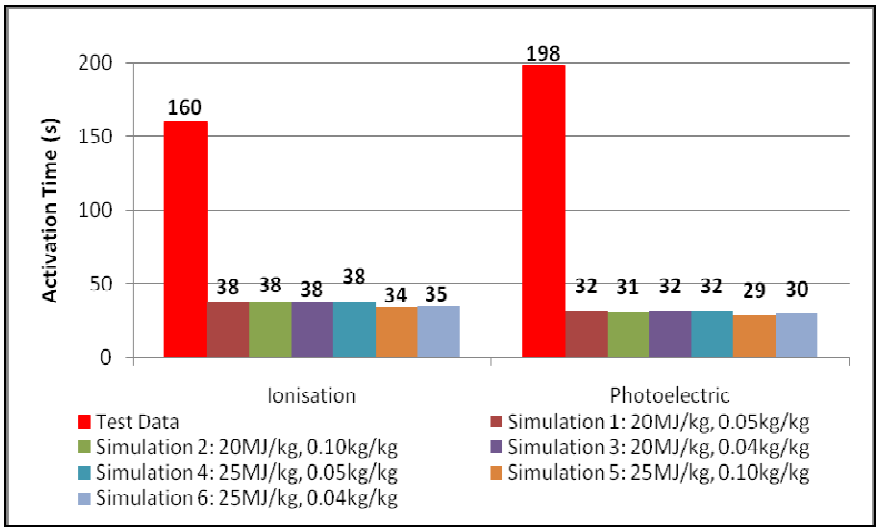

Figure 94 CDT19 Heskestad Method: Entry Hall

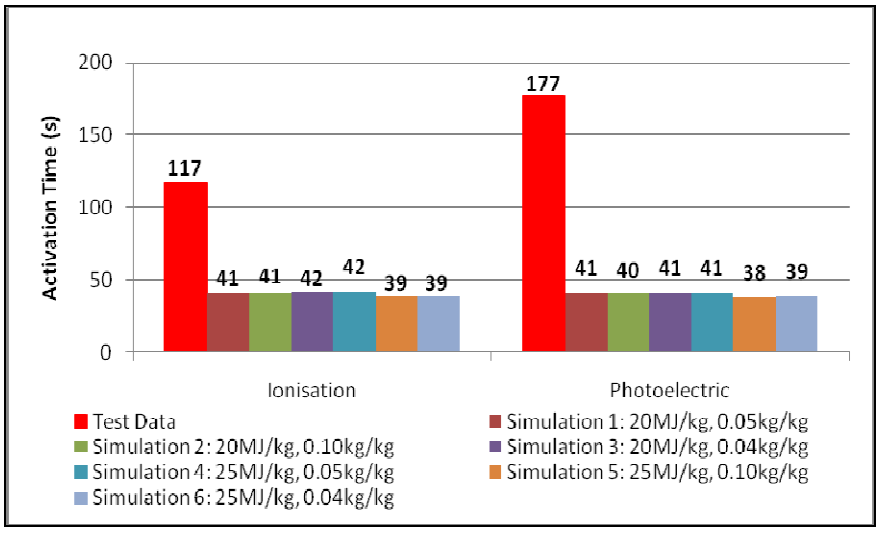

Figure 95 CDT19 Heskestad Method: Landing

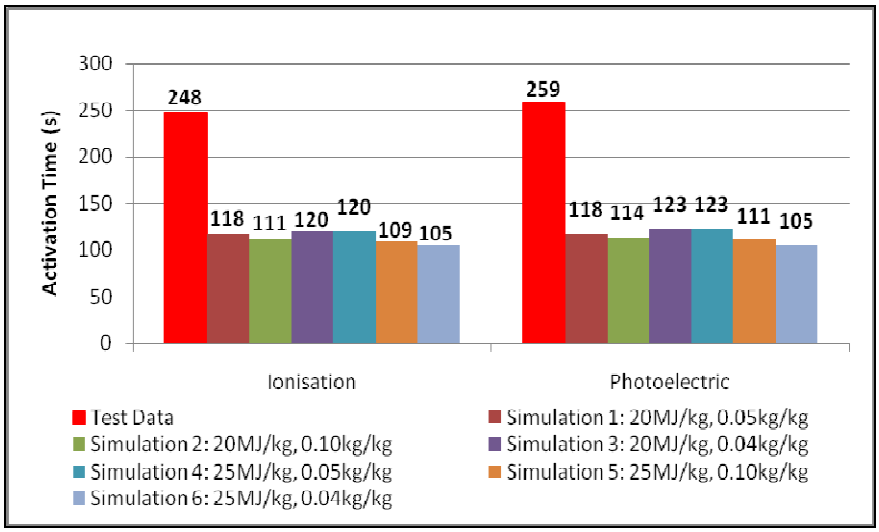

Figure 96 CDT19 Heskestad Method: Bedroom

Comparing the optical density readings within the entry hall and landing at 1.5m above floor level in Figure 97 and Figure 98 respectively, the degree to which it is over predicted is evident. The optical density is seen to increase shortly after ignition within the FDS simulation, however this does not occur until after approximately 150s during the experiment.

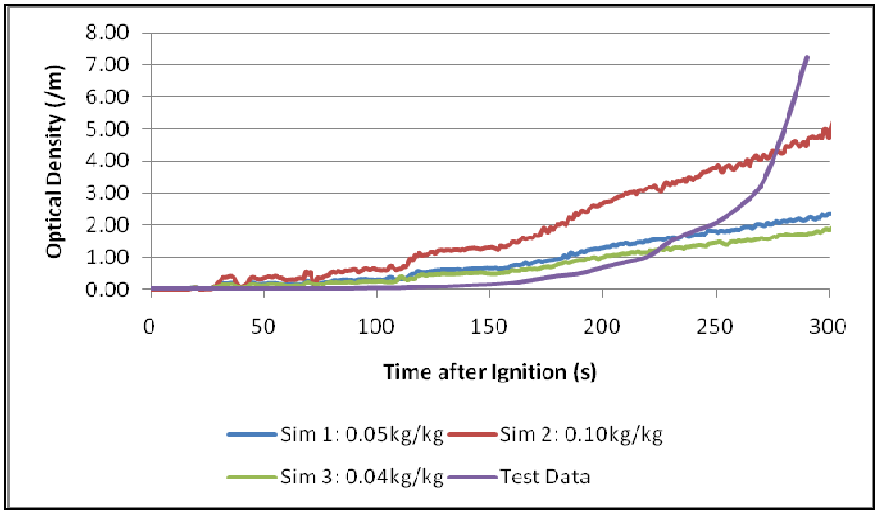

Figure 97 CDT19 Optical Density: Entry Hall at 1.5m above floor level

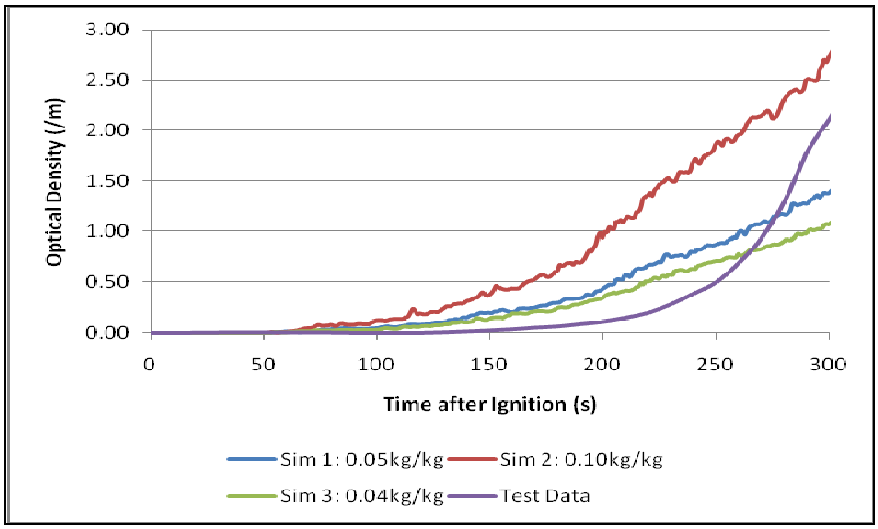

Figure 98 CDT19 Optical Density: Landing at 1.5m above floor level

5.4.3. Cleary Method

The derived activation times from application of Cleary's prediction algorithm to the results of the FDS simulations are comparable to the results provided in Section 5.4.2, with the variance to Heskestad's results being typically only a few seconds. The largest variance occurs within the bedroom, however these activation times are still derived to be no more than 7s apart. The derived activation times within the bedroom are shown in Figure 99 and Figure 100.

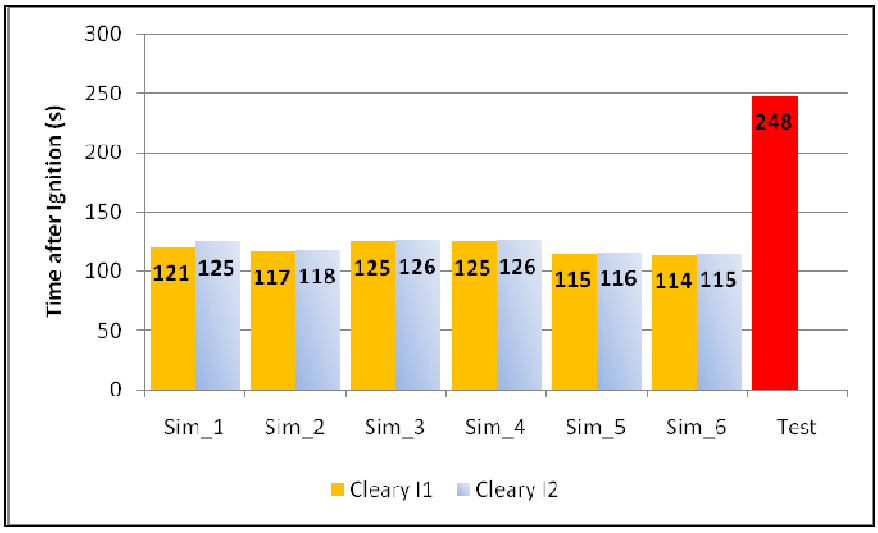

Figure 99 CDT19 Cleary Method: Bedroom Ionisation

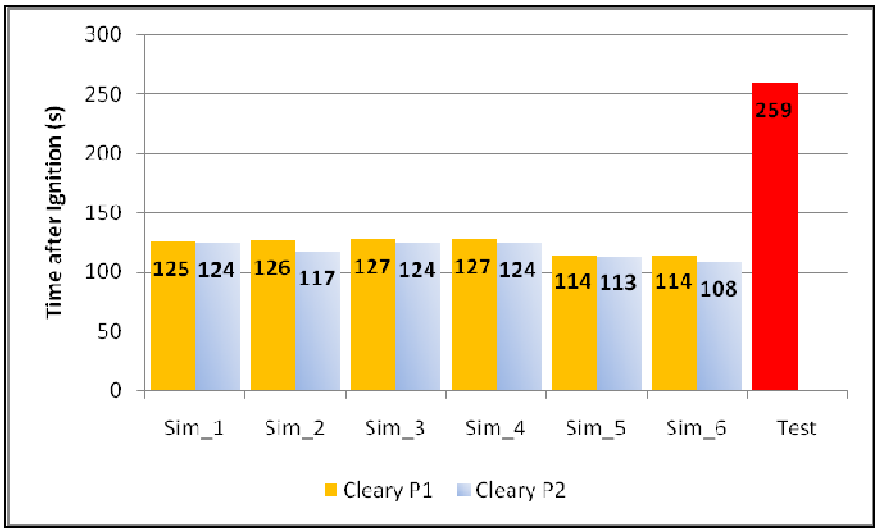

Figure 100 CDT19 Cleary Method: Bedroom Photoelectric

As detailed in the previous section the optical density values derived during the FDS simulations are significantly greater than that recorded during the experiment over time. As a result the predicted activation times are significantly earlier than the experimental test data, with the exception of the lounge ionisation detector where detection occurs shortly after ignition.

6. Discussion

6.1. Comparison to Previous Research – CDT17

6.1.1. Temperature Correlation

As noted previously, Brammer (2002) defined the effective heat of combustion to be 30MJ/kg within his assessment of CDT17. His derived activation times are compared against the average results of Simulations 1, 2 and 3, these being the base case assessments with regards to the effective heat of combustion defined. Figure 101 provides a comparison of the derived results for each of the ionisation detectors, whilst Figure 102 provides similar information for the photoelectric detectors. It is noted that the comparison is made to the average result of Simulations 1, 2 and 3 at each detector location as comparable activation times where derived for the various soot yields, as detailed in Section 5.3.1.

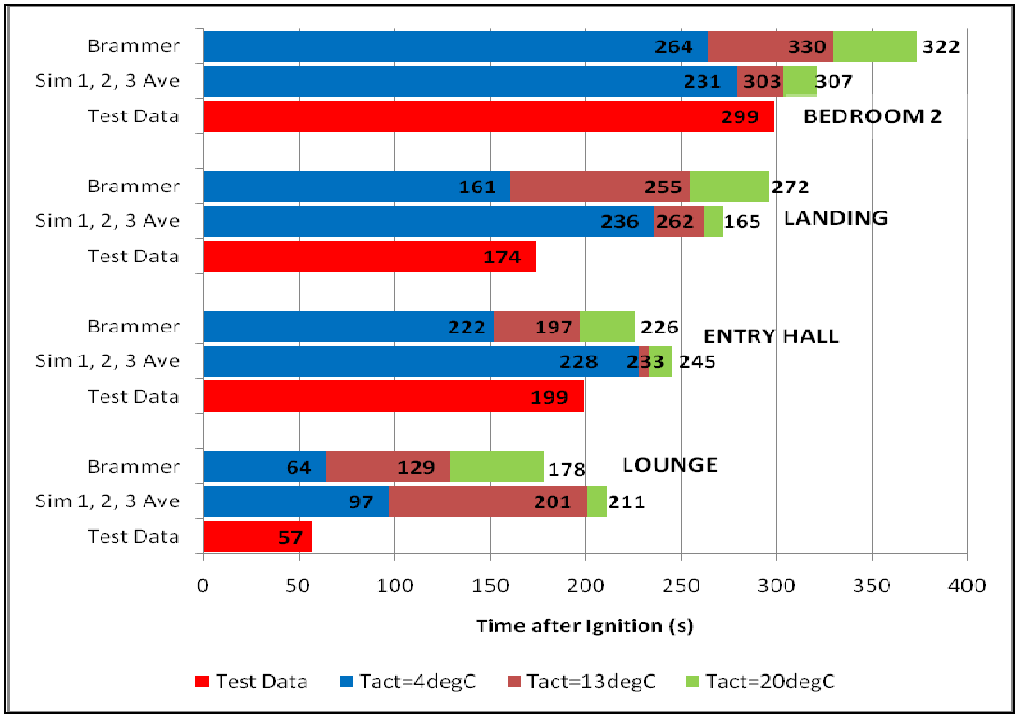

Figure 101 CDT17 Temperature Correlation Method Comparison: Ionisation

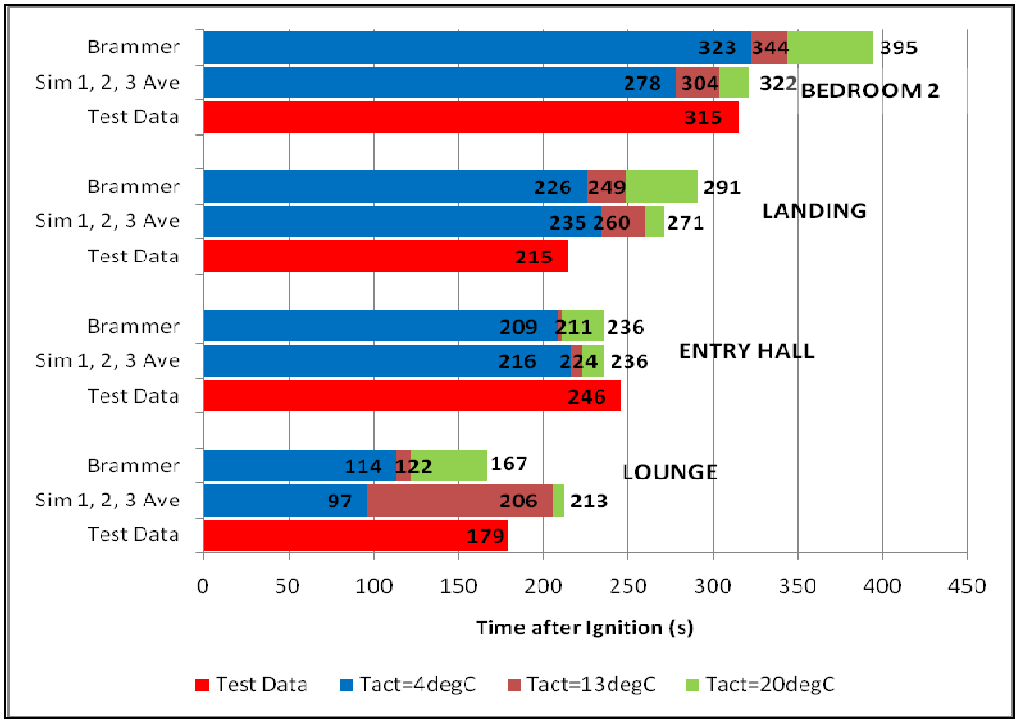

Figure 102 CDT17 Temperature Correlation Method Comparison: Photoelectric

Comparing the average of the derived results there is not seen to be a common degree of variance, i.e. a constant over prediction, constant under prediction or rather results being comparable. For the ionisation detectors, Brammer derived earlier activation times within the lounge and entry hall for each of the acceptance criteria, however not on the landing when considering an activation criterion of 20°C above ambient, or within the bedroom. The difference in margin between the results is also seen to vary.

For the photoelectric detectors, similar activation times where derived in Simulations 1, 2 and 3 to that for the ionisation detectors, as expected. Brammer's results however are seen to vary. Within the lounge, Brammer states an activation criterion of 4°C to derive activation time of 64s at the ionisation detector and 114s at the photoelectric detector, compared to 97s for both detectors in the averaged Simulation 1, 2 and 3 results. The reason for these large variations is unknown and is not commented on by Brammer.

It is expected that Brammer's research would derive earlier activation times given the larger effective heat of combustion defined. Where this is not seen to occur may be a result of differences in the defined heat release rate profiles. Whilst a scientific

approach was adopted to derive the heat release rate defined within Simulations 1, 2 and 3 from the mass data, as detailed in Section 3.5.3, Brammer's heat release rate is understood to be derived from the mass data through a trial and error approach from the information presented within his research report (Brammer 2002). Brammer's resultant heat release rate is subsequently quite smooth, whilst that defined for Simulations 1, 2 and 3 fluctuates over time. This would influence the temperatures derived throughout the model during the simulations, resulting in varied smoke detector activation times.

One similarity of note between the results presented by Brammer and those within this report is the derived activation times of the detectors in the entry hall in comparison to that on the landing. In the experiments the detectors on the landing where seen to activate prior to their counterpart in the entry hall, however this does not occur from the assessment of the FDS results with the temperature correlation method.

6.1.2. Heskestad Prediction Method

Brammer also derived the smoke detector activation times using the Heskestad prediction algorithm. Within his analysis Brammer defined the soot yield to be $0.10kg_{soot}/kg_{fuel,}$ whilst the Simulations undertaken as a component of this research assessed values of $0.05kg_{soot}/kg_{fuel}$, $0.10kg_{soot}/kg_{fuel}$ and 0. $04kg_{soot}/kg_{fuel}$. Brammer found that his defined soot yield and heat release rate results in a significant over prediction of the optical density in the first 300s of the fire simulation. As a result, in order to proceed with the analysis, Brammer simply halved the derived optical density readings before applying Heskestad's algorithm. The only information provided by Brammer is the activation times based on the modified optical density results thus this is provided for comparison within Figure 103 and Figure 104.

Also shown on these Figures are Thomas's (2008) derived activation times. Thomas defined the effective heat of combustion to be 26MJ/kg and soot yield $0.10kg_{soot}/kg_{fuel}$. The activation times derived by Thomas are all earlier that than derived in both the research detailed in this report and that by Brammer. Given the effective heat of combustion and soot yield defined, it would be expected that Thomas's results would

be more comparable. The under prediction of results seen is considered to be due to the use of BRANZFIRE, a zone model, to assess the scenario. A greater degree of assumptions and limitations are present within the derivation of the underlying principles of a zone model in comparison to a field model, influencing the accuracy of the results.

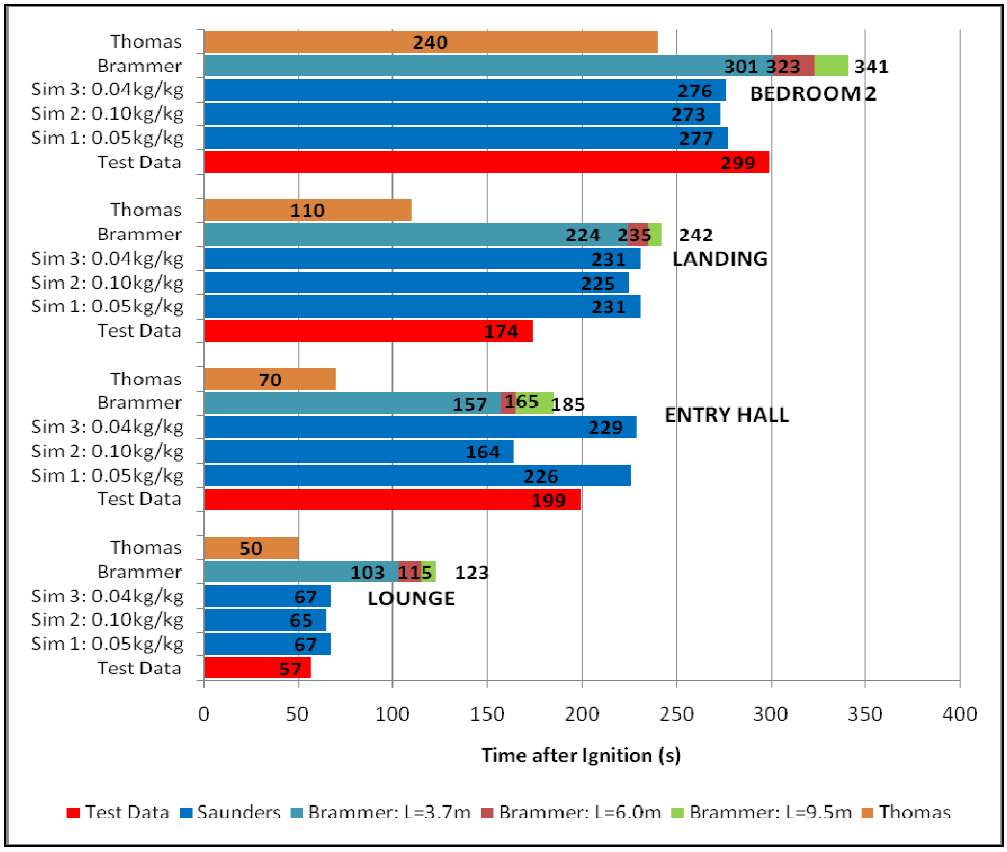

Figure 103 CDT17 Heskestad Method Comparison: Ionisation

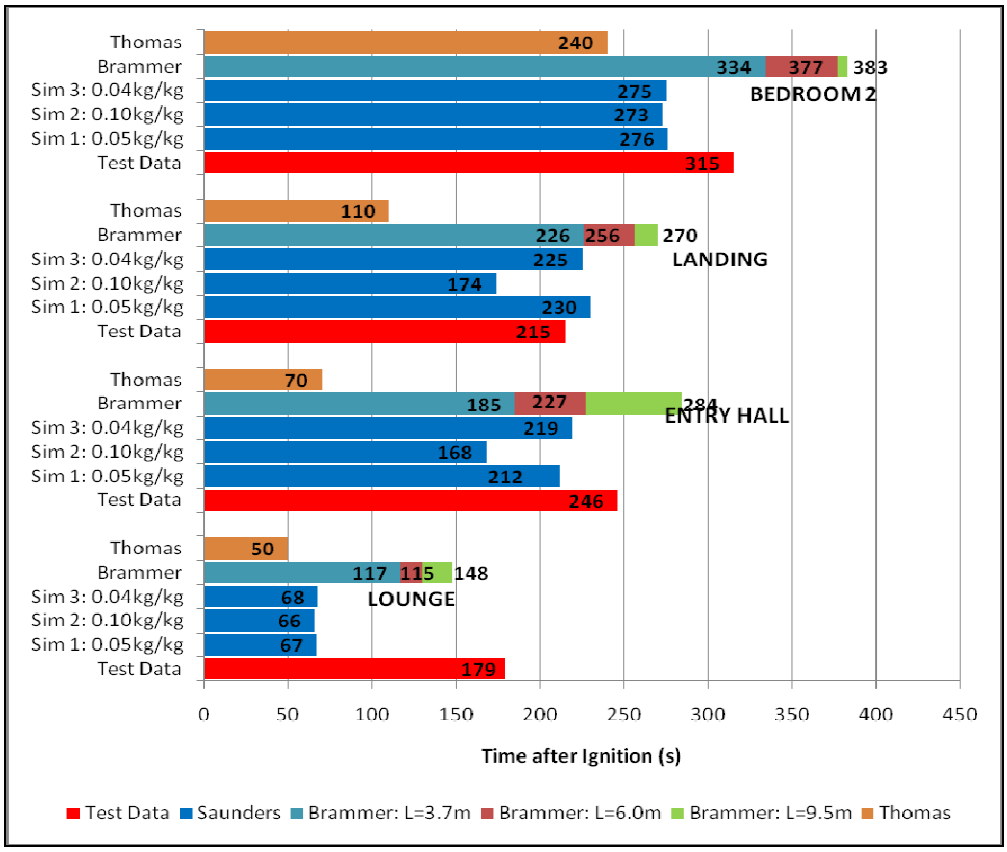

Figure 104 CDT17 Heskestad Correlation Method Comparison: Photoelectric

The Characteristic Length defined to derive the results shown for Simulations 1 to 3, L=1.8m of 1.8m, would be expected to result in activation times earlier than that derived by Brammer. This occurs on some occasions, but not consistently. From the results shown it can however be assumed that had Brammer's actual test data been provided for comparison, these activation times would have been greater than that derived from Simulations 1, 2 and 3.

6.2. Comparison to Previous Research - CDT16

Thomas (2008) assessed CDT16 in addition to CDT17. As in CDT17 the effective heat of combustion was defined to be 26MJ/kg. A comparison to the derived smoke detector activation times to average Heskestad prediction results of Simulations 1, 2 and 3 is provided in Figure 105 and Figure 106. In this fire scenario Thomas's activation times are found to be greater than that of Simulations 1 to 3 within the bedroom and lounge, and less in the entry hall and landing. This is applicable for both

the ionisation and photoelectric detectors. The magnitude of this difference between the results typically varies between 30 and 60s.

Given the effective heat of combustion and soot yields defined, it would initially be expected that Thomas's results would typically indicate earlier detection that that of Simulations 1, 2 and 3. The most comparable results would be expected to occur with the results derived from Simulation 2 where the defined soot yields are equivalent. As detailed previously, the reason this is not seen to occur is assumed to be a result of the use of a zone model by Thomas to assess the fire scenario. A greater degree of assumptions and limitations are seen to be present within the derivation of the underlying principles of a zone model in comparison to a field model, influencing the accuracy of the results.

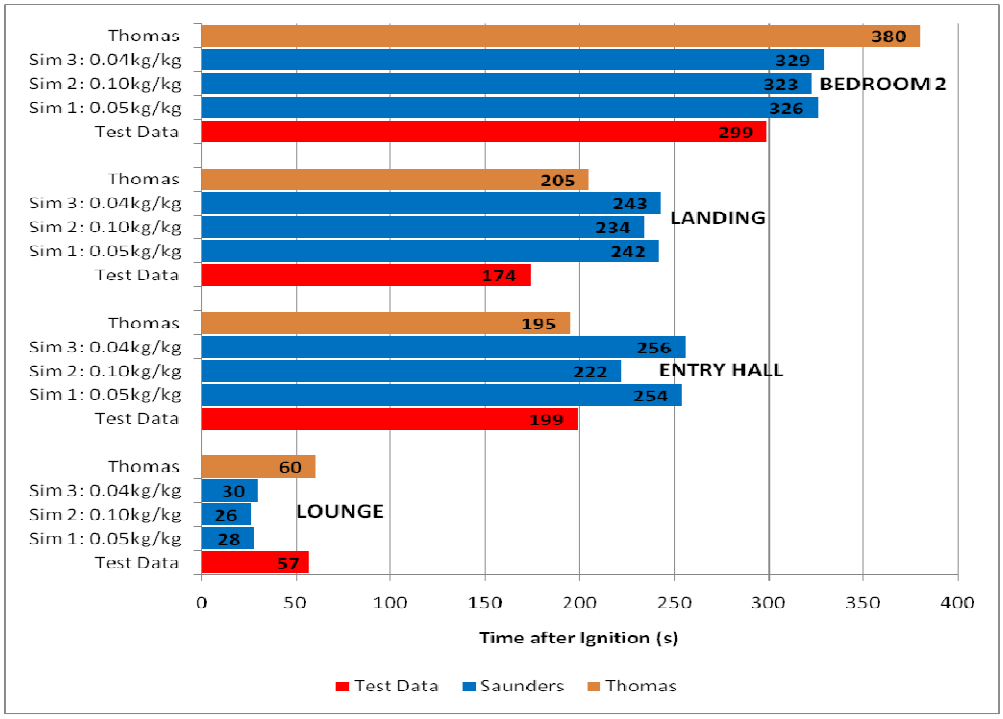

Figure 105 CDT16 Temperature Correlation Method Comparison: Ionisation

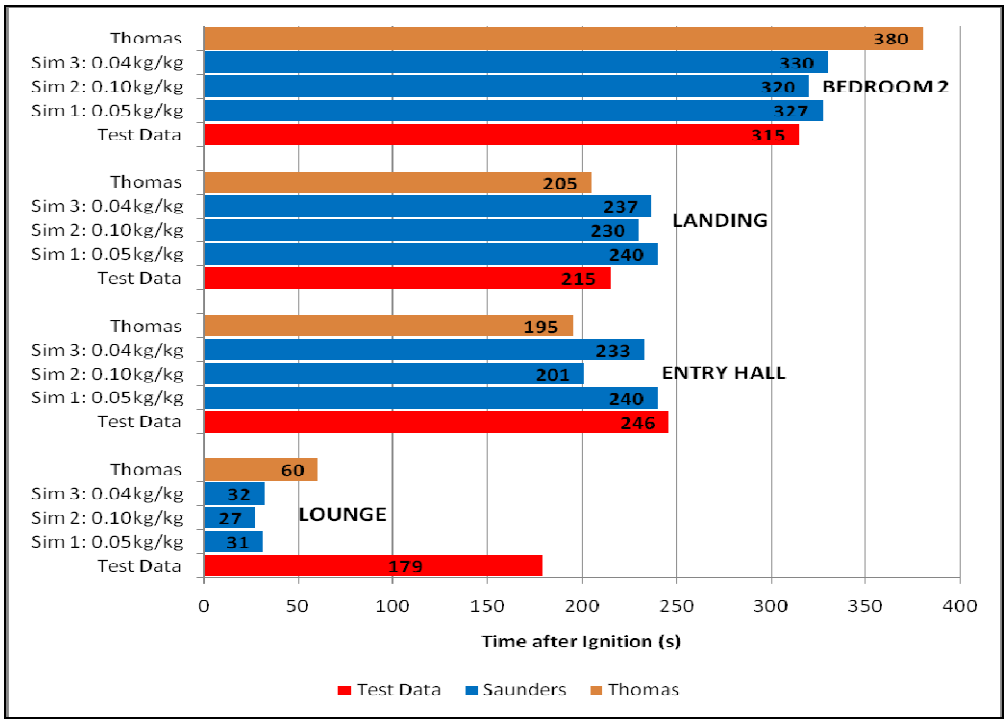

Figure 106 CDT16 Temperature Correlation Method Comparison: Photoelectric

6.3. Smoothing Mass Data

Smoothing of the raw mass data was required to be undertaken due to the level of noise present, this being evident by the increases in mass recorded over periods of time. Prior to the smoothing process being applied some simulations were modelled based on the raw data. Typically, detectors were derived to activate shortly after ignition, due to initial spikes, determined to be present within the heat release rate curve. The process of smoothing the data, thus whilst being necessary to enable the derived environmental conditions to be comparable to that of the experiment, also however resulted in some errors in the defined heat release rate profile which were seen to affect the comparability of the derived smoke detector activation times to the test data.

Within CDT17, the smoothing technique removed the initial perturbations within the mass data, resulting in the time at which growth of the fire occurred being delayed. This subsequently resulted in delayed activation times. Opposed to this, within the assessment of CDT19, the smoothing of the data derived an initial perturbation to be present within the heat release rate profile. The presence of this spike resulted in the

over prediction of hazardous conditions in locations close to the fire and thus typically earlier derived activation times.

In this instance, where observations of the experimental scenarios where provided, modifications could have been applied to the heat release rate profile until the simulation modelled derived results comparable to that detailed. Where such information is available it is recommended that the heat release rate be derived from such a process; i.e. application of a smoothing algorithm to the data, followed by 'minor alterations' to the derived heat release rate profile as required. It is noted that if it is evident that large scale changes are necessary then it is considered likely that an error has occurred at some stage of the process, whether this be within the recording of the data, or the application of the smoothing algorithm.

Typically in an engineering analysis, such data is not available and defined heat release rates are based on assessment of factors such as the available fuel load and ventilation conditions. In this instance smoothing algorithms are not typically required to be applied as the defined heat release rate profile tends to be smooth from the onset, such as that of a typically assumed t^2 growth rate of a fire.

It is noted that use of a t^2 growth rate is likely to provide a conservative analysis to the real fire scenario as the exclusion of any initial spikes in the heat release rate ensures that detection of the fire is not derived to occur until a later time period than may happen in reality.

6.4. Temperature Correlation Method

From the results of the analysis undertaken it is evident that when determining an appropriate activation criterion for use in the temperature correlation prediction method, consideration must be given to detector type, detector location relative to the fire, growth rate of the fire and mode of combustion. As is evident from the varying results derived, no single activation criterion is able to predict accurate smoke detector activation times for all fire scenarios.

Within the room of fire origin, for the fire scenarios considered, the temperature correlation method derived comparable results regarding activation of the ionisation detectors when the lower activation criterion was considered. As the fires were initiated within a wooden crib, with spread to the couch not occurring for a period of time, this criterion significantly under predicts the activation time of the photoelectric detector.

The magnitude of the period between derived activation times for each of the different activation criteria is seen to increase with distance from the fire. For example, the gap between derived activation times for the photoelectric detectors in simulation CDT16_1, for activation criteria of 13°C and 20°C, is 7s in the lounge, 24s in the entry hall and 50s on the landing. Within the bedroom it is noted that activation was not determined to occur within the length of the simulation, thus this difference is at least141s. Furthermore, these times periods are greater when comparing simulations with the lower effective heat of combustion values. This occurrence is considered to be due to the impact of transport effects on the smoke as it travels from the location of fire origin, primarily cooling.

As the distance from the fire increases, a larger volume of energy is required to raise the temperature of the environment and overcome the cooling effects as the hot combustion products mix with the fresh air. Thus, where a heat release rate of lower magnitude is defined, this energy is released over a greater period of time, and subsequently temperatures are seen to increase at a slower rate with distance from the fire.

6.5. Heskestad and Cleary Algorithms

The Heskestad and Cleary algorithms where typically found to derive comparable activation times. The difference between the derived activation times for simulations of equal soot yield but different heats of combustion is seen to increase with distance from the fire. Whilst the prediction algorithms do not consider temperature directly, unlike with the temperature correlation method where the soot yield has no bearing on the derived activation times, temperature does have an impact on the derived activation results. The degree of buoyancy of the smoke particles is directly influenced by

temperature. As distance increases from the fire, the temperature and thus density of smoke at high level also decreases. The difference between activation times for simulations of equivalent soot yield but different soot yields is thus seen to increase with distance from the fire.

6.6. Detector Location

The location of a detector relative to smoke flow patterns was seen to have significant influence on the wether activation was determined to occur at the early stages of a fires development. The small difference in location of the photoelectric and ionisation detectors on the landing resulted in activation times differing by nearly one minute within CDT17 Simulation 2 when considering Heskestad's algorithm.

7. Conclusion

This research continued on from work previously undertaken by Brammer (2002), whereby two-storey house fire experiments where modelled within FDS and derived smoke detector activation times where compared to the test data. A component of the objective of this study was to assess the ability to accurately derive smoke detector activation times when undertaking a typical fire engineering analysis.

Three test fire scenarios were considered, all involving the flaming combustion of upholstered furniture. Base case parameters were established for the modelling of the fire scenario, which were considered to be representative of that which would be used within a typical fire engineering analysis. The soot yields and effective heats of combustion were then varied to assess the impact on derived smoke detector activation times.

The derivation of smoke detector activation was achieved using the temperature correlation method, Heskestad's method and Cleary's method. Within the temperature correlation method activation criterion of 4°C, 13°C and 20°C where considered.

From the results of the simulations and their comparison to the experimental data, and to the work undertaken by Thomas (2008) and Brammer (2002), the following conclusions were made:

- Where possible, heat release rates should be derived from both application of a smoothing algorithm to the mass loss data, followed by minor modifications based on experiment observations of the fire.

- Use of an activation criterion of 4°C provides comparable results when assessing an ionisation detector within the room of fire origin.

- The results supported and reiterated the knowledge that detector algorithms do not provide consideration to the operating mechanism of a detector, nor the type of combustion for a given fire scenario and thus typically derive comparable detector activation times for ionisation and photoelectric

detectors. Where differences are seen between the derived activation times this is typically a results of varying locations of the two detectors.

- No single activation methodology will derive accurate detector activation times for varying detector locations relative to a fire; i.e. near and far.

- The Heskestad and Cleary methods typically derived comparable activation times.

- As distance from the location of the fire increases, so too does the extent which errors within input data affect derived results.

- From comparison with Thomas's work it is not considered that use of a zone model is appropriate for determination of smoke detector activation times within a two storey environment, with the fire initiating on the ground floor.

- The presence of horizontal openings near a detector can have a significant impact on whether the detector is determined to activate during early stages of a fire. This occurs when the detector is located both at the level of the opening or on the floor above. A small difference in position can see a detector not being located within the path of flow of the smoke and thus not activating.

Thus for an appropriate prediction method to be adopted by an engineer to enable an accurate assessment of a given fire scenario with regards to smoke detector activation, consideration must be given to all of the following:

- type of detector being assessed;

- location of the detector relative to the fire;

- mode of combustion (i.e. flaming or smouldering); and the

- growth rate of the fire.

Given the range of results derived when variations to the input parameters where made, it is evident that fire engineers need to either ensure that all such parameters are accurate for a given assessment scenario or ensure that an acceptable safety margin is incorporated. Considering the varied results derived by the three researchers when assessing the same scenario, where all individuals had the same information on the experimental tests available as a starting point, it is evident that such a safety margin should be included within an analysis even when one has confidence in their input parameters.

8. References

Australian Building Code Board (ABCB) (2005) *International Fire Engineering Guidelines*. Australian Building Code Board, Australia.

Babrauskus, V. (2003) *Ignition Handbook*. Fire Science Publishers/Society of Fire Protection Engineers, Issaquah WA.

Beyler, C. (1984) 'A Design Method for Flaming Fire Detection', *Fire Technology*. Vol. 20, No. 4, pp 5 – 16.

Bjorkman, J., Kokkala, M.A. & Ahola, H. (1992) 'Measurements of the Characteristic Lengths of Smoke Detectors', *Fire Technology.* Vol 28, No 2, pp 99 – 106.

Bjorkman, J. Baroudi, D., Latva, R., Tuomisaari, M. & Kokkala, M.A. (2001) 'Determination of Dynamic Model Parameters of Smoke Detectors', *Fire Safety Journal*. Vol 37, pp. 395 – 407.

Brammer, D.R. (2002) A Comparison Between Predicted and Actual Behaviour of Domestic Smoke Detectors in a Realistic House Fire. *Fire Engineering Research Report 2002/2.* University of Canterbury.

BS 5446-1:2000 (2000) *Fire Detection and Fire Alarm Devices for Dwellings – Part 1: Specification for Smoke Alarms*. British Standard Institute, Bristol.

Buchanan, A.H. (ed) (2001) *Fire Engineering Design Guide*. University of Canterbury, New Zealand.

Bukowski, R.W. & Averill, J.D. (1998) 'Methods for Predicting Smoke Detector Activation', *Fire Suppression and Detection Research Application Symposium, Research and Practice: Bridging the Gap.* National Fire Protection Research Foundation, USA, pp 64 – 77.

Cleary, T., Chernovsky, A., Grosshandler, W.L. & Anderson, M. (2000) 'Particulate Entry Lag in Spot-Type Smoke Detectors', *Fire Safety Science. Proceedings: Sixth*

International Symposium. International Association for Fire Safety Science, pp 779 – 790.

Clement, J.M. (2000) *Experimental Verification of the Fire Dynamics Simulator (FDS) Hydrodynamic Model*, University of Canterbury, New Zealand.

Collier, P.C.R. (1996) 'Fire in a Residential Building: Comparison between Experimental Data and a Fire Zone Model', *Fire Technology*. Vol 32, No 3, pp 195 – 217.

Cox, G. & Kumar, S. (2002)'Modelling Enclosure Fires Using CFD', *SFPE Handbook of Fire Protection Engineering, 3rd edn.* Society of Fire Protection Engineers, USA, pp 3-194 – 3-218.

Davis, W.D. & Natarianni, K.A. (1996) *NASA Fire Detection Study: NISTIR 5798,* National Institute of Standards and Technology, Gaithersburg, USA.

Floyd, J.E. et al (2001) *A Mixture Fraction Combustion Model for Fire Simulation Using CFD*. National Institute of Standards and Technology, Gaithersburg, USA.

Ierardi, J.A. & Barnett, J.R. (2000) *A Methodology for Predicting Smoke Detector Response*. WPI Centre for Fire Safety Studies, Worcester.

Farouk, B., Mulholland, G.W. & McGrattan, K.B. (2001) 'Simulation of Smoke Transport and Coagulation for a Standard Test Fire', *AUBE '01 Proceedings of the 12th International Conference on Automatic Fire Detection.* Gaithersburg, USA.

Heskestad, G. (1975) 'Generalised characterisation of smoke entry and response for products-of-combustion detectors*', Proceedings of a Symposium: Fire Detection for Life Safety*. National Research Council, pp 93 – 127.

McGrattan, K., Hostikka, S., Floyd, J., Baum, H., Rehm, R., Mell, W. & McDermott, R. (2009a) *Fire Dynamics Simulator (Version 5) Technical Reference Guide Volume 1: Mathematical Model*. National Institute of Standards and Technology Special Publication 1018-5, Washington, DC.

McGrattan, K., Hostikka, S., Floyd, J., McDermott, R. & Prasad, K. (2009b) *Fire Dynamics Simulator (Version 5) Technical Reference Guide Volume 3: Validation*. National Institute of Standards and Technology Special Publication 1018-5, Washington, DC.

McGrattan, K., Klein, B., Hostikka, S. & Floyd, J. (2009c) *Fire Dynamics Simulator (Version 5) User's Guide*. National Institute of Standards and Technology Special Publication 1019-5, Washington, DC.

Mulholland, G.W. (2002), 'Smoke Production and Properties' *SFPE Handbook of Fire Protection Engineering, 3rd edn.* Society of Fire Protection Engineers, USA, pp 2-258 – 2-268.

Mowrer, F.W. & Friedman, J. (1999) 'Experimental Investigation of Heat and Smoke Detector Response', *Proceedings of* the *Fire Suppression and Detection Research Application Symposium, Research and Practice: Bridging the Gap.* National Fire Protection Research Foundation, Orlando, pp. 256 – 264.

Purser, D.D., Kuipers, F.M. & Wright, J.W. (1995) *Hazards to Life in Smouldering and Vitiated Fires – Mid Term Progress Report*. BRE Client Project CD142/95, Building Research Establishment, Watford.

Purser, D.A., Rowley, J.A. & Bensilum, M. (1998), *A Data Base of Large Scale Enclosed Fires with Life Hazard Analyses for Fire Safety Engineering Design.* Fire Research Station, Building Research Establishment, Watford.

Richardson, L.F. (1993), *Volume 1: Metrology and Numerical Analysis*. Collected Papers, Cambridge University Press, England.

Robbins, A.P. & Wade, C.A. (2007) *Soot Yield Values for Modelling Purposes – Residential Occupancies*. BRANZ Study Report 185, BRANZ Ltd, Porirua, New Zealand.

Shifiliti, R.P. (2001) 'Fire Detection Modelling – The Research – Application Gap', *Proceedings, AUBE '01, Twelfth International Conference on Automatic Fire*

Detection. National Institute of Standards and Technology, Gaithersburg, USA, pp 529 – 560.

Schifiliti, R.P., Meacham, B.J. & Custer, R.L.P (2002) 'Design of Detection Systems' *SFPE Handbook of Fire Protection Engineering, 3rd edn.* Society of Fire Protection Engineers, USA, pp 4-1 – 4-43.

Spearpoint, M.J. (1996) *The Response of Domestic Smoke Alarms to Fires in a Typical Dwelling*. FRDG Publication Number 16/96, Home Office Fire Research and Development Group.

Tewarson, A. (1995) 'Generation of Heat and Chemical Compounds in Fires', *SFPE Handbook of Fire Protection Engineering, 3rd edn.* Society of Fire Protection Engineers, USA, pp 3-82 – 3-161.

Thomas, C.R (2008) Study if Full Scale Fire Test Results Versus BRANZFIRE Zone Model Output. *Fire Engineering Research Report 2008/2.* University of Canterbury.

Wade, C.A. (2004) *A User's Guide to BRANZFIRE 2004*. Building Research Association of New Zealand, Wellington.

Versteeg, H.K. & Malalasekera, W., (1995) *An Introduction to Computational Fluid Dynamics - The Finite Volume Metho.,* Longman Scientific and Technical Publications, Essex, England.

Appendix A – CDT16 Input file

```
&HEAD CHID='CDT16_smoothed_10', TITLE='CDT16, Smoothed Data, Test 10, FDS version 5' /

&TIME T_END=1300 / Length of simulation

&MESH IJK=80,64,50, XB=0.0,8.0,0.0,6.4,0.0,5.0 / 0.1*0.1*0.1m grid

&DUMP DT_RESTART=599.
     DT_DEVC = 1
     DT_HRR = 1 /

&MATL ID = 'CONCRETE'

FYI   = 'Quintiere, Fire Behavior'

SPECIFIC_HEAT  = 0.88
     DENSITY =2100.
     CONDUCTIVITY    = 1.0 /

&MATL ID     = 'GYPSUM BOARD'
     FYI    = 'Quintiere, Fire Behavior'
     CONDUCTIVITY      = 0.48
     SPECIFIC_HEAT  = 0.84
     DENSITY= 1440./

&SURF ID = 'EXTERNAL WALL', ADIABATIC=.TRUE.,RGB = 204,204,178 /

&SURF ID = 'floor'
     RGB = 204,204,178
     MATL_ID = 'GYPSUM BOARD'
     THICKNESS = 0.2 /

&SURF ID = 'WALL'
     RGB = 204,204,178
     MATL_ID = 'GYPSUM BOARD'
```

```
    THICKNESS = 0.1 /

&SURF ID = 'stair'

    RGB=204,153,102

    MATL_ID = 'GYPSUM BOARD'

    THICKNESS = 0.013 /

&SURF ID = 'bannister'

    RGB=155,0,155

    MATL_ID = 'GYPSUM BOARD'

    THICKNESS = 0.013 /

&SURF ID = 'ceiling'

    RGB=204,204,178

    MATL_ID = 'CONCRETE'

    THICKNESS = 0.01 /

&VENT MB='XMIN', SURF_ID='OPEN' / X max boundary of mesh open

&VENT MB='YMIN', SURF_ID='OPEN' / Y max boundary of mesh open

&VENT MB='ZMIN', SURF_ID='OPEN' / Z max boundary of mesh open

&VENT MB='XMAX', SURF_ID='OPEN' / X max boundary of mesh open

&VENT MB='YMAX', SURF_ID='OPEN' / Y max boundary of mesh open

&VENT MB='ZMAX', SURF_ID='OPEN' / Z max boundary of mesh open

------

HOUSE

&OBST XB=0.0,7.9,0.0,0.1,0.0,5.0, SURF_ID='EXTERNAL WALL', COLOR= 'INVISIBLE' /  Front
Wall

&OBST XB=0.0,7.9,5.9,6.0,0.0,5.0, SURF_ID='EXTERNAL WALL' /  Rear Wall

&OBST XB=0.0,0.1,0.0,6.0,0.0,5.0, SURF_ID='EXTERNAL WALL' /  Left Wall

&OBST XB=7.8,7.9,0.0,6.0,0.0,5.0, SURF_ID='EXTERNAL WALL', COLOR= 'INVISIBLE' /  Right
Wall
```

&OBST XB=0.0,7.9,0.0,6.0,0.0,0.0, SURF_ID='EXTERNAL WALL' / Ground Floor

&OBST XB=0.0,7.9,0.0,5.9,2.4,2.6, SURF_ID='floor' / L1 Floor

&OBST XB=0.0,7.9,0.0,5.9,5.0,5.0, SURF_ID='EXTERNAL WALL' / Roof

&OBST XB=0.0,7.9,2.3,2.4,0.0,5.0, SURF_ID='WALL' / EW Wall Gnd & L1

&OBST XB=3.5,3.6,0.0,6.0,0.0,2.4, SURF_ID='WALL' / NS Wall Gnd

&OBST XB=1.8,1.9,0.0,2.3,2.6,5.0, SURF_ID='WALL' / L1 NS Wall 1

&OBST XB=5.6,5.7,0.0,2.3,2.6,5.0, SURF_ID='WALL' / L1 Wall 2

&OBST XB=3.5,3.6,2.4,6.0,2.6,5.0, SURF_ID='WALL' / L1 Wall 3

DOORS

&HOLE XB=4.2,5.0,2.2,2.5,2.6,4.6 / L1 Landing to bedroom2 800 mm door

&HOLE XB=7.6,8.0,1.6,1.7,0.0,2.0 / Front Door Leakage

&HOLE XB=4.4,4.5,2.2,2.5,0.0,1.0 / Lounge door leakage

&HOLE XB=4.0,6.0,5.7,6.1,0.0,0.1 / Lounge to outside leakage

STAIRS

&HOLE XB=3.6,6.2,0.1,1.0,2.3,3.2 / L1 Stairs opening

&OBST XB=3.6,6.0,1.0,1.0,0.0,0.2, SURF_ID='stair'/ Step 1

&OBST XB=3.6,5.8,1.0,1.0,0.2,0.4, SURF_ID='stair' / Step 2

&OBST XB=3.6,5.6,1.0,1.0,0.4,0.6, SURF_ID='stair' / Step 3

&OBST XB=3.6,5.4,1.0,1.0,0.6,0.8, SURF_ID='stair' / Step 4

&OBST XB=3.6,5.2,1.0,1.0,0.8,1.0, SURF_ID='stair' / Step 5

&OBST XB=3.6,5.0,1.0,1.0,1.0,1.2, SURF_ID='stair' / Step 6

&OBST XB=3.6,4.8,1.0,1.0,1.2,1.4, SURF_ID='stair' / Step 7

&OBST XB=3.6,4.6,1.0,1.0,1.4,1.6, SURF_ID='stair' / Step 8

&OBST XB=3.6,4.4,1.0,1.0,1.6,1.8, SURF_ID='stair' / Step 9

&OBST XB=3.6,4.2,1.0,1.0,1.8,2.0, SURF_ID='stair' / Step 10

&OBST XB=3.6,4.0,1.0,1.0,2.0,2.2, SURF_ID='stair' / Step 11

&OBST XB=3.6,3.8,1.0,1.0,2.2,2.4, SURF_ID='stair' / Step 12

&OBST XB=3.6,6.0,0.1,0.1,0.0,0.2, SURF_ID='stair'/ Step 1

&OBST XB=3.6,5.8,0.1,0.1,0.2,0.4, SURF_ID='stair' / Step 2

&OBST XB=3.6,5.6,0.1,0.1,0.4,0.6, SURF_ID='stair' / Step 3

&OBST XB=3.6,5.4,0.1,0.1,0.6,0.8, SURF_ID='stair' / Step 4

&OBST XB=3.6,5.2,0.1,0.1,0.8,1.0, SURF_ID='stair' / Step 5

&OBST XB=3.6,5.0,0.1,0.1,1.0,1.2, SURF_ID='stair' / Step 6

&OBST XB=3.6,4.8,0.1,0.1,1.2,1.4, SURF_ID='stair' / Step 7

&OBST XB=3.6,4.6,0.1,0.1,1.4,1.6, SURF_ID='stair' / Step 8

&OBST XB=3.6,4.4,0.1,0.1,1.6,1.8, SURF_ID='stair' / Step 9

&OBST XB=3.6,4.2,0.1,0.1,1.8,2.0, SURF_ID='stair' / Step 10

&OBST XB=3.6,4.0,0.1,0.1,2.0,2.2, SURF_ID='stair' / Step 11

&OBST XB=3.6,3.8,0.1,0.1,2.2,2.4, SURF_ID='stair' / Step 12

&OBST XB=6.0,6.0,0.1,1.0,0.0,0.2, SURF_ID='stair' / Step 1

&OBST XB=5.8,5.8,0.1,1.0,0.4,0.2, SURF_ID='stair' / Step 2

&OBST XB=5.6,5.6,0.1,1.0,0.6,0.4, SURF_ID='stair' / Step 3

&OBST XB=5.4,5.4,0.1,1.0,0.8,0.6, SURF_ID='stair' / Step 4

&OBST XB=5.2,5.2,0.1,1.0,1.0,0.8, SURF_ID='stair' / Step 5

&OBST XB=5.0,5.0,0.1,1.0,1.2,1.0, SURF_ID='stair' / Step 6

&OBST XB=4.8,4.8,0.1,1.0,1.4,1.2, SURF_ID='stair' / Step 7

&OBST XB=4.6,4.6,0.1,1.0,1.6,1.4, SURF_ID='stair' / Step 8

&OBST XB=4.4,4.4,0.1,1.0,1.8,1.6, SURF_ID='stair' / Step 9

&OBST XB=4.2,4.2,0.1,1.0,2.0,1.8, SURF_ID='stair' / Step 10

&OBST XB=4.0,4.0,0.1,1.0,2.2,2.0, SURF_ID='stair' / Step 11

```
&OBST XB=3.8,3.8,0.1,1.0,2.4,2.2, SURF_ID='stair', PERMIT_HOLE=.FALSE. /  Step 12

&OBST XB=5.8,6.0,0.1,1.0,0.2,0.2, SURF_ID='stair' /  Step 1

&OBST XB=5.6,5.8,0.1,1.0,0.4,0.4, SURF_ID='stair' /  Step 2

&OBST XB=5.4,5.6,0.1,1.0,0.6,0.6, SURF_ID='stair' /  Step 3

&OBST XB=5.2,5.4,0.1,1.0,0.8,0.8, SURF_ID='stair' /  Step 4

&OBST XB=5.0,5.2,0.1,1.0,1.0,1.0, SURF_ID='stair' /  Step 5

&OBST XB=4.8,5.0,0.1,1.0,1.2,1.2, SURF_ID='stair' /  Step 6

&OBST XB=4.6,4.8,0.1,1.0,1.4,1.4, SURF_ID='stair' /  Step 7

&OBST XB=4.4,4.6,0.1,1.0,1.6,1.6, SURF_ID='stair' /  Step 8

&OBST XB=4.2,4.4,0.1,1.0,1.8,1.8, SURF_ID='stair' /  Step 9

&OBST XB=4.0,4.2,0.1,1.0,2.0,2.0, SURF_ID='stair' /  Step 10

&OBST XB=3.8,4.0,0.1,1.0,2.2,2.2, SURF_ID='stair' /  Step 11

&OBST XB=3.5,3.8,0.1,1.0,2.4,2.4, SURF_ID='stair', PERMIT_HOLE=.FALSE. /  Step 12

&OBST XB=5.6,5.7,0.1,1.0,3.2,3.3, SURF_ID = 'ceiling', SAWTOOTH=.FALSE.,
PERMIT_HOLE=.FALSE. / Slope 6

&OBST XB=5.7,5.8,0.1,1.0,3.1,3.2, SURF_ID = 'ceiling', SAWTOOTH=.FALSE.,
PERMIT_HOLE=.FALSE. / Slope 7

&OBST XB=5.8,5.9,0.1,1.0,3.0,3.1, SURF_ID = 'ceiling', SAWTOOTH=.FALSE.,
PERMIT_HOLE=.FALSE. / Slope 8

&OBST XB=5.9,6.0,0.1,1.0,2.9,3.0, SURF_ID = 'ceiling', SAWTOOTH=.FALSE.,
PERMIT_HOLE=.FALSE. / Slope 9

&OBST XB=6.0,6.1,0.1,1.0,2.8,2.9, SURF_ID = 'ceiling', SAWTOOTH=.FALSE.,
PERMIT_HOLE=.FALSE. / Slope 10

&OBST XB=6.1,6.2,0.1,1.0,2.7,2.8, SURF_ID = 'ceiling', SAWTOOTH=.FALSE.,
PERMIT_HOLE=.FALSE. / Slope 11

&OBST XB=6.2,6.3,0.1,1.0,2.6,2.7, SURF_ID = 'ceiling', SAWTOOTH=.FALSE.,
PERMIT_HOLE=.FALSE. / Slope 12

&OBST XB=5.6,6.2,1.0,1.1,2.6,2.7, SURF_ID = 'ceiling', SAWTOOTH=.FALSE.,
PERMIT_HOLE=.FALSE. / Slope Wall 1

&OBST XB=5.6,6.1,1.0,1.1,2.6,2.8, SURF_ID = 'ceiling', SAWTOOTH=.FALSE.,
PERMIT_HOLE=.FALSE. / Slope Wall 2
```

&OBST XB=5.6,6.0,1.0,1.1,2.6,2.9, SURF_ID = 'ceiling', SAWTOOTH=.FALSE., PERMIT_HOLE=.FALSE. / Slope Wall 3

&OBST XB=5.6,5.9,1.0,1.1,2.6,3.1, SURF_ID = 'ceiling', SAWTOOTH=.FALSE., PERMIT_HOLE=.FALSE. / Slope Wall 5

&OBST XB=5.6,5.7,1.0,1.1,2.6,3.2, SURF_ID = 'ceiling', SAWTOOTH=.FALSE., PERMIT_HOLE=.FALSE. / Slope Wall 6

&OBST XB=5.6,6.2,0.0,0.1,2.6,2.7, SURF_ID = 'ceiling', SAWTOOTH=.FALSE., PERMIT_HOLE=.FALSE. / Slope Wall 1

&OBST XB=5.6,6.1,0.0,0.1,2.6,2.8, SURF_ID = 'ceiling', SAWTOOTH=.FALSE., PERMIT_HOLE=.FALSE. / Slope Wall 2

&OBST XB=5.6,6.0,0.0,0.1,2.6,2.9, SURF_ID = 'ceiling', SAWTOOTH=.FALSE., PERMIT_HOLE=.FALSE. / Slope Wall 3

&OBST XB=5.6,5.9,0.0,0.1,2.6,3.1, SURF_ID = 'ceiling', SAWTOOTH=.FALSE., PERMIT_HOLE=.FALSE. / Slope Wall 5

&OBST XB=5.6,5.7,0.0,0.1,2.6,3.2, SURF_ID = 'ceiling', SAWTOOTH=.FALSE., PERMIT_HOLE=.FALSE.

&OBST XB=3.6,5.6,1.0,1.0,2.7,2.8, SURF_ID = 'bannister' / L1 Bannister rung 1

&OBST XB=3.6,5.6,1.0,1.0,2.9,3.0, SURF_ID = 'bannister' / L1 Bannister rung 2

&OBST XB=3.6,5.6,1.0,1.0,3.1,3.2, SURF_ID = 'bannister' / L1 Bannister rung 3

&OBST XB=3.6,5.6,1.0,1.0,3.3,3.4, SURF_ID = 'bannister' / L1 Bannister rung 4

&OBST XB=3.6,5.6,1.0,1.0,3.5,3.6, SURF_ID = 'bannister' / L1 Bannister rung 5

&OBST XB=5.8,6.0,1.0,1.0,0.3,0.4, SURF_ID = 'bannister' / Balustrade rung 1

&OBST XB=5.6,6.0,1.0,1.0,0.5,0.6, SURF_ID = 'bannister' / Balustrade rung 2

&OBST XB=5.4,6.0,1.0,1.0,0.7,0.8, SURF_ID = 'bannister' / Balustrade rung 3

&OBST XB=5.2,6.0,1.0,1.0,0.9,1.0, SURF_ID = 'bannister' / Balustrade rung 4

&OBST XB=5.0,5.8,1.0,1.0,1.1,1.2, SURF_ID = 'bannister' / Balustrade rung 5

&OBST XB=4.8,5.6,1.0,1.0,1.3,1.4, SURF_ID = 'bannister' / Balustrade rung 6

&OBST XB=4.6,5.4,1.0,1.0,1.5,1.6, SURF_ID = 'bannister' / Balustrade rung 7

&OBST XB=4.4,5.2,1.0,1.0,1.7,1.8, SURF_ID = 'bannister' / Balustrade rung 8

&OBST XB=4.2,5.0,1.0,1.0,1.9,2.0, SURF_ID = 'bannister' / Balustrade rung 9

&OBST XB=4.0,4.8,1.0,1.0,2.1,2.2, SURF_ID = 'bannister' / Balustrade rung 10

&OBST XB=3.8,4.6,1.0,1.0,2.3,2.4, SURF_ID = 'bannister' / Balustrade rung 11

&OBST XB=3.6,3.7,1.0,1.0,2.6,3.6, SURF_ID = 'bannister' / Vertical rung 1

&OBST XB=5.9,6.0,1.0,1.0,0.0,1.0, SURF_ID = 'bannister' / Vertical rung 2

&OBST XB=5.5,5.6,1.0,1.0,2.6,3.6, SURF_ID = 'bannister' / Vertical rung 3

&OBST XB=6.7,7.0,2.7,3.5,0.0,0.5, RGB=165,42,42 / Maximum HRR = 0.16*5159 = 825.44 kW

&OBST XB=6.6,6.7,2.8,3.4,0.0,0.5, RGB=165,42,42 / Maximum HRR = 0.16*5159 = 825.44 kW

&OBST XB=6.5,6.6,2.9,3.3,0.0,0.5, RGB=165,42,42 / Maximum HRR = 0.16*5159 = 825.44 kW

&OBST XB=6.4,6.5,3.0,3.2,0.0,0.5, RGB=165,42,42 / Maximum HRR = 0.16*5159 = 825.44 kW

&OBST XB=7.0,7.1,2.8,3.5,0.0,0.5, RGB=165,42,42 / Maximum HRR = 0.16*5159 = 825.44 kW

&OBST XB=7.1,7.2,2.9,3.5,0.0,0.5, RGB=165,42,42 / Maximum HRR = 0.16*5159 = 825.44 kW

&OBST XB=7.2,7.3,3.0,3.5,0.0,0.5, RGB=165,42,42 / Maximum HRR = 0.16*5159 = 825.44 kW

&OBST XB=7.3,7.4,3.1,3.4,0.0,0.5, RGB=165,42,42 / Maximum HRR = 0.16*5159 = 825.44 kW

&OBST XB=6.8,7.2,3.5,3.6,0.0,0.5, RGB=165,42,42 / Maximum HRR = 0.16*5159 = 825.44 kW

&OBST XB=6.9,7.1,3.6,3.7,0.0,0.5, RGB=165,42,42 / Maximum HRR = 0.16*5159 = 825.44 kW

&SURF ID='Heater2kW', TMP_FRONT=81, RAMP_T='HEATER'/

&OBST XB=7.6,7.7,3.7,5.1,0.0,0.7, SURF_ID='Heater2kW', RGB=255,255,0 / Lounge Radiator

&SURF ID='Heater1.5kW', TMP_FRONT=76/

&OBST XB=5.7,6.8,2.1,2.2,0.0,0.7, SURF_ID='Heater1.5kW', RGB=255,255,0 / Entry Hall Radiator

&SURF ID='Heater1kW', TMP_FRONT=66/

&OBST XB=7.6,7.7,4.1,4.9,2.6,3.3, SURF_ID='Heater1kW', RGB=255,255,0 / Bedroom 2 Radiator

&RAMP ID ='HEATER', T=0.00, F=1.00 /

&RAMP ID ='HEATER', T=599., F=1.00 /

&RAMP ID ='HEATER', T=600., F=0.00 /

```
&REAC ID='POLYURETHANE'
    FYI='C_6.3 H_7.1 N O_2.1, NFPA Handbook, Babrauskas'
    SOOT_YIELD=0.05
    C = 6.3
    H = 7.1 /
&SURF ID    = 'FIRE',
    HRRPUA = 320.99,
    RAMP_Q = 'FIRE RAMP'/
&RAMP ID    ='FIRE RAMP',T=600,F=0.00/
&RAMP ID    ='FIRE RAMP',T=610,F=0.00/
&RAMP ID    ='FIRE RAMP',T=620,F=0.0142/
&RAMP ID    ='FIRE RAMP',T=630,F=0.0093/
&RAMP ID    ='FIRE RAMP',T=640,F=0.0071/
&RAMP ID    ='FIRE RAMP',T=650,F=0.0495/
&RAMP ID    ='FIRE RAMP',T=660,F=0.0140/
&RAMP ID    ='FIRE RAMP',T=670,F=0.0300/
&RAMP ID    ='FIRE RAMP',T=680,F=0.0029/
&RAMP ID    ='FIRE RAMP',T=690,F=0.00/
&RAMP ID    ='FIRE RAMP',T=700,F=0.0031/
&RAMP ID    ='FIRE RAMP',T=710,F=0.00/
&RAMP ID    ='FIRE RAMP',T=720,F=0.00/
&RAMP ID    ='FIRE RAMP',T=730,F=0.00/
&RAMP ID    ='FIRE RAMP',T=740,F=0.00/
&RAMP ID    ='FIRE RAMP',T=750,F=0.0114/
&RAMP ID    ='FIRE RAMP',T=760,F=0.0638/
&RAMP ID    ='FIRE RAMP',T=770,F=0.1132/
```

```
&RAMP ID    ='FIRE RAMP',T=780,F=0.1496/
&RAMP ID    ='FIRE RAMP',T=790,F=0.2041/
&RAMP ID    ='FIRE RAMP',T=800,F=0.2444/
&RAMP ID    ='FIRE RAMP',T=810,F=0.2884/
&RAMP ID    ='FIRE RAMP',T=820,F=0.3351/
&RAMP ID    ='FIRE RAMP',T=830,F=0.3980/
&RAMP ID    ='FIRE RAMP',T=840,F=0.4592/
&RAMP ID    ='FIRE RAMP',T=850,F=0.5180/
&RAMP ID    ='FIRE RAMP',T=860,F=0.5888/
&RAMP ID    ='FIRE RAMP',T=870,F=0.6674/
&RAMP ID    ='FIRE RAMP',T=880,F=0.7223/
&RAMP ID    ='FIRE RAMP',T=890,F=0.7856/
&RAMP ID    ='FIRE RAMP',T=900,F=0.8453/
&RAMP ID    ='FIRE RAMP',T=910,F=0.8810/
&RAMP ID    ='FIRE RAMP',T=920,F=0.9243/
&RAMP ID    ='FIRE RAMP',T=930,F=0.9434/
&RAMP ID    ='FIRE RAMP',T=940,F=0.9846/
&RAMP ID    ='FIRE RAMP',T=950,F=0.9758/
&RAMP ID    ='FIRE RAMP',T=960,F=1.0000/
&RAMP ID    ='FIRE RAMP',T=970,F=0.9887/
&RAMP ID    ='FIRE RAMP',T=980,F=0.9846/
&RAMP ID    ='FIRE RAMP',T=990,F=0.9707/
&RAMP ID    ='FIRE RAMP',T=1000,F=0.9248/
&RAMP ID    ='FIRE RAMP',T=1010,F=0.8748/
&RAMP ID    ='FIRE RAMP',T=1020,F=0.8368/
&RAMP ID    ='FIRE RAMP',T=1030,F=0.7824/
```

```
&RAMP ID    ='FIRE RAMP',T=1040,F=0.7385/
&RAMP ID    ='FIRE RAMP',T=1050,F=0.6795/
&RAMP ID    ='FIRE RAMP',T=1060,F=0.5925/
&RAMP ID    ='FIRE RAMP',T=1070,F=0.5555/
&RAMP ID    ='FIRE RAMP',T=1080,F=0.4787/
&RAMP ID    ='FIRE RAMP',T=1090,F=0.4715/
&RAMP ID    ='FIRE RAMP',T=1100,F=0.4652/
&RAMP ID    ='FIRE RAMP',T=1110,F=0.4449/
&RAMP ID    ='FIRE RAMP',T=1120,F=0.4453/
&RAMP ID    ='FIRE RAMP',T=1130,F=0.4585/
&RAMP ID    ='FIRE RAMP',T=1140,F=0.4602/
&RAMP ID    ='FIRE RAMP',T=1150,F=0.4830/
&RAMP ID    ='FIRE RAMP',T=1160,F=0.4945/
&RAMP ID    ='FIRE RAMP',T=1170,F=0.4744/
&RAMP ID    ='FIRE RAMP',T=1180,F=0.4722/
&RAMP ID    ='FIRE RAMP',T=1190,F=0.4826/
&RAMP ID    ='FIRE RAMP',T=1200,F=0.4940/
&RAMP ID    ='FIRE RAMP',T=1210,F=0.5018/
&RAMP ID    ='FIRE RAMP',T=1220,F=0.5121/
&RAMP ID    ='FIRE RAMP',T=1230,F=0.5258/
&RAMP ID    ='FIRE RAMP',T=1240,F=0.5286/
&RAMP ID    ='FIRE RAMP',T=1250,F=0.5321/
&RAMP ID    ='FIRE RAMP',T=1260,F=0.5372/
&RAMP ID    ='FIRE RAMP',T=1270,F=0.5426/
&RAMP ID    ='FIRE RAMP',T=1280,F=0.5142/
&RAMP ID    ='FIRE RAMP',T=1290,F=0.4813/
```

&RAMP ID   ='FIRE RAMP',T=1300,F=0.4644/

&VENT XB=6.7,7.0,2.7,3.5,0.5,0.5, SURF_ID='FIRE', COLOR='RED' /

&VENT XB=6.6,6.7,2.8,3.4,0.5,0.5, SURF_ID='FIRE', COLOR='RED' /

&VENT XB=6.5,6.6,2.9,3.3,0.5,0.5, SURF_ID='FIRE', COLOR='RED' /

&VENT XB=6.4,6.5,3.0,3.2,0.5,0.5, SURF_ID='FIRE', COLOR='RED' /

&VENT XB=7.0,7.1,2.8,3.5,0.5,0.5, SURF_ID='FIRE', COLOR='RED' /

&VENT XB=7.1,7.2,2.9,3.5,0.5,0.5, SURF_ID='FIRE', COLOR='RED' /

&VENT XB=7.2,7.3,3.0,3.5,0.5,0.5, SURF_ID='FIRE', COLOR='RED' /

&VENT XB=7.3,7.4,3.1,3.4,0.5,0.5, SURF_ID='FIRE', COLOR='RED' /

&VENT XB=6.8,7.2,3.5,3.6,0.5,0.5, SURF_ID='FIRE', COLOR='RED' /

&VENT XB=6.9,7.1,3.6,3.7,0.5,0.5, SURF_ID='FIRE', COLOR='RED' /

&DEVC XYZ=5.2,3.9,0.1, QUANTITY='TEMPERATURE', ID='T1.1' / LOUNGE CENTRAL

&DEVC XYZ=5.2,3.9,0.4, QUANTITY='TEMPERATURE', ID='T1.2' /

&DEVC XYZ=5.2,3.9,0.7, QUANTITY='TEMPERATURE', ID='T1.3' /

&DEVC XYZ=5.2,3.9,1.0, QUANTITY='TEMPERATURE', ID='T1.4' /

&DEVC XYZ=5.2,3.9,1.4, QUANTITY='TEMPERATURE', ID='T1.5' /

&DEVC XYZ=5.2,3.9,1.7, QUANTITY='TEMPERATURE', ID='T1.6' /

&DEVC XYZ=5.2,3.9,2.0, QUANTITY='TEMPERATURE', ID='T1.7' /

&DEVC XYZ=5.2,3.9,2.3, QUANTITY='TEMPERATURE', ID='T1.8' /

&DEVC XYZ=4.3,3.2,0.1, QUANTITY='TEMPERATURE', ID='T2.1' / LOUNGE 2

&DEVC XYZ=4.3,3.2,0.4, QUANTITY='TEMPERATURE', ID='T2.2' /

&DEVC XYZ=4.3,3.2,0.7, QUANTITY='TEMPERATURE', ID='T2.3' /

&DEVC XYZ=4.3,3.2,1.0, QUANTITY='TEMPERATURE', ID='T2.4' /

&DEVC XYZ=4.3,3.2,1.4, QUANTITY='TEMPERATURE', ID='T2.5' /

&DEVC XYZ=4.3,3.2,1.7, QUANTITY='TEMPERATURE', ID='T2.6' /

&DEVC XYZ=4.3,3.2,2.0, QUANTITY='TEMPERATURE', ID='T2.7' /

&DEVC XYZ=4.3,3.2,2.3, QUANTITY='TEMPERATURE', ID='T2.8' /

&DEVC XYZ=4.7,2.2,0.1, QUANTITY='TEMPERATURE', ID='T3.1' / ENTRY HALL

&DEVC XYZ=4.7,2.2,0.4, QUANTITY='TEMPERATURE', ID='T3.2' /

&DEVC XYZ=4.7,2.2,0.7, QUANTITY='TEMPERATURE', ID='T3.3' /

&DEVC XYZ=4.7,2.2,1.0, QUANTITY='TEMPERATURE', ID='T3.4' /

&DEVC XYZ=4.7,2.2,1.4, QUANTITY='TEMPERATURE', ID='T3.5' /

&DEVC XYZ=4.7,2.2,1.7, QUANTITY='TEMPERATURE', ID='T3.6' /

&DEVC XYZ=4.7,2.2,2.0, QUANTITY='TEMPERATURE', ID='T3.7' /

&DEVC XYZ=4.7,2.2,2.3, QUANTITY='TEMPERATURE', ID='T3.8' /

&DEVC XYZ=5.3,0.7,0.9, QUANTITY='TEMPERATURE', ID='T4.1' / STAIRS

&DEVC XYZ=5.3,0.7,1.3, QUANTITY='TEMPERATURE', ID='T4.2' /

&DEVC XYZ=5.3,0.7,1.6, QUANTITY='TEMPERATURE', ID='T4.3' /

&DEVC XYZ=5.3,0.7,1.9, QUANTITY='TEMPERATURE', ID='T4.4' /

&DEVC XYZ=5.3,0.7,2.2, QUANTITY='TEMPERATURE', ID='T4.5' /

&DEVC XYZ=5.3,0.7,2.6, QUANTITY='TEMPERATURE', ID='T4.6' /

&DEVC XYZ=5.3,0.7,2.9, QUANTITY='TEMPERATURE', ID='T4.7' /

&DEVC XYZ=5.3,0.7,3.2, QUANTITY='TEMPERATURE', ID='T4.8' /

&DEVC XYZ=3.6,1.7,2.7, QUANTITY='TEMPERATURE', ID='T5.1' / LANDING

&DEVC XYZ=3.6,1.7,3.0, QUANTITY='TEMPERATURE', ID='T5.2' /

&DEVC XYZ=3.6,1.7,3.3, QUANTITY='TEMPERATURE', ID='T5.3' /

&DEVC XYZ=3.6,1.7,3.6, QUANTITY='TEMPERATURE', ID='T5.4' /

&DEVC XYZ=3.6,1.7,4.0, QUANTITY='TEMPERATURE', ID='T5.5' /

&DEVC XYZ=3.6,1.7,4.3, QUANTITY='TEMPERATURE', ID='T5.6' /

&DEVC XYZ=3.6,1.7,4.6, QUANTITY='TEMPERATURE', ID='T5.7' /

&DEVC XYZ=3.6,1.7,4.9, QUANTITY='TEMPERATURE', ID='T5.8' /

&DEVC XYZ=6.0,4.1,2.7, QUANTITY='TEMPERATURE', ID='T6.1' / BEDROOM 2

&DEVC XYZ=6.0,4.1,3.0, QUANTITY='TEMPERATURE', ID='T6.2' /

&DEVC XYZ=6.0,4.1,3.3, QUANTITY='TEMPERATURE', ID='T6.3' /

&DEVC XYZ=6.0,4.1,3.7, QUANTITY='TEMPERATURE', ID='T6.4' /

&DEVC XYZ=6.0,4.1,4.0, QUANTITY='TEMPERATURE', ID='T6.5' /

&DEVC XYZ=6.0,4.1,4.3, QUANTITY='TEMPERATURE', ID='T6.6' /

&DEVC XYZ=6.0,4.1,4.6, QUANTITY='TEMPERATURE', ID='T6.7' /

&DEVC XYZ=6.0,4.1,4.9, QUANTITY='TEMPERATURE', ID='T6.8' /

&DEVC XYZ=5.2,3.9,1.5, QUANTITY='visibility', ID='VLoun' / LOUNGE CENTRAL

&DEVC XYZ=4.7,2.2,1.5, QUANTITY='visibility', ID='VEHall' / ENTRY HALL

&DEVC XYZ=3.6,1.7,4.1, QUANTITY='visibility', ID='VLand' / LANDING

&DEVC XYZ=6.0,4.1,4.1, QUANTITY='visibility', ID='VBed2' / BEDROOM 2

&DEVC XYZ=5.2,3.9,0.5, QUANTITY='optical depth', ID='ODLoung0.5' / LOUNGE CENTRAL

&DEVC XYZ=5.2,3.9,1.5, QUANTITY='optical depth', ID='ODLoung1.5' / LOUNGE CENTRAL

&DEVC XYZ=4.7,2.2,0.5, QUANTITY='optical depth', ID='ODEHall0.5' / ENTRY HALL

&DEVC XYZ=4.7,2.2,1.0, QUANTITY='optical depth', ID='ODEHall1.0' / ENTRY HALL

&DEVC XYZ=4.7,2.2,1.5, QUANTITY='optical depth', ID='ODEHall1.5' / ENTRY HALL

&DEVC XYZ=3.6,1.7,4.1, QUANTITY='optical depth', ID='ODLand1.5' / LANDING

&DEVC XYZ=3.6,1.7,3.1, QUANTITY='optical depth', ID='ODLand0.5' / LANDING

&DEVC XYZ=6.0,4.1,3.1, QUANTITY='optical depth', ID='ODBed2' / BEDROOM 2

&DEVC XYZ=6.0,4.1,4.1, QUANTITY='optical depth', ID='ODBed2' / BEDROOM 2

&PROP ID='Heskestad Smoke Detector', QUANTITY='CHAMBER OBSCURATION', LENGTH=1.8, ACTIVATION_OBSCURATION=3.28 /

&PROP ID='Cleary I1', QUANTITY='spot obscuration', ALPHA_C=0.8, BETA_C=-0.9, ALPHA_E=2.5, BETA_E=-0.7, ACTIVATION_OBSCURATION=3.28 /

```
&PROP ID='Cleary I2', QUANTITY='spot obscuration', ALPHA_C=1.0, BETA_C=-0.8, ALPHA_E=1.8,
BETA_E=-1.1, ACTIVATION_OBSCURATION=3.28 /

&PROP ID='Cleary P1', QUANTITY='spot obscuration', ALPHA_C=1.0, BETA_C=-0.8, ALPHA_E=1.8,
BETA_E=-1.0, ACTIVATION_OBSCURATION=3.28 /

&PROP ID='Cleary P2', QUANTITY='spot obscuration', ALPHA_C=0.8, BETA_C=-0.8, ALPHA_E=1.8,
BETA_E=-0.8, ACTIVATION_OBSCURATION=3.28 /

&DEVC ID='LI.Hesk', PROP_ID='Heskestad Smoke Detector', XYZ=5.8,4.7,2.3 /

&DEVC ID='LI.CI1', PROP_ID='Cleary I1', XYZ=5.8,4.7,2.3 /

&DEVC ID='LI.CI2', PROP_ID='Cleary I2', XYZ=5.8,4.7,2.3 /

&DEVC ID='LI.CP1', PROP_ID='Cleary P1', XYZ=5.8,4.7,2.3 /

&DEVC ID='LI.CP2', PROP_ID='Cleary P2', XYZ=5.8,4.7,2.3 /

&DEVC XYZ=5.8,4.7,2.3, QUANTITY='TEMPERATURE', ID='Lo.Ion' /

&DEVC ID='LO.Hesk', PROP_ID='Heskestad Smoke Detector', XYZ=5.3,4.7,2.3, /

&DEVC ID='LO.CI1', PROP_ID='Cleary I1', XYZ=5.3,4.7,2.3, /

&DEVC ID='LO.CI2', PROP_ID='Cleary I2', XYZ=5.3,4.7,2.3, /

&DEVC ID='LO.CP1', PROP_ID='Cleary P1', XYZ=5.3,4.7,2.3, /

&DEVC ID='LO.CP2', PROP_ID='Cleary P2', XYZ=5.3,4.7,2.3, /

&DEVC XYZ=5.3,4.7,2.3, QUANTITY='TEMPERATURE', ID='Lo.Opt' /

&DEVC ID='HI.Hesk', PROP_ID='Heskestad Smoke Detector', XYZ=5.9,1.6,2.3, /

&DEVC ID='HI.CI1', PROP_ID='Cleary I1', XYZ=5.9,1.6,2.3, /

&DEVC ID='HI.CI2', PROP_ID='Cleary I2', XYZ=5.9,1.6,2.3, /

&DEVC ID='HI.CP1', PROP_ID='Cleary P1', XYZ=5.9,1.6,2.3, /

&DEVC ID='HI.CP2', PROP_ID='Cleary P2', XYZ=5.9,1.6,2.3, /

&DEVC XYZ=5.9,1.6,2.3, QUANTITY='TEMPERATURE', ID='Hall.Ion' /

&DEVC ID='HO.Hesk', PROP_ID='Heskestad Smoke Detector', XYZ=5.0,2.0,2.3, /

&DEVC ID='HO.CI1', PROP_ID='Cleary I1', XYZ=5.0,2.0,2.3, /

&DEVC ID='HO.CI2', PROP_ID='Cleary I2', XYZ=5.0,2.0,2.3, /
```

&DEVC ID='HO.CP1', PROP_ID='Cleary P1', XYZ=5.0,2.0,2.3, /

&DEVC ID='HO.CP2', PROP_ID='Cleary P2', XYZ=5.0,2.0,2.3, /

&DEVC XYZ=5.0,2.0,2.3, QUANTITY='TEMPERATURE', ID='Hall.Opt' /

&DEVC ID='LaI.Hesk', PROP_ID='Heskestad Smoke Detector', XYZ=3.8,1.2,4.9, /

&DEVC ID='LaI.CI1', PROP_ID='Cleary I1', XYZ=3.8,1.2,4.9, /

&DEVC ID='LaI.CI2', PROP_ID='Cleary I2', XYZ=3.8,1.2,4.9, /

&DEVC ID='LaI.CP1', PROP_ID='Cleary P1', XYZ=3.8,1.2,4.9, /

&DEVC ID='LaI.CP2', PROP_ID='Cleary P2', XYZ=3.8,1.2,4.9, /

&DEVC XYZ=3.8,1.2,4.9, QUANTITY='TEMPERATURE', ID='La.Ion' /

&DEVC ID='LaO.Hesk', PROP_ID='Heskestad Smoke Detector', XYZ=4.1,1.2,4.9, /

&DEVC ID='LaO.CI1', PROP_ID='Cleary I1', XYZ=4.1,1.2,4.9, /

&DEVC ID='LaO.CI2', PROP_ID='Cleary I2', XYZ=4.1,1.2,4.9, /

&DEVC ID='LaO.CP1', PROP_ID='Cleary P1', XYZ=4.1,1.2,4.9, /

&DEVC ID='LaO.CP2', PROP_ID='Cleary P2', XYZ=4.1,1.2,4.9, /

&DEVC XYZ=4.1,1.2,4.9, QUANTITY='TEMPERATURE', ID='La.Opt' /

&DEVC ID='BedI.Hesk', PROP_ID='Heskestad Smoke Detector', XYZ=6.1,4.6,4.9, /

&DEVC ID='BedI.CI1', PROP_ID='Cleary I1', XYZ=6.1,4.6,4.9, /

&DEVC ID='BedI.CI2', PROP_ID='Cleary I2', XYZ=6.1,4.6,4.9, /

&DEVC ID='BedI.CP1', PROP_ID='Cleary P1', XYZ=6.1,4.6,4.9, /

&DEVC ID='BedI.CP2', PROP_ID='Cleary P2', XYZ=6.1,4.6,4.9, /

&DEVC XYZ=6.1,4.6,4.9, QUANTITY='TEMPERATURE', ID='Bed.Ion' /

&DEVC ID='BedO.Hesk', PROP_ID='Heskestad Smoke Detector', XYZ=6.1,4.0,4.9, /

&DEVC ID='BedO.CI1', PROP_ID='Cleary I1', XYZ=6.1,4.0,4.9, /

&DEVC ID='BedO.CI2', PROP_ID='Cleary I2', XYZ=6.1,4.0,4.9, /

&DEVC ID='BedO.CP1', PROP_ID='Cleary P1', XYZ=6.1,4.0,4.9, /

&DEVC ID='BedO.CP2', PROP_ID='Cleary P2', XYZ=6.1,4.0,4.9, /

```
&DEVC XYZ=6.1,4.0,4.9, QUANTITY='TEMPERATURE', ID='Bed.Opt' /
```